THE UNIVERSITY OF CALGARY

Structural and Metal Binding Study of Laurentian Fulvic Acid

by

Robert Lewis Cook

A DISSERTATION

SUBMITTED TO THE FACULTY OF GRADUATE STUDIES

IN PARTIAL FULFILMENT OF THE REQUIREMENTS FOR THE

DEGREE OF DOCTOR OF PHILOSOPHY

DEPARTMENT OF CHEMISTRY

CALGARY, ALBERTA

SEPTEMBER, 1997

Abstract

Two organic extracts of the Laurentian soil have been studied. The organic extracts are Laurentian fulvic acid (LFA) and Laurentian humic acid (LHA). These two samples were analysed by cross polarisation magic angle spinning (CP-MAS) ^{13}C NMR, while LFA was also characterised by fluorescence spectroscopy.

A new CP-MAS ^{13}C NMR method was developed, which combined ramped amplitude CP (Ramp-CP), high sample spinning rates, and high field strength (7 T). It is shown both theoretically and experimentally that Ramp-CP gives significantly better qualitative and quantitative spectra than does single amplitude CP (SACP).

The characterisation of LFA and LHA revealed that in terms of size LFA is a more heterogeneous mixture of fragments than LHA. In terms of functionality, it was found that LFA had the majority of its functionality located on its carbohydrate moieties, while LHA had the majority of its functionality located on its aromatic moieties. Based on these findings mesostructures for both LFA and LHA are proposed.

Metal binding by LFA was also investigated by both fluorescence and NMR techniques. From the results it was concluded that the strongest metal binding sites of LFA are predominantly on the carbohydrate moieties, and that the aliphatic moieties are also involved in metal binding via aggregation. These findings also suggest that the majority of luminescence observed for LFA involves Föster resonance or donor/acceptor complexes. The metal binding results also indicate that cellulose may be an important fragment in LFA.

This study leads to a reconceptualisation of LFA in terms of the functionally greater importance of the carbohydrate moieties then the aromatic moieties, and the importance of aggregation and conformation.

Acknowledgements

I wish to extend my deepest thanks to Dr. Cooper H. Langford for believing in me and allowing to go my own way, while at the same time providing guidance, motivation, and support.

I would also like to thank Dr. E.O. Stejskal for many enlightening discussions and Dr. D.E. Axelson, Dr. Cabaniss, Dr. C.M. Preston, Dr. S.O. Smith and Dr. R. Yamdagni for many useful discussions. I cordially thank Mrs. Qiao Wu and Dr. R. Yamdagni for technical assistance, and Dr. G Liu for the use of his instruments.

I would like to extend my thanks to Mike Pullin for the pH dependent fluorescence measurements and for the friendship that developed there after, Jayanti Sharma for aiding in the size exclusion experiment, and Dr. Caroline M. Preston for the liquids state ^{13}C NMR measurements.

I would like to thank Dr. Attila Bérces, Ashfaq Choudhury, Dr. Andrew Kirk, Erwin Schultz, and Dr. Yimmin Xu for their friendship.

I also must thank two teachers from my past Dr. Brown for teaching me how to think, and Dr. Zenious for taking a chance on me, which kept me in chemistry.

For moral support I never had to go far and for this I would like to thank my parents Stuart and Julie Cook as well as my sister Fiona and my brother Malcolm.

Lastly, but by no means leastly, I would like to thank my wife Elzbieta Cook for her love, support, and help which knows no limits.

Dedicated to my Family

Table of Contents

List of Tables

List of Figures

Chapter 1
Introduction

Recently the world ecosystems have been estimated to be worth, in monetary terms, twice the gross national product of the world ($33 trillion [U.S.]),[1.1] and natural organic matter plays a vital role in all ecosystems.

Refractory pedogenic organic matter and its aquagenic analogs play a central role in processes as diverse as water quality, soil quality, soil conditioning, nutrient storage and transport, organic contaminant (e.g. pesticides) binding and transport, and heavy metal binding and transport.[1.2-1.4] This binding and transport of chemical species plays a major role in how toxic chemical species are in the natural environment.[1.5] It has been proposed that the toxicity of a chemical species is most closely related to the concentration of free chemical species and not that of the total chemical species concentration.[1.6-1.8] For metals this is known as the "free metal ion hypothesis".[1.9] Nature buffers the toxicity of chemical species by reducing the lability and activity of the chemical species through complexation or adsorption by complex mixtures of ligands. To date, these complex mixtures have remained the least understood and characterised constituents of soil and water. The best characterised components of these complex mixtures are the polyelectrolyte humic colloid fractions; humic acid and fulvic acid. Both of these are historically defined by base extraction, where humic acids are the higher molecular weight and acid insoluble fractions, while fulvics acids are the low molecular weight and acid soluble fractions.

Humic materials are best described as complex polydisperse polymeric heterogeneous mixtures, whose properties echo their structural diversity, as well as their state of aggregation, conformation and surface charge.

The analysis of complex heterogeneous mixtures has always been a challenge. There are two approaches. The first is the separation or fractionation of the complex heterogeneous mixture, a classic example of this approach is chromatography. However, to date both humic and fulvic acids remain complex mixtures, resistant to fractionation. Indeed, fractionating to individual molecular species would cause a loss of information about critical "emergent" properties dependent upon aggregation, natural conformation, and the electrostatic state of the polyelectrolyte mixture. The second approach to studying complex mixtures is to study the mixture as a whole. The drawback to this approach lies in finding a method which allows one to interrogate the whole mixture in sufficient depth without bias. If this drawback can be overcome this second approach to studying complex mixtures is preferable.

The pre-eminent group of methods in the study of whole humic samples have been degradative (mild oxidation with chemical analysis and physical fragmentation with mass spectroscopy) and spectroscopic techniques. There are, however, inherent problems with the first group of techniques. The most important problems are very low carbon mass recovery, usually in the range of 5%, though in some cases as high as 33% , and the bias towards small aromatic fragments which survive the degradation or fragmentation. There is also a strong possibility of contamination. Many different types of spectroscopic technique have be applied to humic materials. These includes absorption, electron paramagnetic resonance (EPR), Fourier transform infra-red (FT-IR), luminescence, Mössbauer, nuclear magnetic resonance (NMR), Raman, and X-ray photoelectron spectroscopies.[1.2-1.4]

So far, the most useful of these two techniques are luminescence and NMR spectroscopy. Luminescence spectroscopy is of great use because it is highly sensitive,

easy to use, compact, relatively inexpensive, non destructive, four dimensional, and quenched by metal ions. In addition, all humic materials fluoresce.

However, ^{13}C NMR spectroscopy has established itself as the pre-eminent tool for the structural investigation of humic substances.[1.10, 1.11] Although ^{1}H NMR was used first, ^{13}C has several inherent advantages. The first is that the carbon skeleton of the humic material is observed rather than the adjacent protons, which allows functional groups such as ketones to be detected. It also allows fully functionalised aromatic rings to be detected. Secondly, the carbon nuclei are spread over a wider range of chemical shifts in ^{13}C NMR, and consequently individual signals may be observed even when carbons have only a small difference in structural environments. The final advantage is that line widths of signal in ^{13}C NMR are narrower than in ^{1}H, thus signal overlap is less pronounced in ^{13}C NMR. The most important ^{13}C NMR technique for the study of humic materials is cross polarisation magic angle spinning (CP-MAS) ^{13}C NMR spectroscopy.[1.10-1.12]

In chapter 2 a retrospective look at the literature on the use of luminescence and NMR in the study of humic materials is given. This is followed by a theoretical treatment of luminescence and NMR as applied to humic materials in chapter 3.

The quantitative reliability of the ^{13}C CP-MAS technique for insoluble organic matter has long been of concern [1.10-1.15], and has been thoroughly researched for fossil fuels [1.16-1.18]. There are at least three factors which affect the intensity of a particular signal. The first is variation in cross-polarisation rates for different carbon types. The second problem is the loss of intensity and distortion of peak areas by spinning sidebands, especially in the aromatic and carboxyl regions. The third problem is that carbons close to a paramagnetic centre may be undetectable. This is because unpaired electron spins reduce the $T_{1\rho}(^{1}H)$ (spin-lattice relaxation in the rotating frame) of the hydrogens so much that they lose magnetisation too quickly to transfer it to a carbon. For samples low in carbon

and with unpaired electrons, the percentage of carbon actually observed is typically 50% or less, however if the sample is relatively high in carbon and has no paramagnetic species present then the percentage of observable carbons is close to 100%.[1.19-1.22]

The first problem can be addressed by one of several approaches, including acquisition of spectra with varying contact times so that the true intensity distribution can be calculated and Bloch-decay acquisition (without cross-polarisation). The latter generally requires samples high in carbon, and low in paramagnetic species, and/or large (2.5 cm^3) rotors.[1.23] The third problem of low visibility has no easy solution, but thus far, there is no clear indication that the observed C differs substantially from that rendered invisible by proximity to paramagnetic centres, at least for humic substances. For soluble fractions such as fulvic and humic acids, cross-checks of solution and solid-state spectra have shown reasonable agreement.[1.24] If it is not possible to use any of these approaches, a contact time of 1 ms has generally been found to be appropriate for coals and humic substances, giving the best compromise between quantitative intensity distribution and CP intensity enhancement.

For the second problem, some attempts have been made to use mechanical manipulation of the spinning, but these approaches are complex, not commercially available, and not suitable for all types of samples, due to the relatively long delays (0.5 - 5 s) involved.[1.25,1.26] Pulse sequences to suppress sidebands also have their own problems with signal loss and intensity distortions. Faster spinning should be the solution, but it has long been known that high MAS rates can interfere with the cross polarisation process, again leading to loss of signal and distortion of relative intensities.[1.27] For this reason, and because much of the linebroadening in coals is due to chemical shift dispersion, which is not improved by higher fields, it has been recommended that the best CP-MAS results for coals (and humics) will be obtained with low field instruments (2.3 T, ca. 100 MHz for

^{1}H) and slow spinning rates of less than 5 kHz.[1.18] In any event, speeds much above 5 kHz were not readily available until recently.

Two other mechanisms could cause linebroadening in the spectra of non-rigid solids such humic substances. These are motional modulation of the CH coupling, and motional modulation of the resonance frequency by the chemical shift anisotropy (CSA). The latter should make an increasing contribution to linewidths at higher fields, especially for aromatic and carboxyl carbons. As outlined in chapter 3, higher MAS rates should alleviate the broadening due to both of these mechanisms.

Recently, MAS probes have become commercially available that allow spinning rates up to 20 kHz, and this has been coupled with the proliferation of high-field CP-MAS instruments with their greatly enhanced sensitivity. Concurrent with this, modifications have been developed for the CP-MAS pulse sequence to alleviate the CP problems due to high speed spinning. The most promising pulse sequence for large macromolecules such as humic substances, is known as ramped amplitude CP (Ramp-CP).[1.28]

The effects of high fields and high MAS rates when used with Ramp-CP in the CP-MAS ^{13}C NMR investigation of two well-characterised humic substances, the Laurentian fulvic and humic acid (LFA and LHA respectively) are examined in chapter 5.

The formation of chemical species-humus complexes is not as simple as is suggested by model compounds, because there are several possible distributions of complexing sites, as shown in Figure 1.1, whereas in model compounds there is only one. The S-sites correspond to the sites directly involved in the bonding (model compounds), while the L-sites take into consideration the co-ordinating group as well as its environment, both of which can affect complex stability. These L-sites reflect secondary macromolecular effects, and have been divided into three subclasses ((*a*), (*b*), and (*c*) in Figure 1.1) by Buffle.[1.29]

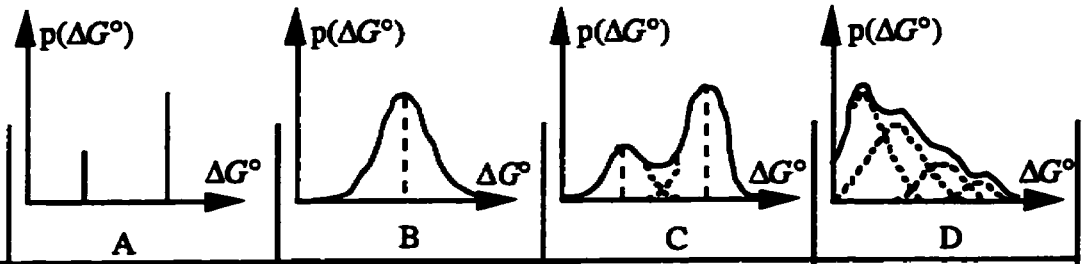

	A	B	C	D
Property	2 different sites S zero (*a*)-(*c*) effects → 2 sites L	Unimodal distribution 1 single site S non-zero (*a*)-(*c*) effects → large number of sites L	Bimodal distribution 2 sites S zero (*a*)-(*c*) effects → large number of sites L	large number of sites S non-zero (*a*)-(*c*) effects →infinity of sites L
Typical examples	mixture of simple ligands (e.g. CO_3^{2-}, amino-acids) or simple ligand with 2 independent sites	homopolysaccharides (site = -COOH) ΔG variation is mostly due to effects (*b*) and (*c*)	peptides (e.g. sites are -COOH and $-NH_2$)	PROM AND AROM (sites = -COOH, Δ-OH, NH_2, -SH, etc...) ΔG variation is mostly due to effects (*a*)-(*c*)

Figure 1.1: Possible distributions of metal binding sites. $p(\Delta G^\circ)$ represents the probability of a site complexing, where ΔG° is the free energy of formation, PROM stands for pedogenic refractory organic matter, and AROM stands for aquagenic refractory organic matter.[1.29]

The (*a*) effects, which cause a distribution $p(\Delta G^\circ)$, are called polyfunctional, and are related to the multifunctionality of the complexing agent, which arises due to the chemical structural diversity of S-sites. The (*b*) effects deal with the dependence of the conformation of the overall complex, on the degree of hydration and the extent of the hydrogen bonding and bridging metal groups. The (*c*) effects are due to the changing electrostatic energy

arising from the polyelectrolyte properties of the complexant (humus material). The extent of binding site occupation will determine the importance of any and all these effects.

Thus, the first step in studying complexation by humic materials is to characterise structurally the humic material under consideration as well as possible. Investigation of humic structures has drawn from three main lines of evidence about chemical functionality: (i) mild oxidative degradation and physical fragmentation with mass spectroscopy;[1.3, 1.4] (ii) titrimetric and specific reactivity determination of functional group distribution;[1.3] and (iii) NMR spectroscopic study of functional group distribution.[1.3, 1.4, 1.11, 1.22] The first line of evidence has tended to emphasise the aromatic fragments which survive the degradative or fragmentative processes. This has generated an emphasis on aromatic small molecule models of functionality and behaviour. The third has corrected the bias in perception of the importance of aromatic as opposed, especially, to carbohydrate functionality, as NMR is non-destructive and requires no fractionation, this is especially true for fulvic acids.[1.3, 1.4, 1.11,1.12] In chapter 6 both LFA and LHA are studied by Ramp-CP-MAS ^{13}C NMR in terms of chemical shift, T_2 relaxation times and dipolar dephasing spectra. LFA is also studied by both emission and synchronous luminescence under different pH conditions.

The next step, and final part of the work presented here, chapter 7, is the study of metal binding by LFA. Due to the ability of humic materials to decrease the toxicity of metal ions, as discussed above, this is of a major environmental importance. The metal ion used for these studies was Cu (II). The reason for choosing Cu (II) was because it has been found that the majority of Cu found in nature is bound to organic matter [1.30], there is also an extensive literature on Cu-FA complexes [1.30-1.32], and Cu is one of the most important trace elements in biology [1.33]. The study uses both luminescence and CP-MAS

^{13}C NMR, and is the first systematic use of NMR to study metal binding as well as being the first study to combine luminescence and NMR results.

References

1.1 Costanza, R.; d'Arge, R.; de Groot, R.; Farber, S.; Grasso, M.; Hannon, B.; Limburg, K.; Naeem, S.; O'Neill, R.V.; Paruelo, J.; Raskin, P.G.; Sutton, P.; van den Belt, M. *Nature*, **1997**, 387, 253.

1.2 Buffle, J. Complexation Reactions in Aquatic Systems. An Analytical Approach; Ellis Harwood Ltd,: Chester, UK, 1988

1.3 Stevenson, F.J. Humus Chemistry. Genesis. Composition. Reactions (2nd ed.); John Wiley & Sons, Toronto, 1992

1.4 Hayes, M.H.B.; MacCarthy, P.; Malcolm, R.L.; Swift, R.S. Humic Substances II. In Search of Structure; John Wiley & Sons, Toronto, 1989.

1.5 Martin, R.B. in Concepts On Metal Ion Toxicity: Vol. 20 of the series: H. Sigel (ed.), Vol. 20 of the series, Metal Ions in Biological Systems; Marcel Dekker, 1986.

1.6 Sunda, W.G.; Lewis, J.A.M. *Limnol. Oceanogr.* **1978**, 23, 870.

1.7 Petersen, R. *Environ. Sci. Technol.* **1982**, 16, 443.

1.8 Morrison, G.M.P. in Trace Element Speciation: Analytical Methods and Problems: G.E. Batley (ed.); CRC Press, Boca Raton, 1989.

1.9 Lund, W. *Fresenius J. Anal. Chem.* **1990**, 337, 557.

1.10 Preston, C.M. *Soil Sci.* **1996**, 161, 144.

1.11 Wilson, M.A. NMR Techniques and Applications in Geochemistry and Soil Chemistry; 1987, Pergamon Press, Oxford (and reference cited there in).

1.12 Wershaw, R.L.; Mikita, M.A. (eds.) NMR of Humic Substances and Coal: Techniques. Problems and Solutions; 1987, Lewis Publishers, Chelsea, MI.

1.13 Axelson, D.E. Solid State Nuclear Magnetic Resonance of Fossil Fuels; Multiscience Publications Ltd: Canadian Government Publishing Centre, Supply and Services Canada, 1985.

1.14 Fründ, R.; Lüdemann, H.-D. *Sci. Total Environ.* **1989**, 81/82, 157.

1.15 Kinchesh, P.; Powlson, D.S.; Randall, E.W. *Eur. J. Soil. Sci.* **1995**, 46, 125-138.

1.16 Jurkiewicz, A.; Maciel, G.E.; *Anal. Chem.* **1995**, 67, 2188.

1.17 Pan, V.H.; Maciel, G.E. *Fuel* **1993**, 72, 451.

1.18 Snape, C.E.; Axelson, D.E.; Botto, R.E.; Delpeich, J.J.; Tekely, P.; Gerstien, B.C.; Pruski, M.; Maciel, G.E.; Wilson, M.A. *Fuel* **1989**, 68, 547.

1.19 Preston, C.M.; Schnitzer, M. *Soil Sci. Soc. Am. J.* **1984**, 48, 305.

1.20 Preston, C.M.; Newman, R.H. *Geoderma*, **1995**, 68, 229.

1.21 Skjemstad, J.O.; Clarke, P.; Taylor, J.A.; Oades, J.M.; Newman, R.H. *Aust. J. Soil Res.* **1994**, 32, 1215.

1.22 Wilson, M.A.; Vassallo, A.M.; Perdue, E.M.; Reuter, J.H. *Anal. Chem.* **1987**, 59, 551.

1.23 Zhang, M.; Maciel, G.E. *Fuel* **1990**, 69, 557.

1.24 Schnitzer, M.; Preston, C.M. *Soil Sci. Soc. Am. J.* **1986**, 50, 326.

1.25 Sardashti, M.; Maciel, G.E. *J. Magn. Reson.* **1987**, 72, 467.

1.26 Zeigler, R.C.; Wind, R.A.; Maciel, G.E. *J. Magn. Reson.* **1988**, 79, 299.

1.27 Pruski, M.; dela Rosa, L.; Gerstein, B.C. *Energy Fuels*, 1990, 4, 160.

1.28 Metz, G.; Wu, X.; Smith, S.O. *J. Magn. Reson. Ser. A.* **1994**, 110, 219.

1.29 Buffle, J. Complexation Reactions in Aquatic Systems. An Analytical Approach; Ellis Harwood Ltd,: Chester, UK, 1988, Chapter 5.

1.30 Tessier, A.; Campbell, P.G.C.; Bisson, M. *Can. J. Earth Sci.* **1980**, 17, 90.

1.31 Shuman, M.S.; Collins, B.J.; Fitzgerald, P.J.; Olson, D.L. in Aquatic and Terrestrial Humic Materials: Christman, R.F.; Gjessing, E.T. (eds.); Ann Arbor Sci., Ann Arbor, Mich., 1983.

1.32 Olson, D.L.; Shuman, M.S. *Anal. Chem.* **1983**, 55, 1103.

1.33 Fraústo da Silva, J.J.R.; Williams, R.J.P. The Biological Chemistry of the Elements: The Inorganic Chemistry of Life; Oxford University Press, New York, 1991.

Chapter 2

A Retrospective of luminescence and NMR spectroscopy studies on humic material

The following section reviews the literature on the use of luminescence and NMR spectroscopy in the study of humic materials in a biased manner. The bias comes from the fact that only the literature pertinent to this study is covered, however there are some more comprehensive (general) reviews in the literature. For luminescence studies a good review is by Senesi,[2.1] while for NMR studies there are several good reviews.[2.2-2.6]

2.1 Luminescence

Coloured waters occur naturally throughout the world. It has long been known that natural waters are coloured and that this colour arises from organic constituents. The first systematic research on what substances caused the coloration of water was performed by Aschan on six Finnish lake and river waters in 1909.[2.7] One year later in 1910 Dienert found that there were luminescent materials present in natural waters and noted that the luminescence was lost on mild oxidation.[2.8] In the early to mid 1960s it was found by a number of workers that humic substances luminesce weakly when irradiated with light of the proper wavelength.[2.9-2.12] In the 1970s and early 1980s attempts were made to obtain structural information from luminescence excitation spectra of humic materials.[2.13-2.15] These attempts were not that successful due to the difficulty of assigning luminescence peaks. Also, in the early 1970s, the quenching of humic luminescence by metal ions was investigated. The first work was followed by several other studies.[2.16-2.20] In 1980 Saar and Weber reported a linear relationship between the amount of complexed Cu^{2+} and the

quenching of the fulvic acids luminescence.[2.21] This linear relationship was then further developed by Ryan and Weber to allow for the determination of complexing capacities and stability constants of fulvic acid.[2.22, 2.23] The fluorescence method was supported by selective ion electrode and model compound studies. The key assumption of Weber and co-workers' method, is that the remaining quenchable luminescence uniformly measures the remaining free ligand concentration. This assumption is highly questionable, since humic substances are mixtures and humic luminophores, Lo, may not be uniformly distributed so that quenching may not be simply proportional to the free ligand concentration as first pointed out by Underdown et. al..[2.24] The vindication of the method with simple molecules is not valid, since they only have one type of Lo while fulvic acid may have at least three.[2.25, 2.26] Moreover, when the binding site is not the Lo itself, some of the binding sites may be partially or fully shielded from the Lo. This will not be obvious for a simple model compound, but in macromolecular systems like those of humic substances this may very well upset Weber and co-workers' linear relationship. The Weber and co-workers' linear relationship has been questioned.[2.27-2.29] This has led to a debate in the literature.[2.30, 2.31] Nevertheless, the literature shows that the humic luminescence approach was (more than 100 citations to the Weber and co-workers' papers) and remains a popular method for attempting to measure the extent of cation binding by humic ligands.

Recently, a new luminescence technique has been used for the study of humic materials, the new technique is known as synchronous luminescence.[2.32, 2.33] It has been found that synchronous luminescence differentially samples the entire distribution of the fulvic acid macromolecular system more effectively, and thus gives spectra with better structure, than either conventional absorbance or emission luminescence spectroscopy.[2.32,

[2.33] It has been shown that the different peaks in humic material synchronous spectra respond differently to changes in pH and metal binding. [2.26,2.34].

In chapter 7 the subject of metal ion quenching of a fulvic acid's luminescence is revisited using emission, synchronous, and time resolved luminescence.

2.2 NMR

2.2.1 Techniques

The first NMR spectrum of a humic materials was published in 1963 by Barton and Schnitzer.[2.35] It was a very poorly resolved liquid state ^1H NMR spectrum obtained on a continuous wave (CW) NMR spectrometer in which no aromatic protons could be monitored. Similar results where obtained in 1968 by Schnitzer and Skinner.[2.36] At the time this was taken to reconfirm the idea that the aromatic moieties of humic materials are highly substituted. These early NMR results seemed to support the degradative and mass spectroscopic results. However Oka et. al.[2.37] and Lundemann[2.38] did observe aromatic hydrogens in poorly resolved spectra in 1969 and 1973, respectively. In 1977 Lentz et. al[2.39] obtained much improved spectra by applying FT techniques instead of CW techniques. One year later this was followed up by Wilson et. al[2.40] who combined FT and high field techniques (6.3 T) to produce even better spectra than those of Lentz et. al.,[2.39] and for the first time the aromatic signal had some resolution. Similar results were obtained by Hatcher et. al.[2.41] using techniques very similar to Wilson's. The results of Wilson et. al.[2.40] and Hatcher et. al.[2.41] demonstrated that spectra with considerable detail could be obtained for humic materials via NMR. Although ^1H NMR has been applied to

humic materials it has taken a back seat to ^{13}C NMR for reasons discussed in chapter 1, such as wider chemical shift range, narrower line widths, and it the carbon skeleton.

This first documented attempt at ^{13}C NMR on humic materials was by Schnitzer and Nyroud[2.42] in 1974. The attempt was on a methylated fulvic acid, but yielded a very poorly resolved spectrum with small but detectable peaks at 53 and 166 ppm, that were assigned to methoxy (-OCH_3) and aromatic carbons bonded to methoxy groups, respectively. However, in 1976 Vila et. al.[2.43] were more successful in obtaining ^{13}C NMR spectra of humic materials. Their data was obtained on two humic acids and a fulvic acid, and yielded spectra consisting of four groups of signals; 220-170 ppm (carboxylic acid groups), 160-100 ppm (aromatic groups), 70-50 ppm (carbon bonded to oxygen in alcohols, esters or sugars, and amino acid CH carbon), and 50-0 ppm (alkyl carbon). Similar findings were reported by Wilson et. al.[2.40] and Ruggiero et. al.[2.44] However, because of nuclear Overhauser enhancements (NOE) and relaxation effects quantification was very difficult, unless it was assumed that these effects were uniform or unimportant as Ogner[2.45] did. This quantification problem was first addressed by Newman et. al.[2.46] From this study it was found that Ogner's assumptions were correct if a delay of 5 or more seconds was allowed for full relaxation between acquisitions. Although one could obtain quantitative spectra with a delay of greater than 5 seconds, this was very time consuming as it can take in the order of 100 000 scans, i.e. 6 days or more, to obtain a spectrum with a good signal to noise ratio. Preston and Blackwell [2.47] showed that qualitative spectra could be obtained with short acquisition times, small pulse angles (the smaller the angle the shorter the delay between acquisitions, but also the less signal one obtains), short delays between acquisitions (about the length of the longest spin-lattice relaxation time [T_1])), and inverse gated decoupling (to remove NOE). However, the time needed to obtain a liquid state ^{13}C NMR spectrum with a good signal to noise ratio was about 3 days, rendering

relaxation and dynamical measurements very time consuming, and almost impossible if the investigator does not have a personal NMR spectrometer.

High resolution solid state ^{13}C NMR became a reality in the 1970s by means of the combination of MAS, CP and high power decoupling. In 1973 Pines et. al.[2.48] combined CP, which was first proposed by Hartmann and Hahn,[2.49] and high power dipolar decoupling to obtain high resolution ^{13}C NMR spectra in the solid state. The CP technique allows for an increase in signal to noise ratio by a theoretical factor of 4 for cross polarisation from ^{1}H to ^{13}C, for each scan. It also allows for the delay between scans to be reduced greatly (for humic material this delay is nearly always 1 second). The high power dipolar decoupling removes linebroadening due to dipole-dipole interactions (see section 3.2.5 for a detailed account). However, the spectra obtained by Pines, Gibby, and Waugh [2.48] still had rather broad lines. It had been shown independently by Lowe [2.50] and Andrews [2.51] that if the sample was spun at the magic angle (54.7 degrees) to the static magnetic field the chemical shift anisotropy (CSA) line broadening terms would reduce to the liquid case, i.e. narrow lines. If the sample could be spun fast enough this technique would also remove all dipolar-dipolar line broadening as well. Thus the reason the angle is called the magic angle. In 1974 Schaefer, Stejskal, and Buchdahl [2.52] reported on the first experiments in which MAS, CP, and high power dipolar decoupling were combined. The combination of these techniques is known as CP-MAS ^{13}C NMR, and demonstrated the almost synergetic relationship that exists between them in terms of resolution and signal enhancement. Their study was on solid glassy polymers and showed the potential of this method for the study of solids. In 1975 Schaefer and Stejskal [2.53] produced CP-MAS ^{13}C NMR spectra of a series of polymers that were of comparable resolution to liquid state ^{13}C NMR spectra, and ushered in modern high resolution solid state ^{13}C NMR. Within two years the CP-MAS ^{13}C NMR technique was discussed in terms of natural organic matter

and applied to coal by Bartuska, Maciel, Schaefer, and Stejkal.[2.54] The CP-MAS ^{13}C NMR was then applied to coals by Retkofsky and VanderHart and Maciel and co-workers [2.55, 2.56] in 1978 and 1979, respectively, and showed its great promise. Within two to three years CP-MAS was applied to humic material. The first work was carried out by Mikinis et. al. in 1979.[2.57] But, it was not until the work of Hatcher et. al.[2.58] in 1980 that CP-MAS ^{13}C NMR was applied to humics for the sole purpose of studying humic materials.[2.58] Also, in 1980 Barron et. al.[2.59] used CP-MAS ^{13}C NMR spectroscopy to study whole soils, and showed two of the major advantages of solid state NMR in studying natural organic matter (NOM) i.e. little to no sample preparation and little to no sample handling. In 1980 work by Newman et al.[2.46] presented CP-MAS ^{13}C NMR as one of, if not, the most promising NMR technique to study humic materials in their extracted and fractionated forms as well as in whole soils. In 1981 Barron and Wilson [2.60] showed that one could obtain higher resolution CP-MAS ^{13}C NMR spectra on higher field instruments (7 T). However, high spinning speeds were not available at the time, and thus CSA linebroadening was a problem. In 1984 the first paper in which two dimensional (2D) CP-MAS ^{13}C NMR was applied was published by Wilson,[2.61] which showed the power of CP-MAS ^{13}C NMR even further as these type of experiments. 2D ^{13}C NMR experiments on humic materials are almost impossible in the liquid state because of time constraints (2D experiments in the liquid state would take about 96 days, compared to about 5 days in the solid state). From this early work CP-MAS ^{13}C NMR spectroscopy has become one of the most important tools in the study of humic materials, and has fostered a quantum leap in the understanding of humic materials.

Although CP-MAS ^{13}C NMR is a very powerful technique, there have been many questions as to its quantitative reliability. These questions started to emerge as soon as the technique was introduced.[2.2, 2.3, 2.62-2.66] The majority of the questions were in terms of

the possible biases in CP. The biased nature of CP is inherent, since the more protons attached or close to the carbon being monitored the more favourable the CP process is. The first systematic investigation was carried out by Dudley and Fyfe in 1982 [2.67] on coals and related materials. This work was followed by the work of Sullivan and Maciel in the same year.[2.68] In both these works it was found that a contact time of 1 ms gave the most reliable qualitative CP-MAS ^{13}C NMR spectra, but all the CP-MAS parameters have to be checked for each sample. The quantitative reliability of the CP-MAS ^{13}C NMR technique when applied to humic materials was also investigated. The first work was by Preston and Ripmeester [2.69] in 1982. This work compared liquid ^{13}C NMR spectra and CP-MAS ^{13}C NMR spectra and found that only qualitative comparisons could be made. However, the samples they monitored where high in ash content, and hence had paramagnetic impurities which may have heavily affected the NMR measurements, as shown by the conflicting results obtained in the presence of paramagnetic impurities.[2.70, 2.71] However, a study by Schnitzer and Preston [2.72] in 1986 found that a contact time of 1 ms gave liquid like spectra for a series of humic materials. As mentioned above, paramagnetic impurities are of major concern when performing any type of NMR, especially CP-MAS ^{13}C NMR. It has been shown by Botto et. al.[2.73] for coals with a high concentration of stable free radicals and low H/C content, that only a fraction of the carbons are observed, and this fraction can be as low as 25%. However, it was found by Vassallo et. al.[2.74] that a low concentration of stable free radicals in humic materials does not make any of the carbons invisible (97% are visible via spin counting experiments). But, in the same work by Vassallo et. al.[2.74] and in previous work by Wilson [2.75] it was shown that humic materials must have a low content of inorganic paramagnetic centres (impurities) for all the carbons to be sampled correctly. In 1987 it was reported by Earl et. al.[2.76] that low temperature (-60°C) should be used to obtain the most reliable spectra. But, Hatcher and Wilson showed that this was not

necessary as long as the humic sample was not highly hydrated.[2.77] Under normal humic materials sample handling there is no hydration problem.

Another problem with the CP-MAS is that MAS interferes with CP. This was shown experimentally in 1977 by Stejskal, Schaefer and Waugh.[2.78] This interference was further investigated by Maciel and co-workers.[2.79, 2.80] It was found that sample spinning narrowed the frequency range over which good CP could take place by the narrowing of the Hartmann-Hahn match (see Chapter 3 for a more detailed account of this phenomenon). It was suggested by Maciel and co-workers that this problem could be overcome by mechanical manipulation of the spinning [2.81]. But, these approaches are complex, not commercially available, and not suitable for all types of samples due to the relatively long delays (0.5 - 5 s) involved. It was suggested by Zhang and Maciel to use Bloch-decay acquisition (without cross-polarisation) for samples high in carbon, and low in paramagnetic species, and/or large (2.5 cm^3) rotors.[2.82] However, currents can be produced in these large rotors which in turn cause magnetic field inhomogeneity problems.

In 1989 a seminal paper was published in which it was stated that the best and most quantitatively reliable CP-MAS ^{13}C NMR spectra can be obtained with low field instruments and slow spinning speeds.[2.83] From the discussion above the standard protocol for CP-MAS ^{13}C NMR on humic materials has become: spinning rate of 5 kHz or less (rotors and spinning systems capable of higher spinning speeds were not commercially available until recently, and were in fact only available in very few labs [approximately 5 to 10 laboratories in the world]); a contact time of 1 ms; a delay of 1 s; use of a low field instrument (2.3 T) if it is available; and use of single amplitude CP.

However, since 1989 MAS probes have become commercially available which allow spinning rates up to 20 kHz, and this has been coupled with the proliferation of high-field CP-MAS instruments with their greatly enhanced sensitivity. Concurrent with this,

modifications have been developed for the CP-MAS pulse sequence to alleviate the CP problems caused by high speed spinning. These pulse sequences can be grouped into the following categories: Hartmann-Hahn cross polarisation sequences with with the following modifications phase manipulation [2.84-2.88], frequency manipulation [2.89], or amplitude manipulation [2.90-2.95]; pulsed polarisation-transfer methods [2.96, 2.97]; or adiabatic polarisation-transfer methods [2.48, 2.98-2.101]. In principle, a method which uses transfer through an adiabatic demagnetisation-demagnetisation scheme in the rotating frame would be the method of choice, as this approach leads theoretically to the maximum achievable transfer of spin order.[2.102] However, in practice this approach has many limitations, as has been pointed out by Ernst and co-workers.[2.99, 2.100] As well, this approach is of extremely limited applicability to complex heterogeneous samples. The most promising pulse sequence for large macromolecules such as humic substances, is known as ramped amplitude CP (Ramp-CP).[2.94] With recent advances, it is appropriate to examine the effects of high fields and high MAS rates when used with Ramp-CP-MAS NMR for humic substances, as is discussed in chapter 5.

2.2.2 The Functionality and Structure of Humic Materials

The use of NMR on humic materials, quite simply put, turned the whole study of humic materials up-side-down. The reason for this is that from the first NMR studies, the importance of aliphatic and carbohydrate moieties became much more apparent. It also became obvious that aromatic moieties were not the highly dominant components they had been believed to be (mainly based on degradative studies). The degradative findings are based on less than a 1/3 carbon mass recovery, usually in the range of 5% or less. Because of this and other concerns, these studies have been questioned.[2.103, 2.104] NMR

spectroscopy is now considered the reference method for analysis of humic materials, but as discussed above it is not perfect and great care must be taken in carrying out the experiments and in the interpretation of the data.

As discussed above, the early ^{1}H NMR studies on humic materials by Schnitzer and co-workers showed no aromatic signal. These results were interpreted as indicating that aromatic rings must be highly substituted.[2.35, 2.36] Due to the poor quality of the spectra, little could be established. It seems that there may have been a belief that the poor quality spectra were interpreted as indicating that there where no other moieties in the sample other than fully functionalised aromatic rings (this is the only interpretation that can be made by this author). Further study showed that aromatic hydrogens could be detected by ^{1}H NMR for humic materials, as discussed above. This was then followed by ^{13}C NMR studies. In 1976 Vila et. al. obtained the first truly resolved ^{13}C NMR spectra of two humic acids and a fulvic acid in which some aromatic signal was found.[2.43] These findings where supported by more improved ^{13}C NMR work on humic materials in 1980 and 1981.[2.46, 2.58-2.60] From this work it was also found that humic acids were more aromatic in nature than fulvic acids, and that on the whole humic acids contained between 25% and 33% aromatic carbon. However, a ^{13}C NMR study by Hatcher, Schnitzer, Dennis, and Maciel in 1981 reported that some humic materials were found to be between 35% and 92% aromatic, with 6 out of the 10 tested being 50% or more aromatic in nature.[2.105] In the same year Hatcher, Maciel, and Dennis published another paper in which ^{13}C NMR results indicated that no humic acid had an aromatic content higher than 46%.[2.106] It is also interesting to note that one of the samples was the same in both studies (Armadale humic acid), and was tested under the same conditions. In the first study (ref. 2.105) this sample was reported to have 35% of its detectable carbons aromatic, while in the other study (ref. 2.106) it was found that only 25% of its detectable carbons were

aromatic. In 1985 a strong question was raised about results on humic materials which gave high aromatic content.[2.103] This led to a debate in the literature.[2.104, 2.107] In 1987 a comprehensive study was published in which it was concluded that humic materials were not highly aromatic, and that the notion that carboxyl groups in humic substances are always attached to aromatic rings is clearly inappropriate.[2.74] It is now well established that humic materials are not as highly aromatic as once believed, and that in some cases aromatic moieties may be a very small minority.

However, the role aromatic and carbohydrate moieties play in structure and, especially, functionality has not been well established. Apparently, no systematic NMR study of a fulvic acid and humic acid from the same source has been carried out (no published report could be found). In Chapter 6 a systematic study of LFA and LHA in terms of functionality and structure (structure in humic materials is an elaborated concept compared to classic chemistry and is more akin to the concept of structure in biochemistry) is reported.

2.2.3 Metal Binding Study

Only two references to humic material metal binding studies by NMR could be found. Neither of the two studies was systematic. In the work by Preston et. al. naturally bound copper produced the observed effect [2.108], and in the study by Pfeffer et. al. only one concentration of Fe(III) was added to a humic material from a sewage waste treatment plant.[2.109] In both studies it was found that it was the carbohydrate moiety signal which was affected by metal ions and not the aromatic moieties, in contrast to long held concept that it is the aromatic moieties which play a major role in metal binding.[2.108, 2.109]

In chapter 7 the first systematic NMR study of metal binding to humic material is presented. These results are then compared to the luminescence metal binding results also reported in chapter 7.

References

2.1 Senesi, N. *Anal. Chim. Acta* **1990**, 232, 77.

2.2 Wilson, M.A. *J. Soil Sci.* **1981**, 32, 167.

2.3 Wershaw, R.L.; Mikita, M.A. (eds.) NMR of Humic Substances and Coal: Techniques, Problems and Solutions; 1987, Lewis Publishers, Chelsea, MI.

2.4 Wilson, M.A. NMR Techniques and Applications in Geochemistry and Soil Chemistry; 1987, Pergamon Press, Oxford.

2.5 Fründ, R.; Guggenberger, G.; Haider, K.; Knicker, H.; Kögel-Knabner, I.; Lüdemann, H.-D.; Luster, J.; Zech, W.; Spiteller, M. Z. *Pflanzenernähr. Bodenk.* **1994**, 157, 175.

2.6 Preston, C.M. *Soil Sci.* **1996**, 161, 144.

2.7 Aschan, O. *J. Prakt. Chem.* **1909**, 77, 172.

2.8 Dienert, F. *Compt. Rend.* **1910**, 150, 487.

2.9 Black, A.P.; Christman, R.F. *J. Am. Water Works Assoc.* **1963**, 55, 753.

2.10 Seal, B.K.; Roy, K.B.; Mukherjee, S.K. *J. Indian Chem. Soc.* **1964**, 41, 212.

2.11 Kononova, M.M. Soil Organic Matter; Pergamon Press, Oxford, 1966, pp. 103-106.

2.12 Ghassemi, M. Christman, R.F. *Limnol. Oceanogr.* **1968**, 13, 583.

2.13 Datta, C.; Ghosh, K.; Mukherjee, S.K. *J. Indian Chem. Soc.* **1971**, 48, 279.

2.14 Ghosh, K.; Schnitzer, M. *Can. J. Soil Sci.* **1980**, 60, 373.

2.15 Ghosh, K.; Schnitzer, M. *Soil Sci.* **1980**, 129, 266.

2.16 Banerjee, S.K.; Mukherjee, S.K. *J. Indian Soc. Soil Sci.* **1972**, 20, 13.

2.17 Lévesque, M. *Soil Sci.* **1972**, 113, 346.

2.18 Cline, J.T.; Holland, J.F. in Biological Implications of Metals in the Environment: Proc. Fifteenth Hanford Life Sci Symp.; Richland, WA, 1975, Tech. Info. Ctr. Energy Res. Developement Admin., 1977.

2.19 Cline, J.T.; Holland, J.F. *ERDA Symp. Ser.* **1977**, 42, 264.

2.20 Schnitzer, M.; Ghosh, K. *Soil Sci. Soc. Am. J.* **1981**, 45, 25.

2.21 Saar, R.A.; Weber, J.H. *Anal. Chem.* **1980**, 52, 2095.

2.22 Ryan, D.K.; Weber, J.H. *Anal. Chem.* **1982**, 54, 986.

2.23 Ryan, D.K.; Weber, J.H. *Environ. Sci. Technol.* **1982**, 16, 866.

2.24 Underdown, A.W.; Langford, C.H.; Gamble, D.S. *Environ. Sci. Technol.* **1985**, 19, 132.

2.25 Power, J.F.; Lesgae, R.; Sharma, D.K.; Langford, C.H. *Environ. Technol. Lett.* **1986**, 7, 425.

2.26 Cook, R.L.; Langford, C.H. *Anal. Chem.* **1995**, 67, 174.

2.27 Fish, W.; Morel, F.M.M. *Can. J. Chem.* **1985**, 63, 1185.

2.28 Cabaniss, S.E.; Shuman, M.S. *Anal. Chem.* **1986**, 58, 398.

2.29 Cabaniss, S.E.; Shuman, M.S. *Anal. Chem.* **1988**, 60, 2418.

2.30 Ryan, D.K.; Ventry, L.S. *Anal. Chem.* **1990**, 62, 1523.

2.31 Cabaniss, S.E.; Shuman, M.S. *Anal Chem.* **1990**, 62, 1526.

2.32 Miano, T.M.; Sposito, G.; Martin, J.P. *Soil Sci. Soc. Am. J.* **1988**, 52, 1016.

2.33 Senesi, N.; Miano, T.M., Provenzano, M.R., Brunetti, G. *Sci. Total Environ.* **1989**, 81, 143.

2.34 Cabaniss, S.E. *Environ. Sci. Technol.* **1992**, 26, 1133.

2.35 Schnitzer, M.; Barton, D.H.R. *Nature* **1963**, 198, 217.

2.36 Schnitzer, M.; Skinner, S.I.M. Isotopes and Radiation in Soil Organic Matter Studies. Proceedings of the Second International Atomic Energy Agency. Vienna, 1968.

2.37 Oka, H.; Sasaki, M.; Itoh, M.; Suzuki, *A. Nenryo Koyokai-shi*, **1969**, 48, 295.

2.38 Ludemann, H.D. *Erdoel und Kohle, Ergas, Petrochemie vereinigt mit Brennstoff-Chemie*, **1973**, 26, 506.

2.39 Lentz, H.; Ludemann, H.D.; Ziechmann, W. *Geoderma*, **1977**, 18, 325.

2.40 Wilson, M.A.; Jones, A.J., Williamson, B. *Nature*, **1978**, 276, 487.

2.41 Hatcher, P.G.; Rowan, R.; Mattingly, M. *Org. Geochem.* **1980**, 2, 113.

2.42 Schnitzer, M.; Neyroud, J.A. *Can. J. Chem.* **1974**, 52, 4123.

2.43 Vila, F.J.; Lentz, H.; Ludemann, H.D. *Biochem. Biophys. Res. Comm.* **1976**, 72, 1063.

2.44 Ruggiero, P.; Interesse, F.S.; Sciacovelli, R. *Geochim. Cosmochim. Acta* **1979**, 44, 603.

2.45 Ogner, G; Gronneberg, T. *Geoderma* **1977**, 19, 237.

2.46 Newman, R.H.; Tate, K.R.; Barron P.F.; Wilson, M.A. *J. Soil Sci.* **1980**, 32, 623.

2.47 Preston, C.M.; Blackwell, B.A. *Soil Sci.* **1985**, 139, 88.

2.48 Pines, A.; Gibby, M.G.; Waugh, J.S. *J. Chem. Phys.* **1972**, 56, 1776

2.49 Hartmann, S.R.; Hahn, E.L. *Phys. Rev.* **1962**, 128, 2042.

2.50 Lowe, I.J. *Phys. Rev. Ltters* **1959**, 2, 285.

2.51 Andrews, E.R. *Progr. Nucl. Magn. Reson. Spectrosc.* **1971**, 8, 1.

2.52 Schaefer, J.; Stejskal, E.O.; Buchdahl, R. *Macromolecule* **1975**, 8, 291.

2.53 Schaefer, J.; Stejskal, E.O. *J. Am. Chem. Soc.* **1976**, 98, 1031.

2.54 Bartuska, V.J.; Maciel, G.E.; Schaefer, J.; Stejskal, E.O. *Fuel* **1977**, 56, 354.

2.55 Retkofsky, H.L.; VanderHart, D.L. *Fuel* **1978**, 57, 421.

2.56 Maciel, G.E.; Bartuska, V.J.; Miknis, F.P. *Fuel* **1979**, 58, 391.

2.57 Mikinis, F.P.; Maciel, G.E.; Bartuska, V.J. *Org. Geochem.* **1979**, 1, 169.

2.58 Hatcher, P.G.; Vanderhart, D.L.; Earl, W.L. *Org. Geochem.* **1980**, 2, 87.

2.59 Barron, P.F.; Wilson, M.A.; Stephens, J.F.; Cornell, B.A.; Tate, K.R. *Nature* **1980**, 286, 585.

2.60 Barron, P.F.; Wilson, M.A. *Nature* **1981**, 289, 275.

2.61 Wilson, M.A. *J. Soil Sci.* **1984**, 35, 209.

2.62 Alemany, L.B.; Grant, D.M.; Pugmire, R.J.; Alger, T.D.; Zilm, K.W. *J. Am. Chem. Soc.* **1983**, 105, 2133.

2.63 Alemany, L.B.; Grant, D.M.; Pugmire, R.J.; Alger, T.D.; Zilm, K.W. *J. Am. Chem. Soc.* **1983**, 105, 2142.

2.64 Axelson, D.E. Solid State Nuclear Magnetic Resonance of Fossil Fuels; Multiscience Publications Ltd: Canadian Government Publishing Centre, Supply and Services Canada, 1985.

2.65 Fründ, R.; Lüdemann, H.-D. *Sci. Total Environ.* **1989**, 81/82, 157.

2.66 Kinchesh, P.; Powlson, D.S.; Randall, E.W. *Eur. J. Soil. Sci.* **1995**, 46, 125.

2.67 Dudley, R.L.; Fyfe, C.A. *Fuel* **1982**, 61, 651.

2.68 Sullivan, M.J.; Maciel, G.E. *Anal. Chem.* **1982**, 54, 1615.

2.69 Preston, C.M.; Ripmeester, J.A. *Can. J. Spectrosc.* **1982**, 27, 99.

2.70 Worobey, B.L.; Webster, G.R.B. *Nature* **1981**, 292, 526.

2.71 Newman, R.H.; Tate, K.R. *J. Soil Sci.* **1984**, 35, 47.

2.72 Schnitzer, M.; Preston, C.M. *Soil Sci. Am. J.* **1986**, 50, 326.

2.73 Botto, R.E.; Wilson, R.; Winans, R.E. *Energy Fuels* **1987**, 1, 173.

2.74 Vassallo, A.M.; Wilson, M.A.; Collin, P.J.; Oades, J.M.; Waters, A.G.; Malcolm, R.L. *Anal. Chem.* **1987**, 59, 558.

2.75 Wilson, M.A.; Vassallo, A.M.; Perdue, E.M.; Reuter, J.H. *Anal. Chem.* **1987**, 59, 551.

2.76 Earl, W.L.; Wershaw, R.L.; Thorn, K.A. *J. Magn. Reson.* **1987**, 76, 264.

2.77 Hatcher, P.G.; Wilson, M.A. *Org. Geochem.* **1991**, 17, 293.

2.78 Stejskal, E.O.; Scaefer, J.; Waugh, J.S. *J. Magn. Reson.* **1977**, 28, 105.

2.79 Sardashi, M.; Maciel, G.E. *J. Magn. Reson.* **1987**, 72, 467.

2.80 Wind, R.A.; Dec, S.F.; Lock, H.; Maciel, G.E. *J. Magn. Reson.* **1988**, 79, 136.

2.81 Ziegler, R.C.; Wind, R.A.; Maciel, G.E. *J. Magn. Reson.* **1988**, 79, 299.

2.82 Zhang, M.; Maciel, G.E. *Fuel* **1990**, 69, 557.

2.83 Snape, C.E.; Axelson, D.E.; Botto, R.E.; Delpeich, J.J.; Tekely, P.; Gerstien, B.C.; Pruski, M.; Maciel, G.E.; Wilson, M.A. *Fuel* **1989**, 68, 547.

2.84 Levitt, M.H.; Suter, D.; Ernst, R.R. *J. Phys. Chem.* **1986**, 84, 4243.

2.85 Barbara, T.M.; Williams, E.H. *J. Magn. Reson.* **1992**, 99, 439.

2.86 Green, H.; Titman, J.J.; Spiess, H.W. *Chem. Phys. Letters* **1993**, 213, 145.

2.87 Wu, X; Zilm, K.W. *J. Magn. Reson. Ser. A* **1993**, 104, 154.

2.88 Lee, Y.K.; Helmle, M.; Johannessen, O.G.; Nielsen, N.C.; Levitt, M.H. *Chem. Phys. Letters* **1995**, 242, 304.

2.89 Kolbert, A.C.; Bielecki, A. *J. Magn. Reson. Ser. A* **1995**, 116, 29.

2.90 Hediger, S.; Meier, B.H.; Ernst, R.R. *Chem. Phys. Letters* **1993**, 213, 627.

2.91 Peersen, O.B.; Wu, X.; Kustanovich, I.; Smith, S.O. *J. Magn. Reson. Ser. A* **1993**, 104, 334.

2.92 Peersen, O.B.; Wu, X.; Smith, S.O. *J. Magn. Reson. Ser. A* **1994**, 106, 127.

2.93 Zhang, S. *J. Magn. Reson. Ser. A* **1994**, 110, 73.

2.94 Metz, G.; Wu, X.; Smith, S.O. *J. Magn. Reson. A* **1994**, 110, 219.

2.95 Zhang, S; Czekaj, C.L.; Ford, W.T. *J. Magn. Reson. A* **1994**, 111, 87.

2.96 Hing, A.W.; Vega, S.; Schaefer, J. *J. Magn. Reson.* **1992**, 96, 250.

2.97 Hing, A.W.; Vega, S.; Schaefer, J. *J. Magn. Reson. A* **1993**, 103, 151.

2.98 Anderson, A.G.; Hartmann, S.R. *Phys. Rev.* **1962**, 128, 2023.

2.99 Hediger, S.; Meier, B.H.; Kurur, N.D.; Bodenhausen, G.; Ernst, R.R. *Chem. Phys. Letters* **1994**, 223, 283.

2.100 Hediger, S.; Meier, B.H.; Ernst, R.R. *Chem. Phys. Letters* **1995**, 240, 449.

2.101 Hediger, S.; Signer, P.; Tomaselli, M.; Ernst, R.R.; Meier, B.H. *J. Magn. Reson.* **1997**, 125, 291.

2.102 Ernst, R.R.; Bodenhausen, G.; Wokaun, A. Principles of Nuclear Magnetic Resonance in One and Two Dimensions; Oxford University Press, New York, 1987, Chapter 4.

2.103 Framer, V.C.; Pisaniello, D.L. *Nature* **1985**, 313, 474.

2.104 Framer, V.C. *Nature* **1985**, 316, 658.

2.105 Hatcher, P.G.; Schnitzer, M.; Dennis, L.W.; Maciel, G.E. *Soil Sci. Soc. Am. J.* **1981**, 45, 1089.

2.106 Hatcher, P.G.; Maciel, G.E.; Dennis, L.W. *Org. Geochem.* **1981**, 3, 43.

2.107 Schnitzer, M. *Nature* **1985**, 316, 658.

2.108 Preston, C.M.; Dudley, R.L.; Fyfe, C.A.; Mathur, S.P. *Geoderma* **1984**, 33, 245.

2.109 Pfeffer, P.E.; Gerasimowicz, W.V.; Piotrowski, E.G. *Anal. Chem.* **1984**, 56, 734.

Chapter 3
Theory

The following section is aimed at giving readers the theoretical background they need to understand the remainder of the presented work. Basic NMR theory is not covered here there are many excellent monographs on the subject.[3.1-3.11] This chapter is a compilation of reference works and seminal papers pertinent to the presented work, there are also new insights as well. There are two sections. In section 3.1, Solid State NMR: the pertinent core solid state NMR theory is presented along with more advanced theory which allows the reader a deeper and fuller understanding of CP, MAS, and their interaction. This more advanced theory is needed to fully appreciate the CP-MAS NMR approach developed in Chapter 5 and applied in Chapters 6 and 7. The basic theory is mainly based on the following works 3.6, 3.7, 3.9, 3.10, 3.12, 3.13. For the more advanced theory references are given in the text. In section 3.2, Luminescence: basic luminescence theory is presented, as well as more advanced theory on synchronous luminescence spectroscopy and luminescence quenching. The basic luminescence theory is mainly based on the following works 3.14-3.19, for the more advanced theory references are given in the text.

The very basic theory has been covered in most undergraduate programs in chemistry. However, typically NMR and fluorescence receive little attention, especially as analytical tools. Yet, both techniques are important and very powerful tools in environmental science.[3.20-3.22] In addition, NMR is coming of age in the field of environmental chemistry as is indicated by a very recent monograph (1997) entitled "Nuclear Magnetic Resonance Spectroscopy In Environmental Chemistry".[3.23] Also, the

more NMR is used for environmental studies, the more its application in environmental studies will grow and expand.

3.1 Solid State NMR

NMR can be done in the gas, liquid, and solid state. However, due to its inherent insensitivity, NMR is not usually carried out in the gas phase, because of concentration limits. Based on this concentration argument it would seem that the best state to do NMR on is the solid state. In fact, the first true NMR publication by Purcell et. al.[3.24] was on the solid state, very quickly followed by Bloch et. al.[3.25] NMR work on the liquid state. It should be noted that the two groups independently developed their work and submitted for publication within a month. However, over time the liquid state proved to be much more conducive to NMR. There are two major reason for this. The first is that without special techniques the solid state gives very broad spectral linewidths compared to the linewidths obtained in the liquid state. Also, spin-lattice relaxation times (T_1s) in the solid state are very long in comparison to the T_1s in the liquid state, while the spin-spin relaxation times (T_2s) are very short. However, over the last two decades special techniques have been developed which have allowed solid state NMR to achieve high resolution. These techniques have opened new doors to material scientists and, more recently, environmental scientists. High resolution solid state and liquid state ^{13}C NMR have revolutionised the way in which we look at humic matter, as it allows one to look at functionality, molecular dynamics, metal binding, and other properties in an entirely new light. Solid state ^{13}C NMR is the dominant NMR method for interrogating humic matter, and it is also the reference method. In the discussion below the theory behind the techniques which allow

for high resolution solid state NMR are discussed with focus towards on very complex heterogeneous mixtures such as humic matter.

3.1.1 Line Broadening

Line broadening in the solid state occurs mainly because of dipolar-dipolar interactions and chemical shift anisotropy (CSA).

3.1.1.1 Dipolar-Dipolar Interactions

The reason the dipolar-dipolar interactions cause line broadening is that the Zeeman energy levels are shifted slightly by local fields around the nucleus caused by the neighbouring nuclei. These local fields will vary depending on the number of nuclei that have spin up or down. These variations in local fields cause variations in the Zeeman energy levels, and correspond to slight shifts in the NMR frequency. These slight shifts in NMR frequency are be random and cause line broadening.

The dipolar-dipolar interactions can be expressed mathematically as follows:

$$H_D' = \sum_{i<j} (h'^2/2)\gamma_i\gamma_j r_{ij}^{-3}(3\cos^2\theta_{ij} - 1)(\mathbf{I}_i \bullet \mathbf{I}_j - 3I_{iz}I_{jz}) \qquad (3.1.1)$$

In the liquid state $\cos^2\theta_{ij}$ is 1/3, because of random time averaging (see below). In the liquid state there is random motion and reorientation due to Brownian motion, thus the time-average value of $\cos^2\theta_{ij}$ will be:

$$\cos^2\theta_{ij} = (1/4\pi)\int_0^{4\pi}\cos^2\theta d\Omega$$

$$= (1/4\pi)\int_0^{2\pi} d\phi \int_0^{\pi}\cos\theta\sin\theta d\theta \qquad (3.1.2)$$

$$= 1/3.$$

Thus, $3\cos^2\theta_{ij} - 1$ time-averages to zero, due to the random and rapid molecular tumbling due to Brownian motion, and dipolar-dipolar broadening vanishes in the liquid state.

However, in the solid state this is not the case. For solids equation (3.1.1), in the time-averaged form, is;

$$H_D' = (h'^2/4)(3\cos^2\beta - 1)\sum_{i>j}\gamma_i\gamma_j r_{ij}^{-3}(3\cos^2\beta_{ij}' - 1)(\mathbf{I}_i \bullet \mathbf{I}_j - 3I_{iz}I_{jz}), \qquad (3.1.3)$$

where β is the angle between the macroscopic sample and the applied magnetic field, $\mathbf{B}_0$.

3.1.1.2 Chemical Shift Anisotropy

Before we can understand how chemical shift anisotropy (CSA) influences linebroadening, we must first explain CSA. CSA arises from a non spherical electron density distribution around the nuclei. For ^{13}C NMR it is particularly important for aromatic, carboxyl, and alkene moieties. If one now considers two aromatic rings, one with its plane normal to the external field and the other with its plane parallel to the magnetic field, the effect of the $\mathbf{B}_0$ field will be very different. Thus, the local field, $\mathbf{B}_{loc}$, will be different which means there will be an anisotropy in the chemical shift, i.e. CSA.

In liquids, because of rapid and random molecular tumbling CSA, linebroadening is not a problem. But, once again for solids this is not true. In solids different nuclear sites

will have, in general, different orientations with respect to $\mathbf{B}_0$. This means that here will be a distribution of local fields, hence a distribution of NMR frequencies, which leads to linebroadening. In solids the chemical shielding parameter, σ_{izz}, is;

$$\sigma_{izz} = (1/2)(\sin^2\beta)(\sigma_{i1} + \sigma_{i2} + \sigma_{i3}) + (1/2)(3\cos^2\beta - 1)\sum_p \sigma_{ip}\cos^2\chi_{ip}, \quad (3.1.4)$$

where β is the angle between $\mathbf{B}_0$ and the macroscopic sample (i.e. the rotor or sample holder), while χ is the angle between $\mathbf{B}_0$ and the principal axes (e.g. the planes of the aromatic rings) of the sample.

3.1.2 The Magic Angle and Magic Angle Spinning

Upon inspection of equations (3.1.3) and (3.1.4) it can be seen that by allowing $3\cos^2\beta - 1 = 0$, both equations reduce to the liquid form. Thus, by choosing $\beta = 54.7^\circ$, the two major line broadening mechanisms in solid state NMR are overcome. This angle is known as the "magic" angle for obvious reasons. In order to time-average the sample must be spun. Thus, by macroscopic sample rotation about an axis tilted at the magic angle to the static external field, $\mathbf{B}_0$, a liquid like condition is reached (note vector notation is dicontinued from here as it is not needed). This technique first proposed by Lowe and Andrews independently, and is known as magic angle spinning (MAS).[3.26, 3.27]

In practice MAS can actually also cause line broadening. The two most important causes of this effect for non rigid solids are discussed below. This discussion is abstracted from much more detailed works on the subject [3.28-3.31], to which the reader is referred for a full theoretical explanation.

3.1.2.1 Motional Modulation of the CH Coupling in a CP Experiment

Motional modulation can provide pathways for relaxation in a solid and thus cause line broadening. One such mechanism comes about by molecular motion at the frequency, ω_{1H}, which corresponds to the decoupling field strength, B_{1H}, where $\omega_{1H} = 2\pi\upsilon_{1H} = \gamma_H B_{1H}$. The ensuing transverse relaxation time, T_{2m}, contributes $(\pi T_{2m})^{-1}$ to the ^{13}C line width. If the proton irradiation is applied exactly on resonance, the sample spinning frequency (rate), $\omega_r = 2\pi\nu_r$, is much smaller than ω_{1H}, and the motions dominating T_{2m} occur at frequencies much smaller than the carbon Larmor frequency. The expression for the motional induced relaxation time is;

$$(T_{2m})^{-1} = 0.5 M_2^{CH} J_m(\omega_{1H}), \qquad (3.1.5)$$

where M_2^{CH} is the carbon-proton VanVleck second moment expressed in rad^2/sec^2 and $J_m(\omega_{1H})$ is the spectral density of motion at ω_{1H} given by $J_m(\omega) = \int g(\tau) \exp(i\omega\tau)\, d\tau$.

For motion that is isotropic with a single correlation time, τ_c, and an exponential auto correlation function $g(\tau)$, $J_m(\omega_{1H})$ is given by;

$$J_m(\omega_{1H}) = 2\tau_c(1 + \omega_{1H}^2\tau_c^2)^{-1}. \qquad (3.1.6)$$

Thus, in the slow motion regime, $\tau_c^2 >> (\omega_{1H})^{-2}$, so that $J_m(\omega_{1H}) \approx 2(\omega_{1H})^2$ and hence $T_{2m} \propto \omega_{1H}$. In fast motion regime $\tau_c^2 << (\omega_{1H})^{-2}$, thus $J_m(\omega_{1H}) \approx 2\tau_c$, hence T_{2m} is independent of ω_{1H}.

3.1.2.2 Motional Modulation of the Resonance Frequency Via Chemical Shift Anisotropy

A loss of phase coherence in the transverse ^{13}C magnetisation resulting from motional modulation of the resonance frequency via the ^{13}C CSA is the second mechanism for line broadening in ^{13}C spectra resulting from molecular motion.

When a sample is being spun at the magic angle, each ^{13}C resonance undergoes periodic changes in resonance frequency such that all of the mean resonance values are the same for chemically equivalent carbons over a rotational period, T_r. Hence, at $t = nT_r$, where n is a positive integer, there will be a macroscopic coherence in the transverse magnetisation. These periodic coherences are known as "spin echoes". For the understanding of line broadening due to the modulation of the CSA, it is essential to recognise that the mean frequency averaged over the T_r is uniform. If a molecule executes a reorientational jump at some point during a T_r interval a specific phase error will be induced at the next echo. The phase error, and consequently, the line broadening will depend on the geometries involved and on the relative time of the jump within the interval. These jumps are simple changes in spatial orientation which leave the isotropic chemical shifts unaffected, as opposed to jumps between conformational minima which do produce changes in the isotropic chemical shifts. Because of averaging over a collection of spins these individual phase errors appear as a decrease in the amplitude of the next echo, thus producing relaxation described by transverse relaxation time $T_{2\sigma}$ and linewidth $\Delta\upsilon_\sigma = (\pi T_{2\sigma})^{-1}$. The dephasing effects of a jump are not cumulative over subsequent intervals unless the mean frequency changes, as it might in conformational jumping.

In order to estimate linewidth contributions attributable to these reorientational jumps, a distinction is made between two limiting cases for which a single jump usually

causes either a large or a small random phase error at the time of the next echo. These two regimes are known as the "strong" and "weak" collision cases, respectively.

A single event usually produces a large phase error in the strong collision case when the two following conditions prevail, as shown by equations (3.1.7) and (3.1.9) below.

$$-\omega_r << \gamma B_0 \Delta\sigma \tag{3.1.7}$$

where $\Delta\sigma$ = root-mean-square instantaneous change in chemical shift due to the jump, and $\tau_c >> \omega^{-1}{}_r$, where τ_c = the mean time between jumps. When this is the case, $T_{2\sigma}$, the transverse ^{13}C relaxation time associated with the mechanism, is:

$$T_{2\sigma} \cong \tau_c. \tag{3.1.8}$$

In the weak collision case the $T_{2\sigma}$ must consist of weak events and the relaxation corresponds to the diffusional loss of phase coherence. If one or both of the following conditions prevail

$$-\omega_r >> \gamma B_0 \Delta\sigma \tag{3.1.9}$$

or

$$-\tau_c^{-1} >> \omega_r \geq \gamma B_0 \Delta\sigma, \tag{3.1.10}$$

then;

$$T_{2\sigma}^{-1} = (\gamma B_0 \Delta\sigma)^2 \tau_c (1 + \omega_r^2 \tau_c^2)^{-1}. \qquad (3.1.11)$$

The above equation can be simplified in terms of slow or fast motion of the molecule. In the case of slow molecular motion (fast sample spinning) $\tau_c^2 >> (\omega_r)^{-2}$, and $T_{2\sigma}^{-1}$ is proportional to $\omega_r^{-2}\tau_c^{-1}$; whereas for fast motion, $\tau_c^2 << (\omega_r)^{-2}$, and $T_{2\sigma}$ is proportional to τ_c. Since it is normally desired to choose as fast a sample spinning frequency as is needed to prevent spinning sideband interference it is usual for equation (3.2.9) to apply.

In the intermediate region where $\sqrt{2}\omega_r \tau_c \cong 1$, both coherent spatial averaging (which permits line narrowing in the strong collision limit) and incoherent averaging (which allows line narrowing in the weak collision limit) destructively interfere with one another resulting in broadened NMR lines.

The following two equations can be derived from the discussion above. For a diffusional model;

$$T_2^{-1} = 1/15\,\omega_0^2\sigma^2(1 + n^2/3)(\tau_c(1 + 4\omega_r^2\tau_c^2)^{-1} + 2\tau_c(1 + \omega_r^2\tau_c^2)^{-1}), \qquad (3.1.12)$$

and for an anisotropic diffusional model;

$$T_2^{-1} = 1/45\,\omega_0^2\sigma^2 n^2(\tau_c(1 + 4\omega_r^2\tau_c^2)^{-1} + 2\tau_c(1 + \omega_r^2\tau_c^2)^{-1}). \qquad (3.1.13)$$

Both of these equations suggest that at a sample spinning frequency, υ_r, of 0.25σ there should be substantial line narrowing.

3.1.3 Spinning Sidebands Due to CSA through MAS

The CSA interaction, in the time dependent form due to sample spinning, can be expressed as:[3.32]

$$H_C = \sum_i \sum_{p=1}^{3} I_{iz} B \sigma_{ip} [\cos^2\beta \cos^2\chi_{ip} + 2\cos\beta \sin\beta \cos\chi_{ip} \sin\chi_{ip} \cos(\omega_r t + \psi_{ip}) + \sin^2\beta \sin^2\chi_{ip} \cos^2(\omega_r t + \psi_{ip})] \quad (3.1.14)$$

From equation (3.1.14) it can be seen that the interaction is periodic with respect to the sample spinning frequency, $\omega_r / 2\pi = f_r$. It can be shown that this time-dependence gives rise to a series of echoes separated by a time interval of f_r^{-1}. These echoes arise because of a refocusing of the magnetisation due to the spinning of the sample. In the spectrum these echoes will appear as spinning sidebands separated from the central line at frequency intervals equal to the spinning frequency ω_r. Spinning sidebands will only appear if the CSA interaction exceeds the spinning frequency ω_r. Thus, as one spins the sample faster one not only spreads out the sidebands but also reduces the intensity of the sidebands.

3.1.4 Magic Angle Spinning Speed

From the discussion above it can be seen that there are many reason why one would wish to spin the sample as rapidly as possible. Due to physical reasons there is an upper limit to the speed at which one can continuously spin the sample. However, it must always be kept it mind that high sample spinning speeds are advantageous in terms of reducing line broadening and spinning sideband spectral distortions.

3.1.5 Dipolar Decoupling

In practice, MAS is used only to remove CSA line-broadening effects and the homonuclear dipolar-dipolar interactions of the sparse spins, *S* (in this work ^{13}C, however the discussion will stay general and use a generalised nucleus *S*). On the other hand, dipolar decoupling is used to remove line broadening due to heteronuclear and homonuclear dipolar-dipolar interactions of the abundant spins, *I* (in this work ^{1}H, however the discussion will stay general and use *I*). The reason for this is that the spinning speeds of approximately 80 kHz are needed to ensure that all line broadening due to dipolar-dipolar interactions are removed. To put this type of rotational speed and the forces it causes into perspective, consider a 10 mm outer diameter rotor. If one spins this rotor at 10 kHz one has gone supersonic and the rotor will experience a centripetal acceleration (force) of 2 million times that of gravity at the edge.

An alternative method of removing the abundant spin dipolar interaction is to operate on the spin part of the interaction rather than the spatial term. This approach is much more effective. The method is to modulate the orientation on the abundant spins with respect to B_0, by forcing the spins to change states at a very fast rate compared to the frequency of the *I*-*S* and *I*-*I* interactions, thus reducing H_D^I to zero. To accomplish this one must apply r.f. irradiation at the *I* spin frequency at sufficient amplitude to "decouple" the interactions. The power required to cause complete decoupling is on the order of 1 kW, and the technique is known as dipolar decoupling. For comparison, typical power levels used for scalar decoupling, decoupling *J*-couplings, is on the order of 1 to 3 W.

3.1.6 The Sensitivity Problem, Long ^{13}C T_1, and Cross Polarisation

The low sensitivity of NMR has always been a problem. This has been especially the case when one studies a nucleus that is scarce and has a low susceptibility value, for example ^{13}C. It would be very nice to transfer some of the signal from an abundant and highly susceptible (in NMR terms) nucleus, e.g. ^{1}H, to the scarce and low susceptiblity nuclei. This can be achieved by a technique known as cross polarisation (CP). For solids it is sufficient to use a thermodynamic treatment to understand the cross polarisation phenomena. However, for liquids a more detailed quantum mechanical treatment is in order. For our purposes a simplified thermodynamic model will be used. A full and detailed thermodynamical treatment has been given by Levitt et. al..[3.33] Also, the treatment given here uses the "graphical interface" developed by Marks and Vega.[3.34]

Cross polarisation can be achieved by many mechanisms of which the most widely used is via simultaneous spin locking of two species This technique is known as the Hartmann-Hahn method.[3.35] The Hartmann-Hahn method allows for cross polarisation in the rotating frame. For nuclear spin systems having two nuclear types, an abundant spin species, I, and a sparse spin species, S, the experiment can be achieved by the pulse sequence shown Figure 3.5a. Preceding the 90°_y pulse, thermal equilibration in a large static magnetic field B_0 has taken place. The first step is to create a large polarisation of the abundant spins, I, along the rotating frame field via a 90°_y pulse. The 90°_y pulse is immediately followed by applying two simultaneous strong radio frequency, r.f., fields B_{1I} and B_{1S} at the I and S Larmor frequencies, respectively, for a period of time, commonly called the contact time.

The spin locking procedure of the I spin system causes the magnetisation to precess about B_{eff} in the rotating frame, and the magnetisation will decay with a time constant $T_{1\rho}$.

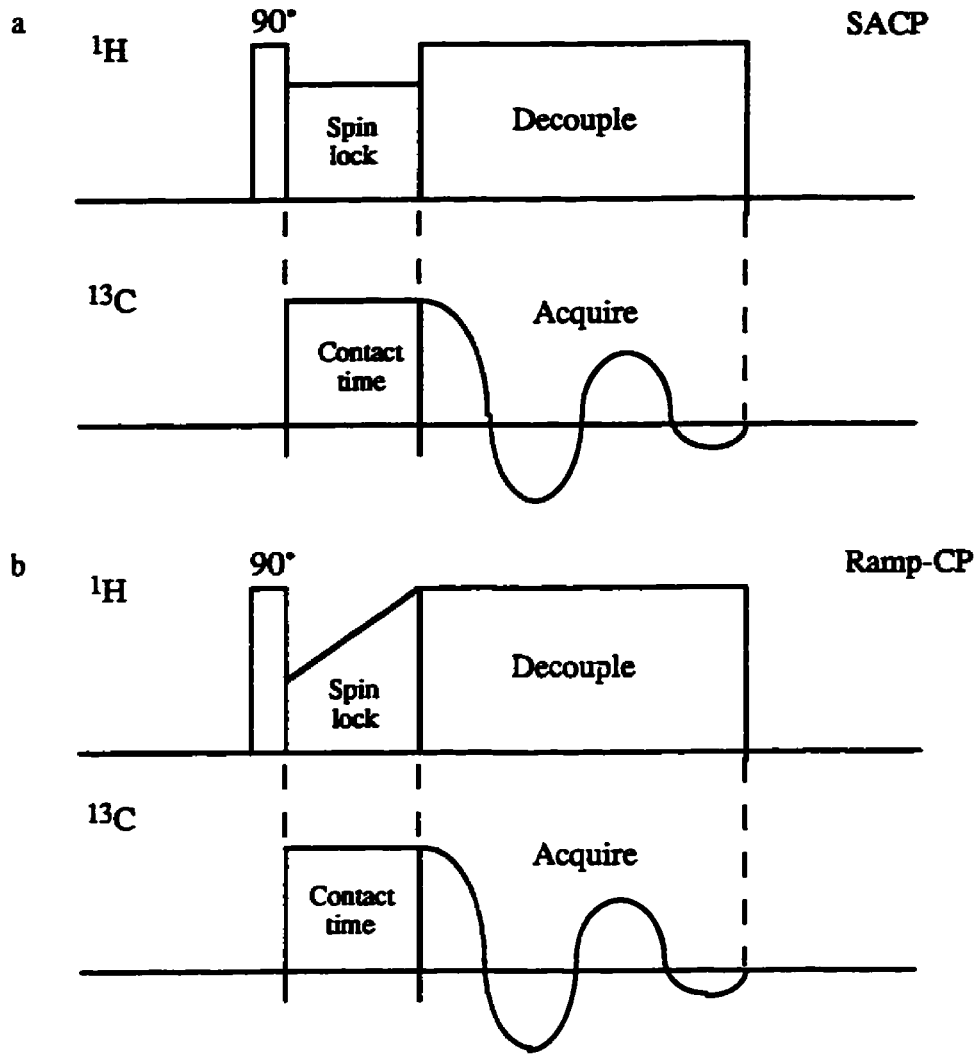

Figure 3.1: a) Single amplitude CP and b) Ramp-CP pulse sequences.

It should be noted that the spin temperature of the abundant spins is now very low. The reason for this can be shown by considering what we have just done to the proportion of spins in the lower energy state. Under normal conditions this is;

$$N_{-\frac{1}{2}} / N_{+\frac{1}{2}} = \exp(-h'\gamma_I B_0 / kT_L), \qquad (3.1.15)$$

where T_L is the temperature of the lattice. But, under the spin lock state in the rotating frame equation (3.2.15) becomes ;

$$N_{-\frac{1}{2}} / N_{+\frac{1}{2}} = \exp(-h'\gamma_I B_{\text{eff}} / kT_S), \tag{3.1.16}$$

where T_S is the spin temperature. From equations (3.1.15) and (3.1.16) the following relationship can be derived:

$$B_0 / B_{\text{eff}} = T_L / T_S. \tag{3.1.17}$$

Because $B_0 >> B_{\text{eff}}$, which means that $T_L >> T_S$, we have induced a large magnetisation of the I spin system via spin locking on the *y*-axis in the rotating frame.

At the same time the *I* spin system is spin locked the *S* spin system is subjected to r.f. irradiation at its own resonance frequency in the external magnetic field, B_0:

$$\omega_0 = \gamma_S B_0. \tag{3.1.18}$$

Since the r.f. irradiation is continuous, the r.f. field it produces is constant so that in the rotational frame the *S* spins precess about B_{1S} with the following angular frequency;

$$\omega_{1S} = \gamma_S B_{1S}. \tag{3.1.19}$$

Similarly:

$$\omega_{1I} = \gamma_I B_{1I}. \qquad (3.1.20)$$

A double resonance probe is needed to spin lock both the S and I spin systems at the same time as discussed above.

From the above discussion it should be noted that, in the rotating frame, both the S spin and I spin magnetisation have a component along the z-axis. Under the right condition this allows communication between the two spin systems via the Zeeman energy levels. When the Zeeman levels are approximately matched the spin systems can exchange energy via the coupling produced by the I-S dipolar interaction. The rate at which energy is exchanged, i.e cross polarisation, is strongly dependent on the magnitudes of B_{1I} and B_{1S}, and reaches a maximum when the Hartmann-Hahn condition is fulfilled:

$$\gamma_I B_{1I} = \gamma_S B_{1S} \qquad (3.1.21)$$

This condition is known as the Hartmann-Hahn match, HH, and assures that the nutation frequencies of the two nuclear species, ω_{1I} and ω_{1S}, in their respective rotating frames are equal. This allows for the maximum interaction and thus the maximum exchange (where I the abundant nuclear spin species is in most cases the protons, and S the sparse nuclear spin species, is commonly ^{13}C). Each type of $I_N S$ system, where N is the number of Is associated with an S in terms of CP, will have its own distinct HH, but this is not a problem in most cases due to the broadness of the HH profile (see below).

In terms of spin temperature, there is a thermal contact between the two spin systems at the HH. This thermal contact between the two systems will lead to a warming of the I system (very slight though because of the systems large heat capacity and the large size of the reservoir). At the same time, there will be a considerable cooling of the S

system, manifested as a significant decrease in the spin temperature of the sparse spin system down to;

$$T_S^{cp} = T_I = (B_{1I} / B_0)T_L = (\gamma_S / \gamma_I)(B_{1S} / B_0)T_L, \qquad (3.1.22)$$

based on equations (3.1.17) and (3.1.21). The cooling of the S spins results in a large increase in the polarisation (the population difference between the two energy levels), and thus a large increase in the observable signal intensity. In other words, we have sensitivity enhancement by CP. The energy transferred by this process is then transferred to the lattice by the I spin-lattice relaxation processes at a rate of T_1I (for this work $T_1{}^1$H).

From equation (3.1.21) or (3.1.22) it can be shown that the maximum theoretical sensitivity enhancement provided by cross polarisation is γ_I/γ_S. For ^{1}H to ^{13}C cross polarisation this enhancement factor is 4. Also, because the cross polarisation repetition rate is based on the proton spin-lattice relaxation rate (which is 2 or 3 orders of magnitude shorter than the carbon-13 spin-lattice relaxation, $T_1{}^{13}$C, an extreme example of $T_1{}^{13}$C is the crystalline component of polyethylene where the $T_1{}^1$H is about 1 second, while the $T_1{}^{13}$C is about 5200 seconds!), it may be much higher. Since the signal-to-noise ratio is proportional to the square root of the number of scans, increasing the number of spectra averaged leads to a large sensitivity enhancement for a set collection time.

The system that we are considering consists of two nuclear spins species, I and S. Because the S spins are sparse, S-S interactions can be ignored. In addition, the system can be considered as a set of subsystems, each consisting of a large number of I spins and a single S spin. The spin Hamiltonian for this type of system, in the double rotating frame, can be written as follows (after the usual high-field truncations):[3.33]

$$H = H_I + H_S + H_{IS} + H_{II}. \tag{3.1.23}$$

The H_{IS} Hamiltonian represents the heteronuclear dipolar interactions, and the H_{II} Hamiltonian represents the homonuclear dipolar interactions.

The HH can also be shown graphically, as in Figure 3.2. In Figure 3.2 there are two coupled spin manifolds |Mα> and |M+1β>. It can be shown that when there is a full energy overlap of the two manifolds the HH condition is satisfied:[3.34]

$$E_{\alpha}^{M} = E_{\beta}^{M+1} \tag{3.1.24}$$

which leads to;

$$-M\omega_{1I} - \frac{1}{2}\omega_{1S} = -(M+1)\omega_{1I} + \frac{1}{2}\omega_{1S}, \tag{3.1.25}$$

and thus:

$$\omega_{1I} = \omega_{1S}. \tag{3.1.26}$$

The heteronuclear dipolar interaction governs the coupling between the manifolds. Thus, the stronger the heteronuclear dipolar interaction the stronger the coupling between the manifolds, $|\bar{b}|$. The larger the number of *I*s connected or in close proximity to the *S* in question, the stronger the heteronuclear dipolar interactions. Hence, the stronger the coupling between the manifolds. The energy spread of the manifolds, $|\bar{a}|$, is determined by the homonuclear dipolar interactions. Only the proton homonuclear dipolar interaction need to be considered. This means that the weaker the homonuclear dipolar interactions, the narrower the energy spread of the manifolds. Figure 3.2 shows two cases, in Figure 3.2

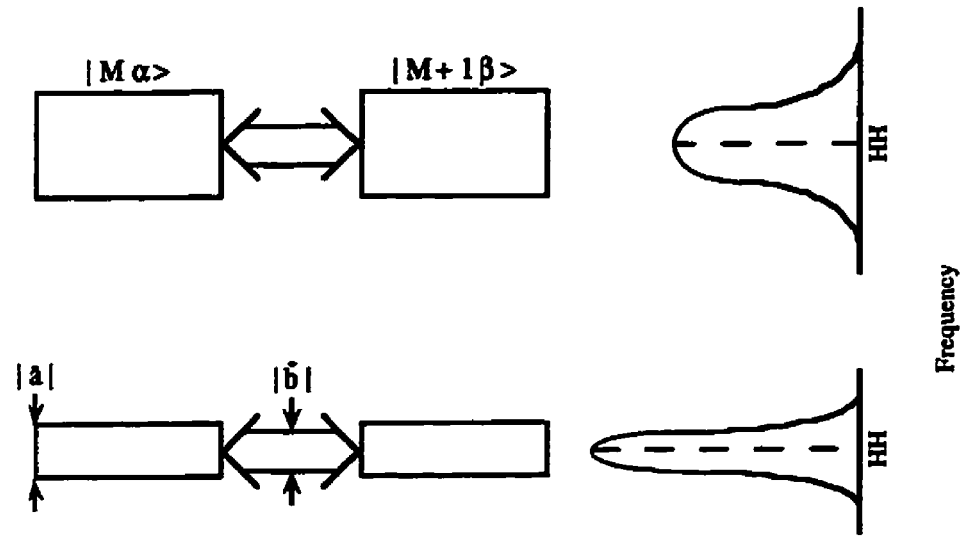

Figure 3.2: The energy overlap of the coupled |Mα> and |M+1β> manifolds at the HH. The HH profile is shown to the right as a vertical projection (see text for further details).

(top) the homonuclear dipolar interactions are strong, while in Figure 3.2 (bottom) the homonulear dipolar interactions are weak. It can be seen that the stronger the homonuclear dipolar interaction, the larger the energy overlap and the broader the HH. It has been shown that the S spin polarisation efficiency falls off from the HH on both the higher and lower r.f. field strengths of ω_{1S} as a Lorentzian function.[3.33] Thus, a relationship can be identified between the width of the HH and the homonuclear dipolar interactions. This relationship is a modification a formula already introduced by Levitt et. al.[3.33]

$$\lambda^2 = \frac{1}{4} f(H_{II}) M_2^I N, \qquad (3.1.27)$$

where λ is the width at half-height of a Lorentzian function, M_2^I is the second moment of the I spin resonance line, N is the number of I spins involved, and $f(H_{II})$ is a function of

the homonuclear dipolar interactions. This Lorentzian function is known as a HH profile, and is shown in Figure 3.2, on the vertical axis. The narrower the HH profile, the more important it is to have an exact HH.

From the above discussion it can be seen that for highly protonated carbons in a rich proton environment (e.g. aliphatic carbons) an exact HH is less important than for sparsely protonated carbons in a proton poor environment (e.g. carboxylic carbons). Thus, the HH condition is much more stringent for carboxyl type carbons in comparison to aliphatic type carbons.

3.1.7 Cross Polarisation and Sample Spinning

Up to this point, the sample considered in the cross polarisation discussion has been static. However, in the majority of solid state experiments, magic angle spinning (MAS) of the sample is used. In MAS macroscopic sample rotation about an axis tilted at the magic angle ($arc\ \cos(1/\sqrt{3}) = 54.7^{\circ}$) to the static field is used. This macroscopic rotation averages the inhomogeneous anisotropic interaction. Spinning sidebands appear if the magnitude of the interaction exceeds the spinning rate ω_r. The closer ω_r is to the magnitude of these interaction the smaller the spinning sidebands. These spinning sidebands are separated by ω_r. Thus, to eliminate sidebands from the spectra, one would wish to spin the sample at very high speeds.

Sample spinning also interferes with CP.[3.36-3.39] To understand this one must consider first how sample spinning affects the spin manifolds. For simplicity we will concentrate only on the $|M\alpha\rangle$ manifold, but the same effects occur in the $|M+1\beta\rangle$ manifold. With spinning, the $|M\alpha\rangle$ manifold becomes a set of $|M\alpha n\rangle$ manifolds. The $|M\alpha n\rangle$ manifolds are a series of states $|M\alpha n+k\rangle$, where the states are separated by ω_r. In

other words, sample spinning splits a narrow continuum into a series of states. Figure 3.3 represents this graphically. As the spinning rate increases so does the separation between these states. Also, as the spinning rate increases the magnitude of $|\bar{a}_{eff}|$ (the energy spread of the manifolds under the influence of sample spinning) decreases, due to a weakening of the homonuclear dipolar interaction. Hence, the faster the sample is spun the smaller the energy spread of the manifold.

For CP to take place, one of the |Mαn> states has to be coupled to one of the |M+1βn> states, as is shown in Figure 3.4. This coupling of manifolds can also be expressed in terms of an HH profile, as is shown on the right of Figure 3.4. The most effective couplings are the 1 and -1 couplings, followed by the 2 and -2 couplings, while the 0 coupling is weaker. All other sidebands are weaker still. Thus, the faster one spins the sample, the smaller the energy spread of each of the |Mαn> and |M+1βn> states and the

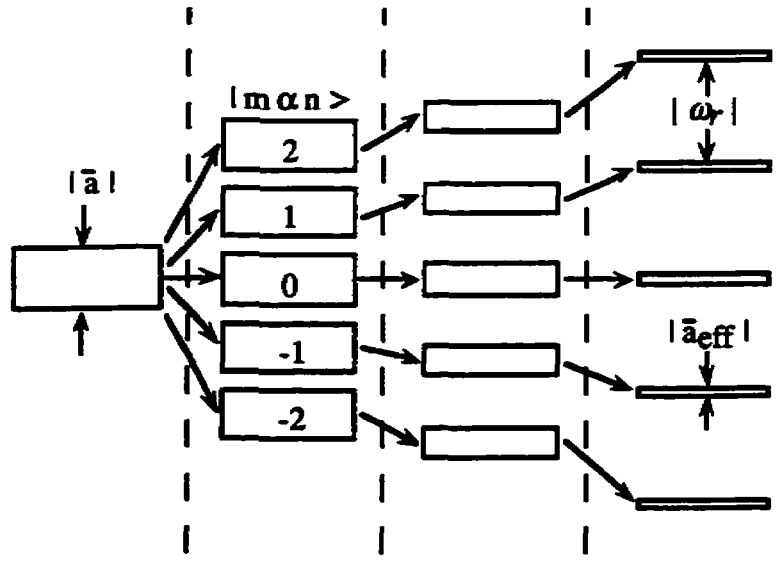

Figure 3.3: The effect of sample spinning on the energy spread manifolds (see text for further explanation).

lower the probability of these states overlapping. This in turn means that the higher the sample spinning rate, the narrower are the matching sidebands in the HH profile. In experimental terms this means that the faster one spins the sample, the more precise the condition needed for a HH.

The heteronuclear dipolar interactions are also affected by sample spinning. This effect was first pointed out by Stejskal et. al.[3.36] and is a series of sidebands analogous to the matching sidebands in the HH profile. However, the sidebands are a function of CP rate, and CP is the fastest at the sideband's maximum. The weaker the coupling, the longer the mixing time (CP pulse contact time) needed for polarisation equilibrium. Thus, the fastest polarisation transfer takes place on the -1 and 1 sidebands, followed by the -2 and 2 sidebands, and finally the central band (higher sidebands are not considered). If a long enough contact time is allowed for CP on the centre band, the same amount of polarisation will be transferred as the -1 sideband (if relaxation is neglected).[3.34] However, if the CP

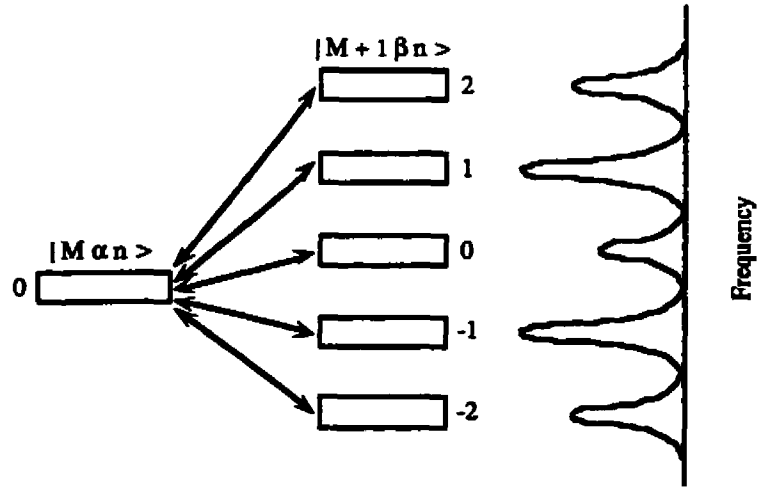

Figure 3.4: The coupling of the one of the |Mαn> states to the -2, -1, 0, 1, and 2 |M+1βn> states (see text for further explanation).

contact time is too long, then the S magnetisation will be lost due to the relaxation of the I spins. Thus there is an optimum CP contact time, T_{SI}. This is because of the interplay between CP rate and the I spin-lattice relaxation in the rotating frame, characterised by a relaxation time of $T_{1\rho}I$. This interplay can be expressed by the expression:[3.40, 3.41]

$$M(t) = M_0\Gamma(1-\exp\{\frac{-\Gamma t_{ct}}{T_{SI}}\})\exp\{\frac{-t_{ct}}{T_{1\rho}I}\} \qquad (3.1.28)$$

where;

$$\Gamma = 1+\frac{T_{SI}}{T_{1\rho}S}-\frac{T_{SI}}{T_{1\rho}I} \approx 1-\frac{T_{SI}}{T_{1\rho}I}. \qquad (3.1.29)$$

$M(t)$ is the resulting time-dependent S magnetisation, M_0 is the maximum equilibrium magnetisation of the S system in contact with the I system in the absence of relaxation processes, t_{ct} is the cross polarisation contact time, and $T_{1\rho}S$ is the S rotating frame relaxation time.

From equation (3.1.28) it can be seen that for a mixture of different I_NS systems there will be an optimum contact time in which the interplay between T_{SI} and $T_{1\rho}I$ produces a spectrum that is the closest to the real spectrum.

3.1.8 Samples with multiple HHs

So far it has been demonstrated that the faster the sample is spun the narrower the HH profile, and hence the more precise the HH condition, $\omega_{1I} = \omega_{1S}$, must be. In terms of experimental reality, if the sample is not being spun at all or is spun slowly, the HH condition can be represented by $\omega_{1I} \approx \omega_{1S}$. The reason for this approximation is the width

of the matching sidebands in the HH profile. However, when one spins the sample at a high rate, the matching sidebands in the HH profile become narrower. The weaker the homonuclear dipolar interactions, the narrower the matching sidebands in the HH profile become. Thus, for groups with weak homonuclear dipolar interactions at high sample spinning speeds the HH condition becomes $\omega_{1I} = \omega_{1S}$ rigorously. Experimentally, this means that there may be multiple HHs for complex heterogeneous samples such as humic materials. For this type of sample the classic single amplitude cross polarisation (SACP) method, shown in Figure 3.1a, will bias CP for some I_NS subsystems, and possibly fail to allow for CP altogether. This bias will be most noticeable as a loss of signal intensity for I_NS subsystems with weak homonuclear dipolar interaction such as carboxylic groups in fulvic acids.

3.1.9 Ramp-CP and Multiple HHs

In order to satisfy multiple HHs so that unbiased CP can take place, one of two approaches can be adopted. The first approach is to broaden out the matching sidebands. Although this may sound simple, it is difficult to do correctly and requires some knowledge of the sample's HH profile. The second approach is to try to achieve matching of all the HHs. At first this may sound extremely difficult, yet it has been made feasible via the ingenious ramped amplitude cross polarisation (Ramp-CP) method proposed by Metz, Wu and Smith.[3.42] This is a modification of variable amplitude CP, and is shown in Figure 3.1b. Standard SACP, shown in Figure 3.1a, allows for only one HH to be satisfied for the duration of the contact time (the duration of the spin lock condition [CP]), as the spin lock condition is maintained on both channels for the entire contact time. On the other hand, in Ramp-CP, only one spin lock is maintained at a fixed magnitude, while the

amplitude of the other spin lock is ramped. In Figure 3.1b the ramp is applied on the *I* channel, but it can as easily be applied to the *S* channel. The same results are obtained no matter on which channel the ramp is placed,[3.42] or whether the ramp is ascending or descending. To understand why this is so is to understand what the ramp is doing.

In simplest terms, the ramp is applied to only one of the channels, while the amplitude of the other channel is set so that at the centre of the ramp the spin lock is exactly HHed to the non ramped channel for a reference nucleus, such as the ketonic carbon in glycine. Another way of expressing this is that the ramp, when applied on the *I* channel causes $\omega_{1I} < \omega_{1S} > \omega_{1I}$, where at the centre of the ramp $\omega_{1I} = \omega_{1S}$, to the reference nucleus. Thus, whether the ramp is applied to the *I* or the *S* channel the range of frequency over which the spin-lock condition is varied in search of an exact HH is the same.

It should be noted at this point that amplitude and frequency can be a linear function of one another if the amplifier is linear (see Appendix A). Hence, the importance of applying the ramp on the channel with the most linear response in terms of amplitude and frequency. Thus, by ramping the amplitude on a linear amplifier we are also ramping the frequency.

The faster the sample is spun, the narrower the matching sidebands become. For SACP, if one is slightly off the centre of the matching sideband, this error will show up more and more the faster the sample is spun. This is especially the case if there are weak homonuclear dipolar interactions, when even the slightest mismatch can cause a substantial decrease in the CP efficiency. This, in turn, leads to the loss of signal. This is not the case for Ramp-CP since the ramp covers a range of spin-lock frequencies, and will hit on the one corresponding to the HH for each nucleus. Thus, Ramp-CP overcomes the burdensome, if not impossible, task of finding, setting, and maintaining an exact HH, which is necessary when spinning the sample at high speeds.

Moreover, and of special interest here, if the sample has multiple HHs then SACP fails. At low sample spinning speeds this is not a serious problem due to the broadness of matching sidebands, as can be seen in Figure 3.5 (left). Even at high spinning speeds, one would expect that where there are strong homonuclear dipolar interactions the sidebands will still be broad enough to limit the impact of a slight Hartmann-Hahn mismatch. However, if there are weak homonuclear dipolar interactions, and the sample is being spun at a high spinning speed, SACP will lead to very poor CP, as can be seen in Figure 3.5 (right). This in turn will lead to distorted spectra. Ramp-CP overcomes this by sweeping the spin-lock conditions of one of the channels. Hence, it can satisfy multiple HHs, as seen in Figure 3.5 (right). Thus, Ramp-CP is very likely to give better-resolved spectra and a more accurate depiction of all *S*s in a sample than the classic SACP method of CP.

Ramp-CP also overcomes the motional modulation of the CH coupling caused by spinning the sample at a high rate, by changing one of the spin-lock conditions to compensate for the spinning effect.[3.43]

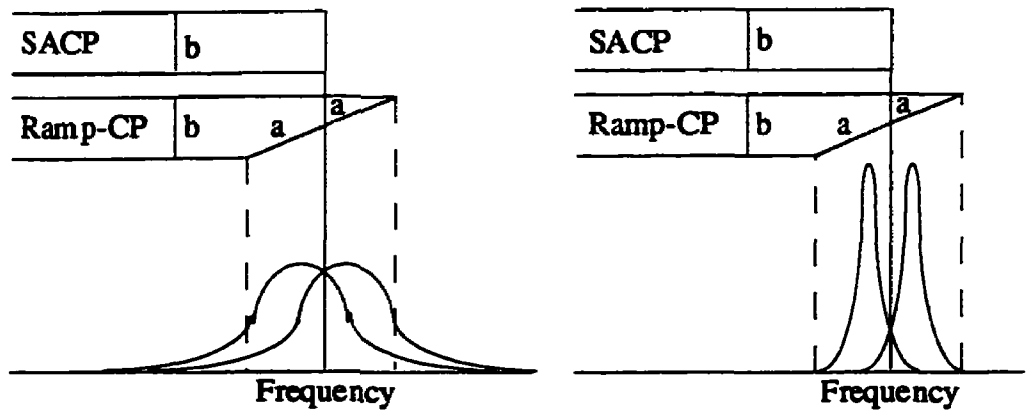

Figure 3.5: A comparison of SACP and Ramp-CP for a sample in which there are two subsystems, each having its own HH. Slow spinning rate and broad HH profiles (left) and high spinning rate and narrow HH profiles (right). See text for further explanation.

3.1.10 Other Advantages of Ramp-CP

Ramp-CP will compensate for inhomogeneous B_1 fields.[3.44] It has been suggested that Ramp-CP may also take place via quasi-adiabatic CP.[3.45] But, to date, there has been no clear evidence that the signal enhancement of Ramp-CP is not solely due to the compensation of B_1 field inhomogeneities. Also, the quasi-adiabatic interpretation has been questioned.[3.46]

3.1.11 NMR Spectra Line Widths and Relaxation Rates

There is a direct inverse relationship between T_2 and line width, as given by equation (3.1.30):

$$T_2 = \frac{1}{\pi \Delta \upsilon_{1/2}}, \tag{3.1.30}$$

where $\Delta\upsilon_{1/2}$ (measured in Hz) is the spectral line width at half-peak height. T_1 is also related to spectral line widths by molecular motions that cause noise. The effect of induced transition between energy levels to restore the thermal equilibrium (as discussed above) contribute to the spin lattice relaxation rate $1/T_1$. The lifetimes of the energy states are reduced by these transitions which leads to a loss of phase coherence between the precessing spins. Because the lifetime of an excited state is reduced by relaxation processes, the uncertainty in measuring the energy is increased by ($\Delta E \bullet \Delta t \sim h$) leading to spectral line broadening in accordance to Heisenberg's Uncertainty Principle. Thus, any process which increase spin-lattice relaxation rate ($1/T_1$) increases line broadening and T_2

relaxation. Thus an increase in spin-lattice or spin-spin relaxation rates ($1/T_1$ or $1/T_2$) alleviate saturation, but cause line broadening.

3.1.12 Paramagnetic Relaxation, Line Broadening, and Spectral Simplification

It is known that paramagnetic ions cause an increase in relaxation rates for both the spin-lattice and spin-spin modes. This is due to the magnetic moments of unpaired electrons being ca. 10^3 times greater than those of the nuclear magnetic moments, which causes them to generate much greater local fields. The fluctuations in these local fields lead to enhanced relaxation and the larger fields resulting from the presence of paramagnetic species give more efficient nuclear relaxation.

The relaxation times of nuclei near paramagnetic sites can be represented by the Solomon-Bloembergen equations [3.47, 3.48]. Assuming that the electronic Larmor precession frequency (ω_e) is much greater than the nuclear Larmor precession frequency (ω_n), they are:

$$\frac{1}{T_2}=\frac{2}{15}\frac{\gamma^2 g^2 S(S+1)\beta_N^2}{r^6}\left(\frac{3\tau_{cn}}{1+\omega_n^2\tau_{cn}^2}+\frac{7\tau_{cn}}{1+\omega_e^2\tau_{cn}^2}\right)+\frac{2}{3}S(S+1)\left(\frac{A}{h'}\right)^2\left(\frac{3\tau_{sc}}{1+\omega_e^2\tau_{sc}^2}\right), \tag{3.1.30}$$

and

$$\frac{1}{T_2}=\frac{1}{15}\frac{\gamma^2 g^2 S(S+1)\beta_N^2}{r^6}\left(4\tau_{cn}+\frac{3\tau_{cn}}{1+\omega_n^2\tau_{cn}^2}+\frac{13\tau_{cn}}{1+\omega_e^2\tau_{cn}^2}\right)+\frac{1}{3}S(S+1)\left(\frac{A}{h'}\right)^2\left(\frac{3\tau_{sc}}{1+\omega_e^2\tau_{sc}^2}+1\right. \tag{3.1.31}$$

The first term in both equations comes about because of dipole-dipole interactions between the electrons, *e*, and the nuclear spin, *n*, which is characterised by a correlation time τ_{cn}. The second term in both equations arises due to the modulation of the scalar interactions characterised by a correlation time of τ_{sc}. $\frac{A}{h'}$ is the electron-nuclear hyperfine coupling constant in Hz, γ is the magnetogyric ratio of the nucleus being monitored, β_N^2 is the Bohr magneton, *S* is the total electron spin, and *r* is the distance between the nucleus and the paramagnetic ion. τ_{cn} and τ_{sc} are defined in equations (3.1.30) and (3.1.31):

$$\frac{1}{\tau_{cn}} = \frac{1}{\tau_S} + \frac{1}{\tau_M} + \frac{1}{\tau_R}, \tag{3.1.32}$$

and

$$\frac{1}{\tau_{sc}} = \frac{1}{\tau_S} + \frac{1}{\tau_M}, \tag{3.1.33}$$

where τ_M is the life-time of a nucleus in the bound site, τ_R is the rotational correlation time of the bound paramagnetic ion, and τ_S is the electron-spin relaxation time. From equations (3.1.30) and (3.1.31) it can be seen that the most important factor in how much effect the paramagnetic centre has on a nucleus is the distance between the two. From this section it can be concluded that paramagnetic ions will cause a large decrease in the spin-lattice and spin-spin relaxation times, although this effect may be less if paramagnetic centres are already present in the system (as is a concern when dealing with fulvic acid). But, one would still expect to see decrease in both relaxation times from the presence of a metal paramagnetic ion.

Thus, paramagnetic relaxation manifests itself in the spectra via line broadening which can easily cause certain signals to "disappear" into the baseline. Thus, the regions

affected by paramagnetic relaxation are altered by loss of apparent signal intensity. Because of the $1/r^6$ distance dependence of dipolar couplings, paramagnetic relaxation is highly diagnostic of the location of the paramagnetic ion. This paramagnetic line broadening will cause spectral changes, as can be seen in Figure 3.6. Figure 3.4 illustrates the effect on a simple five component spectrum. In Figure 3.6a there is no paramagnetic ion, while in Figure 3.6b a paramagnetic ion is bound at a site. The bound paramagnetic ion causes this site spectral component to broaden (2nd from the right) and it also causes spectral broadening of the neighbouring site (2nd form the left). Note that the overall envelope is simplified and the unperturbed components emerge for easier identification. Thus, the region of the spectrum which corresponds to the moiety or moieties to which the paramagnetic relaxation agent has bound will be altered by loss of signal intensity.

As well, in CP-MAS paramagnetic relaxation affects the CP process via a reduction in the $T_{1\rho}{}^1H$ (spin-lattice relaxation in the rotating frame) of the protons. The $T_{1\rho}{}^1Hs$ can be so severely reduced that they relax before CP can take place. Thus, in a CP ^{13}C NMR

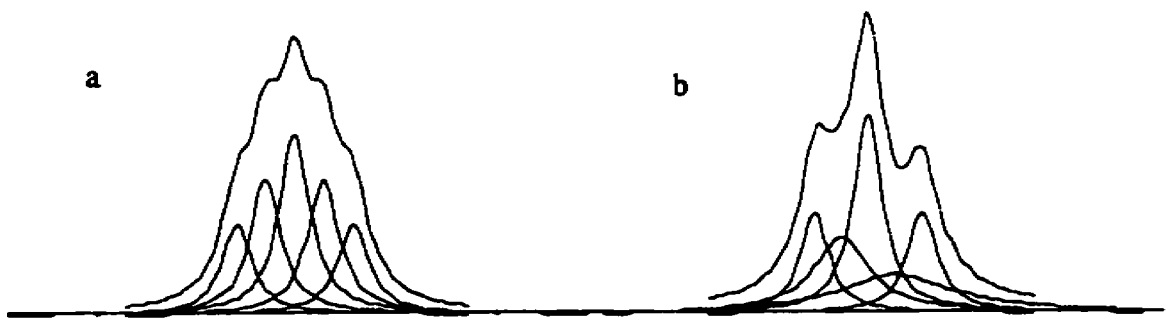

Figure 3.6: The effect of a paramagnetic centre on line broadening in NMR. a) is a hypothetical spectrum with no bound paramagnetic ion, while b) is the same but with a paramagnetic ion bound (see text for details).

experiment the carbon connected to these protons would be rendered invisible and lead to further simplification of the spectrum.

3.2 Luminescence

Luminescence refers to any emission of electromagnetic radiation (usually in the ultraviolet or visible region of the spectrum) from an excited state. There are two main forms of organic luminescence: fluorescence, a spin allowed transition from the singlet excited state (S_1) to the singlet ground state (S_0); and phosphorescence, a formally spin forbidden transition from the triplet excited state (T_1) to the singlet ground state (note: that in this section *I*, S, and T are redefined). This is shown graphically in Figure 3.7.

3.2.1 Absorption of Light as an Analytical Measurement

Consider a molecule in its lowest energy state, known as the electronic ground state (S_0). When this molecules absorbs light, the molecule is promoted to an electronic excited state (S_1). When a molecule absorbs the light the radiation power of the exciting light beam is decreased. Molecules will only absorb light of specific wavelength or wavelengths, which can be chosen by the use of a monochromator (a prism, grating, or a filter). If one knows the radiant power (energy per unit time per unit area) of the light beam before, P_0, and after, P, it passes through a sample, then one can define transmittance, T:

$$T = P / P_0. \qquad (3.2.1)$$

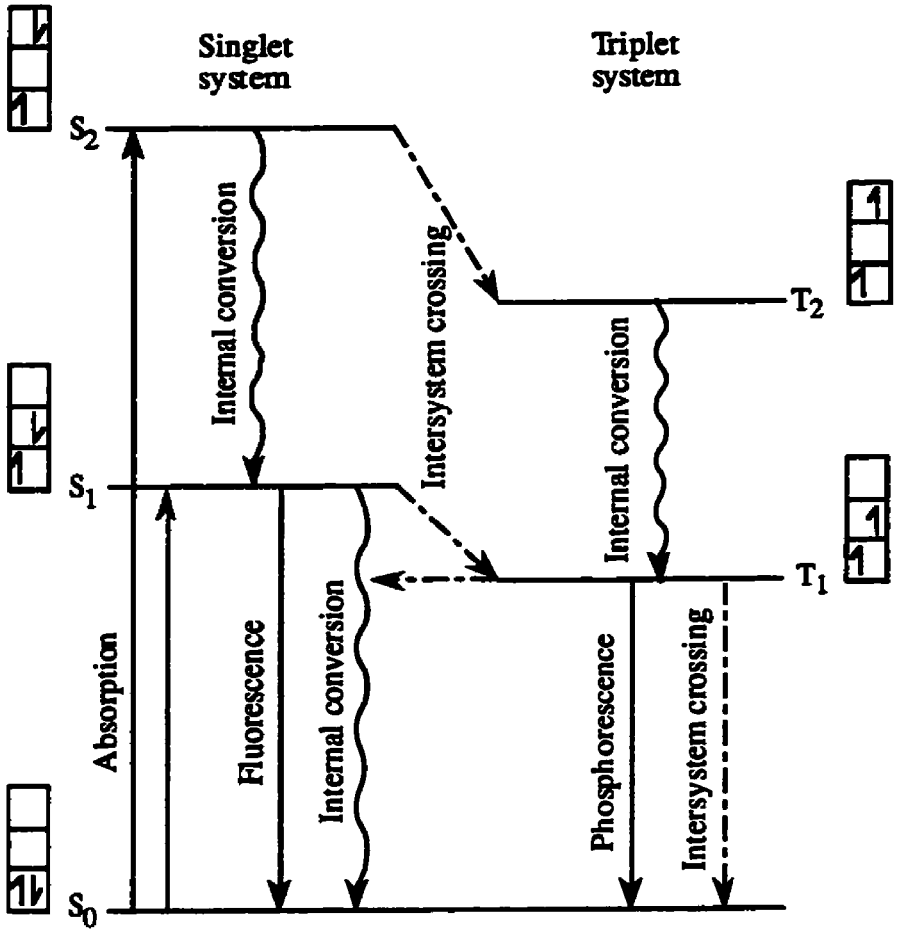

Figure 3.7: Some of the physical processes that take place after a molecules adsorbs a photon (see text for further details).[3.14, 3.15, 3.18, 3.19]

If we now consider what happens to P when the light beam passes through an infinitesimally thin layer of solution with a thickness of dx then;

$$dP = -\vartheta P c dx, \tag{3.2.2}$$

where dP is the decrease in power, c is the concentration of the absorbing species in molar units, and ϑ is a proportionality constant. If we rearrange and integrate equation (3.2.2) with the following limits $P=P_0$ at $x=0$ and $P=P$ at $x=b$, then:

$$-\log(P/P_0) = (\vartheta / \ln 10)cb. \qquad (3.2.3)$$

Defining absorbance, A, as $A=-\log(P/P_0)$, and molar absorptivity (or extinction) coefficient, ε, as $(\vartheta / \ln 10)$, equation (3.2.3) can be rewritten as:

$$A = \varepsilon bc. \qquad (3.2.4)$$

Equation (3.2.4) is known as the Beer-Lambert law (more commonly called the Beer's law). Equation (3.2.4) needs to be modified to take into account the wavelength dependence of absorbance. Thus, the Beer-Lambert law in its final form is;

$$A_\lambda = \varepsilon_\lambda bc, \qquad (3.2.5)$$

where λ stands for the wavelength of light. The molecule, or its part, responsible for the absorption is known as a chromophore.

3.2.2 Relaxation of the Excited State

The excited state must return down to the ground state. The processes resposible for this are collectively known as relaxation. There are two major forms of relaxation. The first is via non-radiative relaxation pathways, while the second is via radiative relaxation pathways. The first set of pathways, are as follows:

- internal conversion; an organic molecule can convert its excited state by passing from a low vibrational level of the upper state to a high vibrational level of the lower state having the same spin as the initial excited electronic state, and
- intersystem crossing; an organic molecule typically crosses from a singlet excited state into the corresponding excited vibrational level of the triplet excited state, e.g. S_1 to T_1, from the T_1 state the molecule can intersystem cross into a highly excited vibrational state of S_0.

The second set of pathways, luminescence relaxation by the emission of a photon, are as follows:

-fluorescence; an organic molecule typically returns to S_0 from S_1 via the emission of a photon in a spin allowed process, and

-phosphorescence: a molecule returns to S_0 from T_1 via the emission of a photon in a spin forbidden process.

All the above processes are graphically depicted in Figure 3.7.

As mentioned above, transitions between states of different multiplicity e.g. between singlets and triplets, are theoretically forbidden. However, in reality, these transitions do take place because of spin-orbit coupling, although with low probability in comparison to singlet-singlet or triplet-triplet transitions. Low transition probability leads to weak absorption bands and the radiative lifetime for the reverse transition ($T_1 \rightarrow S_0$) will be long. Thus, phosphorescence usually takes longer than fluorescence i.e. phosphorescence lifetime are usually longer than fluorescence lifetimes. However, this is not always the case, a classic example is delayed fluorescence.

3.2.3 Luminescence as an Analytical Measurement

Figure 3.8 shows a block diagram of a fluorescence spectrophotometer. If we let the incident radiation interacting with the sample be P_0. Via the Beer-Lambert law, the following relationship can be derived after the light has travelled through the system some distance b_1 near the centre of the cell;

$$P_0' = P_0 10^{-\epsilon_{ex} b_1 c}, \tag{3.2.6}$$

where ϵ_{ex} is the molar absorptivity for the excitation wavelength. After the light has

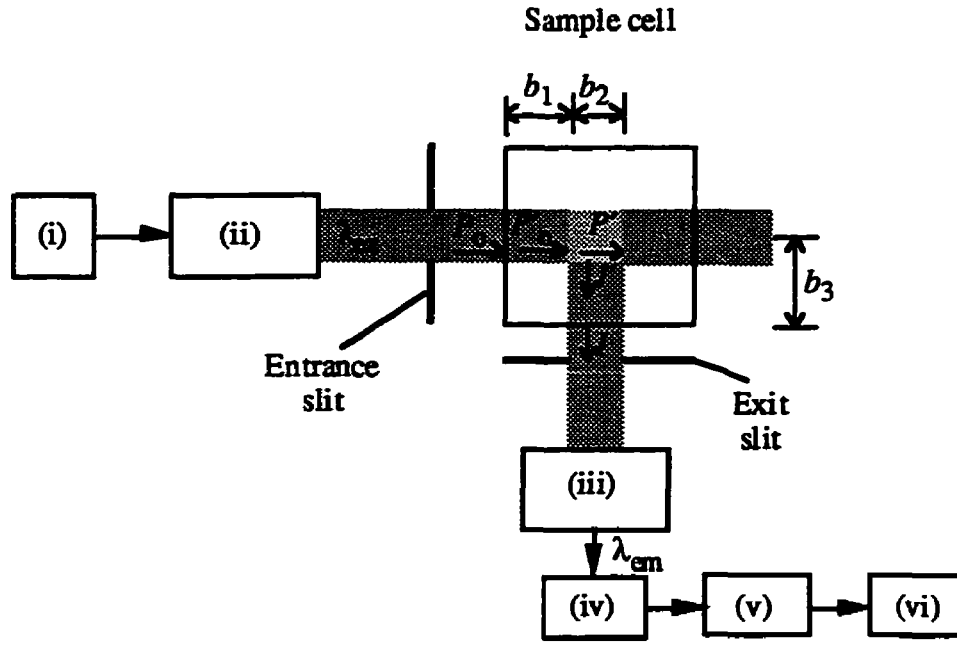

Figure 3.8: A block diagram of a fluorimeter, where (i) is the radiation source, (ii) is the excitation monochromator, (iii) is the emission monochromator, (iv) is the detector, (v) is the amplifier, and (vi) is the recorder.[3.19]

travelled through the sample some further distance b_2 just beyond the centre, the radiation is:

$$P' = P'_0 10^{-\varepsilon_{ex} b_2 c}. \qquad (3.2.7)$$

Since only the radiation reaching the centre of the cell will cause the emission, which is monitored by a slit matching the centre of the cell, this emission intensity, I', should be proportional to the irradiating power absorbed in this central region of the cell;

$$I' = k'(P'_0 - P'), \qquad (3.2.8)$$

where k' is a proportionality constant which arises from, and depends on, the experimental condition and the emitting molecule. The radiation emitted from the centre of the cell, I, has to pass through the sample. However, some will be absorbed by the solution in accordance to the Beer-Lambert Law;

$$I = I' 10^{-\varepsilon_{em} b_3 c}, \qquad (3.2.9)$$

where ε_{em} is the molar absorptivity at the emission wavelength and b_3 is the distance from the centre of the cell to its side, as shown in Figure 3.8. This absorption of emitted radiation by the solution is known as the "inner filter effect", and implies that for optimal quantitative fluorescence analysis the solution should have a very low absorbance of the emitted radiation. From equation (3.2.9) it can be seen that this is the case if ε_{em} , b_3, or c are small. Because, only b_3 or c can be experimentally controlled, and the simplest of these

two to control is c, luminescence measurements are commonly performed on dilute solutions.

The expression for the observed emission intensity can be obtained if one combines equations (3.2.8) and (3.2.9):

$$I = k'(P_0' - P')10^{-\varepsilon_{em} b_3 c}. \qquad (3.2.10)$$

If equations (3.2.6) and (3.2.7) are substituted into equation (3.2.10), then the following expression emerges:

$$I = k'(P_0 10^{-\varepsilon_{ex} b_1 c} - P_0 10^{-\varepsilon_{ex} b_1 c} 10^{-\varepsilon_{ex} b_2 c}) 10^{-\varepsilon_{em} b_3 c}$$

$$= k' P_0 10^{-\varepsilon_{ex} b_1 c}(1 - 10^{-\varepsilon_{ex} b_2 c}) 10^{-\varepsilon_{em} b_3 c}. \qquad (3.2.11)$$

Thus, with equation (3.2.11) we now have the ability to calculate observed emission as a function of concentration. However, the relationship is not a simple or linear one. If the concentration is sufficiently low then equation (3.2.11) is greatly simplified, since $10^{-\varepsilon_{ex} b_1 c}$, $10^{-\varepsilon_{ex} b_2 c}$, and $10^{-\varepsilon_{em} b_3 c}$ will all tend to unity. While it is allowable for $10^{-\varepsilon_{ex} b_1 c}$ and $10^{-\varepsilon_{em} b_3 c}$ to become unity, care must be taken in not allowing $10^{-\varepsilon_{ex} b_2 c}$ to become unity at low concentrations in order to prevent equation (3.2.11) from becoming equal to zero. If these conditions are satisfied then equation (3.2.11) becomes quite simple:

$$I = k' P_0 (1 - 10^{-\varepsilon_{ex} b_2 c}). \qquad (3.2.12)$$

If the following relation $10^{-A} = (e^{\ln 10})^{-A} = e^{-A \ln 10}$ and the power series expansion of e^x: $e^x = 1 + x/1! + x^2/2! + x^3/3!..$ are applied to equation (3.2.12) then;

$$1-10^{-\varepsilon_{ex}b_2c} = \varepsilon_{ex}b_2c\ln 10, \qquad (3.2.13)$$

which leads to the simplification of equation (3.2.12):

$$I = k'P_0\varepsilon_{ex}b_2c\ln 10. \qquad (3.2.14)$$

If all the constants are collapsed into one i.e. $k = k'\varepsilon_{ex}b_2 \ln 10$, then equation (3.2.12) is even further simplified to its final form;

$$I = kP_0c, \qquad (3.2.15)$$

Thus, fluorescence intensity shows a linear dependence of c (and P_0).

Luminescence is a much more sensitive measurement than conventional absorption (although sophisticated absorption techniques such as thermal lensing and laser ring-down cavity absorption are very sensitive analytical methods). The first thing that must be noted is that absorption is the difference between two large numbers to obtain a small number, while fluorescence is the direct measurement of a small number. A delightful analogy of the difference between absorption and luminescence notes that; absorption is akin to trying and find out a captain's weight by weighing the ship with and without the captain, while luminescence is akin to just weighing the captain. The second thing that should be noted is that we can increase the sensitivity of the luminescence measurement just by increasing P_0, while increasing P_0 has little advantage in absorption. Along the same lines, one can also increase the sensitivity of a luminescence measurement just by increasing the sensitivity of

the detector. Thus, luminescence enjoys a large sensitivity advantage over conventional absorption since luminescence's intensity is directly proportional to the incident radiant power, P_0, while absorption is proportional to the $\log(P_0/P)$.

3.2.4 Some Characteristics of the Excited State

A molecule in its ground state has a certain geometry and solvation. When the molecule is first excited it still possesses its ground state geometry. The reason for this is that light absorption takes place within about 10^{-15} s, i.e. within the period of vibration of the light wave. However, during this time period the nuclei of the atoms in the molecule do not appreciably change their position or momenta, due to their much higher mass. Thus, the nuclear configuration and relative motions in the excited state are identical to those in the ground state immediately before absorption occurred. This is known as the Frank-Condon principle. However, very shortly after the excitation the solvation and geometry relax to the most favourable values for the excited state. When a molecule luminesces it returns to the ground state but temporarily retains the geometry and solvation of the excited state

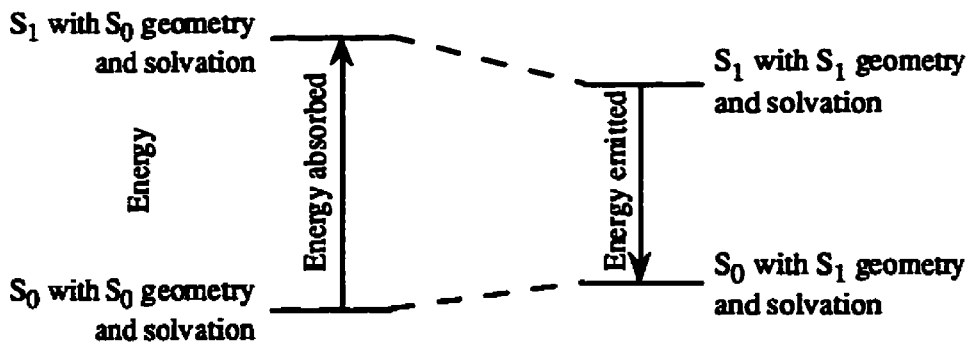

Figure 3.9: The reason why there is a red shift in the emission spectrum compared to the absorption spectrum.[3.19]

before it relaxes to the most favourable geometry and solvation of the ground state. This is shown in Figure 3.9. The net effect is that the energy emitted is less than the energy absorbed during excitation. In terms of wavelength, the emission wavelength will always be longer than the excitation wavelength. This is called the Stokes shift.

The excited state is also characterised by a lifetime τ. When the excitation source is withdrawn, the luminescence intensity decays in accordance to a first-order rate equation, i.e. exponentially with time;

$$I = I_0 e^{-t/\tau}, \tag{3.2.16}$$

where I_0 is the intensity of emission when the excitation source is present, I is the intensity at time t after the excitation source is removed, and τ. is constant defined as the mean decay time for the emission process or the mean lifetime of the excited state. Alternatively;

$$\tau = 1/k_L, \tag{3.2.17}$$

where k_L refers to the luminescence decay rate constant corresponding to the lifetime τ. However, τ. is the observed lifetime but not the intrinsic lifetime, τ_0 for radiative decay. The lifetimeτ., is determined by all the deactivation processes, both radiative and non radiative; thus;

$$\tau_0 \Phi_L^0 = \tau, \tag{3.2.18}$$

where Φ_L^0 is the luminescence quantum yield which, in the absence of external quenching, is defined as follows:

$$\Phi_L^0 = \frac{\text{number of luminescence quanta emitted}}{\text{number of quanta absorbed to a single excited state}}. \qquad (3.2.19)$$

3.2.5 Synchronous Fluorescence [3.49-3.53]

As can be seen in Figure 3.10 fluorescence has four dimensions. Theseare: excitation wavelength, λ_{ex}; and emission wavelength, λ_{em}; (both typically controlled by a monochromator), lifetime of the excited state; and the emission intensity (neither instrumentally controlled). The emission wavelength and the excitation wavelength can both be manipulated by the instrument operator. This manipulation can be done to yield four types of spectra:

- an emission spectrum; to obtain this type of spectrum one maintains a constant λ_{ex}, and varies λ_{em} at higher wavelengths;
- an excitation spectrum; to obtain this type of spectrum one maintains a constant λ_{em}, and varies λ_{ex} at lower wavelengths;
- a synchronous spectrum; to obtain this type of spectrum one varies both λ_{ex} and λ_{em} with a constant offset (with the λ_{ex} being at lower wavelengths); and
- a 3D spectrum; to obtain this type of spectrum one, in effect, combines a complete set of emission spectra for all excitation wavelengths in the region of interest to yield emission intensity as a function of both λ_{ex} and λ_{em}.

Both emission and excitation luminescence spectroscopy are common while the 3D technique is gaining popularity (due to the advent of computer control). However, for complex multicomponent systems such as humic materials, synchronous luminescence spectroscopy has its own unique advantages. The synchronous luminescence advantage lies in how it scans the sample versus emission or excitation luminescence spectroscopy. For simplification we will only compare emission spectroscopy to synchronous

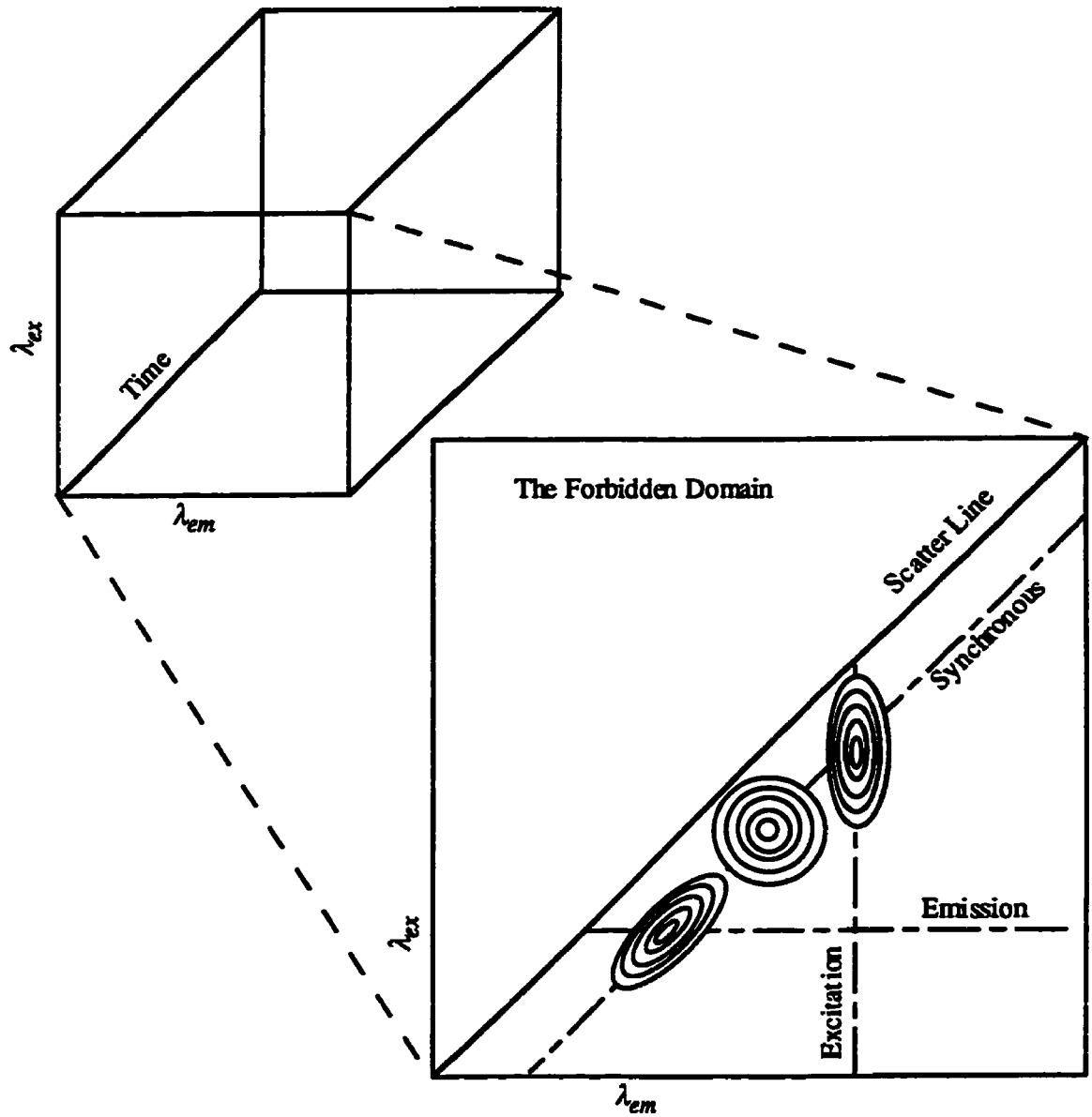

Figure 3.10: The four dimensions of luminescence (see text for details).

spectroscopy, but the same holds true for excitation spectroscopy versus synchronous spectroscopy. One obtains a synchronous spectrum by exciting at λ_{ex} and monitoring the emission at $\lambda_{ex}+\Delta\lambda$ and then repeat this at a higher λ'_{ex} scanning step and monitoring at

$\lambda'_{ex}+\Delta\lambda$, where $\Delta\lambda$ is the offset between the emission and excitation monochromators. This is continued until the whole spectral region of interest has been monitored.

Figure 3.10 shows how all four types of spectra are obtained. It can be seen that emission, excitation, and synchronous spectra can each be treated as a subset of the 3D spectrum. From Figure 3.10 it can be seen that an emission spectrum is, in reality, a horizontal slice through the 3D spectrum, and can be looked at as a 2D signal matrix, consisting of an intensity (I_e) and an emission wavelength (λ_{em}), and can be expressed in the following manner;

$$I_e = f(\lambda_{em}). \tag{3.2.20}$$

Synchronous luminescence can be looked at as an alternatice 2D slice of the three dimensional signal matrix, as shown in Figure 3.10, consisting of a intensity (I_s), excitation wavelength (λ_{ex}), and emission wavelength (λ_{em}), and can be expressed in the following manner;

$$I_s = f(\lambda_{ex}, \lambda_{em}). \tag{3.2.21}$$

But, λ_{ex} can be made a function of λ_{em} as shown below:

$$\lambda_{ex} = \lambda_{em} - \Delta\lambda, \tag{3.2.22}$$

where $\Delta\lambda$ is the constant offset between the excitation and emission monitors. Thus equation (3.2.21) becomes:

$$I_S = f(\lambda_{ex}, \lambda_{ex}+\Delta\lambda). \qquad (3.2.23)$$

From equation (3.2.23), the following equation can be derived:[3.51]

$$I_S = KcbE_{ex}(\lambda_{em} - \Delta\lambda)E_{em}\lambda_{em}, \qquad (3.2.24)$$

where K is a constant, c is the concentration of the analyte, b is the thickness of the sample, and E_{ex} and E_{em} are defined as the intensity distribution patterns of the excitation and emission, respectively. Equation (3.2.24) can also be written in the following form:

$$I_S = KcbE_{ex}(\lambda_{ex})E_{em}(\lambda_{ex} + \Delta\lambda). \qquad (3.2.25)$$

Equation (3.2.24) can be considered an emission spectrum with a synchronously scanned excitation wavelength, and equation (3.2.25) can be considered an excitation spectrum with a synchronously scanned emission wavelength.

Synchronous luminescence interrogates the luminophores, Lo, very differently than emission luminescence. In emission luminescence only a single excitation is used per spectrum, and if the chosen λ_{ex} does not excite every Lo then only a fraction of luminophores will show up in the spectrum. In synchronous luminescence it is the $\Delta\lambda$ that determines how many luminophores will show up in the spectrum. Due to the Stokes shift phenomena, the distribution of luminophores shown in Figure 3.10 is actually a close representation of what the real distribution of luminophores would be in a complex multicomponent system such as a humic material. Thus, if one chooses the correct $\Delta\lambda$ all three luminophores will be sampled. In other words, synchronous luminescence directly excites the Lo which is being monitored for a series of wavelengths. On the other hand it

would take three separate emission spectra to sample all three luminophores in Figure 3.10.

Synchronous luminescence will also generally give spectra with greater detail than emission luminescence. The reason for this arises from the fact that to obtain structure in an emission spectrum the intensity distribution of the emission must have structure. On the other hand, for synchronous luminescence if the intensity distribution of the either emission or the excitation has structure then the synchronous luminescence spectra will have structure. Also, the peaks in synchronous luminescence are narrower and simplified than

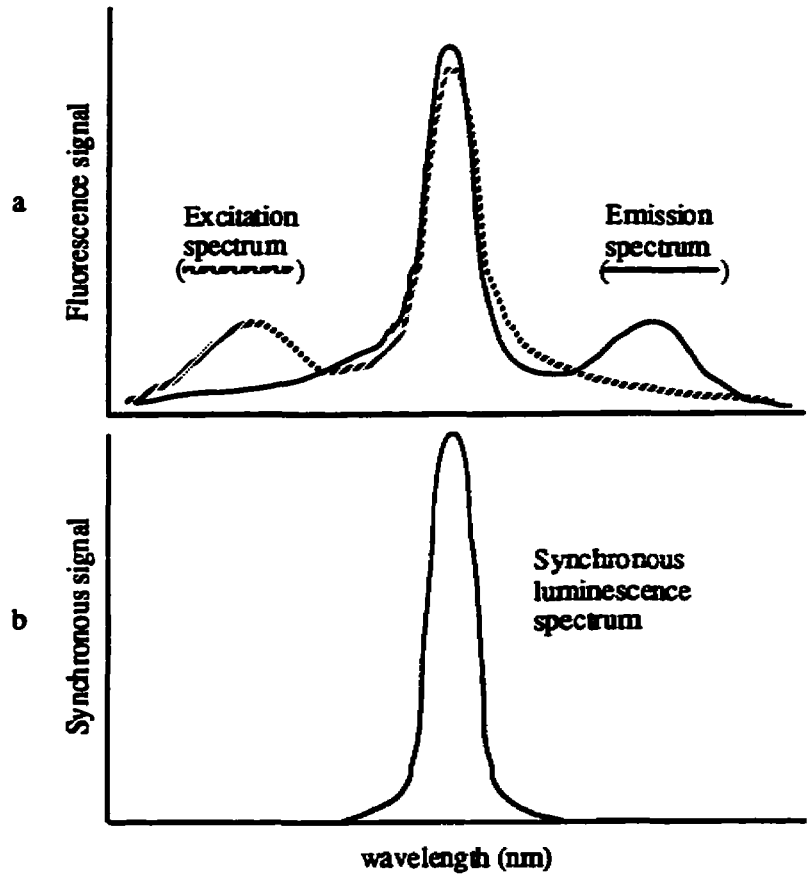

Figure 3.11: a) Excitation and emission spectra, and b) the synchronous luminescence signal, of a hypothetical luminophore.[3.51]

those in emission luminescence, as shown graphically in Figure 3.11. The line narrowing can be as much as $1/\sqrt{2}$.[3.51]

Since synchronous luminescence samples a wider range of luminophores and it does so in finer detail, synchronous luminescence is a more explicit tool and better at resolving the individual components of the luminescence signal.

3.2.6 Fluorescence Quenching

The luminescence intensity for a Lo that one observes is proportional to the amount of Lo in the excited state, Lo*. If there is constant illumination at an appropriate wavelength then a constant population of the excited state is established. Thus $d\mathrm{Lo}^*/dt = 0$. The differential equations describing Lo* in the absence and presence of a quencher are as follows:

$$d\mathrm{Lo}^*/dt = f(t) - \nabla \mathrm{L}^* = 0 \tag{3.2.26}$$

$$d\mathrm{Lo}^*/dt = f(t) - (\nabla + k_q[\mathrm{Q}])\mathrm{L}^* = 0, \tag{3.2.27}$$

where $f(t)$ is the constant excitation function, $\nabla = \tau^{-1}$ is the decay of the Lo in the absence of a quencher, k_q is the bimolecular quenching constant, and [Q] is the concentration of the quencher. Equations (3.2.26) and (3.2.27) yield;

$$L_0/L = (\nabla + k_q[\mathrm{Q}])/\nabla = 1 + k_q\tau[\mathrm{Q}], \tag{3.2.28}$$

where L_0 and L are the observed luminescence intensities in the absence and presence of

quencher, respectively. Another way of obtaining equation (3.2.28) is to consider the proportion of excited Lo, relative to the total, which decay by emission, this consideration leads to;[3.18]

$$L/L_0 = \nabla/(\nabla + k_q[Q]) = 1/(1 + K_D[Q]), \qquad (3.2.29)$$

where K_D is the Stern-Volmer quenching constant. Both equation (3.2.28) and (3.2.29) are the Stern-Volmer equation for collisional quenching can be written in a very generalised form as:

$$L_0/L = 1 + k_q\tau'[Q] = 1 + K_D[Q]. \qquad (3.2.30)$$

Up to this point only quenching resulting from diffusive encounters during the lifetime of the excited state has been considered. This is a time-dependent process. However, quenching can take place by complexation, where the new complex does not luminesce. This type of quenching is known as static quenching.

The dependence of the luminescence intensity on the quencher's concentration can be obtained if one considers the association constant for the complex formation, which is;

$$K_S = [LoQ]/[Lo][Q], \qquad (3.2.31)$$

where [LoQ] is the concentration of the complex and [Lo] is the concentration of the uncomplexed luminophore. Thus the total concentration of the Lo is;

$$[Lo]_0 = [Lo] - [LoQ]. \qquad (3.2.32)$$

By substitution of equation (3.2.32) into equation (3.2.31) one obtains;

$$K_S = ([Lo]_0 - [Lo])/[Lo][Q] = [Lo]_0/[Lo][Q] - 1/[Q]. \quad (3.2.33)$$

If the luminophore concentrations are replaced by the luminescence intensities, equation (3.2.33) becomes;

$$L_0/L = 1 + K_S[Q], \quad (3.2.34)$$

which is once a again the Stern-Volmer equation, and K_S is the Stern-Volmer quenching constant.[3.18]

It should be noted that the complexed luminophores do not luminesce, thus only the uncomplexed Lo is observed. This means the uncomplexed fraction is unperturbed, and hence the lifetime is τ'. Therefore, for static quenching, $\tau'/\tau = 1$. In contrast, for dynamic quenching, $L_0/L = \tau'/\tau$.

However, humic materials are, in all likelihood, multiple luminophore systems (in fact LFA is a multiple luminophore system as shown in Chapter 6). A slight modification must be made to the Stern-Volmer equation to take this into account.[3.54] In the following derivation a two-luminophore equation is derived. The two luminophores have different accessibility (quenchers have different accessibility to these two luminophores), and it is assumed that all luminophores will adhere to the Stern-Volmer law;

$$L_0 = L_{0a} + L_{0b}, \quad (3.2.35)$$

where the "0" subscript once again refers to the luminescence in the absence of a quencher.

If we now consider the extreme case where L_{0b} is not accessible to the quencher then the Stern-Volmer equation becomes;

$$L = L_{0a}/(1 + K[Q]) + L_{0b}, \tag{3.2.36}$$

where K is the Stern-Volmer quenching constant. Subtraction of equation (3.2.36) from (3.2.35) yields;

$$\Delta L = L_0 - L = L_{0a}(K[Q]/(1 + K[Q]). \tag{3.2.37}$$

This equation can be rearranged by inverting equation (3.2.37) followed by division into equation (3.2.35);

$$L_0/\Delta L = 1/f_a K[Q] + 1/f_a, \tag{3.2.38}$$

where f_a is the fraction of the initial luminescence accessible to a quencher;

$$f_a = L_{0a}/(L_{0a} + L_{0b}). \tag{3.2.39}$$

Thus, if there are only two types of luminophores a plot of $\Delta L / L_0$ versus [Q] will give a linear plot, with a slope $f_a K$ of and an intercept of f_a.

Also, when dealing with polymeric system such as humic materials, luminescence can be quenched by aggregation changes which can disturb the special relations needed for emission from donor/acceptor complexes or Förster resonance excitation transfer to the Lo.[3.55]

References

3.1 Abragam, A. The Principles of Nuclear Magnetism; Oxford University Press, New York, 1961.

3.2 Dwek, R.A. Nuclear Magentic Resonance (N.M.R.) in Biochemistry: Applications to Enzyme Systems; Oxford University Press, New York, 1973.

3.3 Knowles, P.F.; Marsh, D.; Rattle, H.W.E Magnetic Resoance of Biomolecules: An Introduction to the Theory and Practice of NMR and ESR in Biological Systems; John Wiley & Sons, New York, 1976.

3.4 Leyden, D.E.; Cox, R.H. Analytical Applications of NMR; John Wiley & Sons, New York, 1977.

3.5 Sohár, P. Nuclear Magentic Resonance Spectroscopy: Volume 1; CRC Press Inc. Boca Raton, Florida, 1983.

3.6 Harris, R.K. Nuclear Magnetic Resonance Spectroscopy: A Physiochemical View; Longman Science & Technical, Essex, England, 1986.

3.7 Sanders, J.K.M.; Hunter, B.K. Modern NMR Spectroscopy: A Guide for Chemists; Oxford University Press, New York, 1993.

3.8 Freeman, R A Handbook of Nuclear Magnetic Resonance; Longman Science & Technical, Essex, England, 1988.

3.9 Ernst, R.R.; Bodenhausen, G.; Wokaun, A. Principles of Nuclear Magnetic Resonance in One and Two Dimensions; Oxford University Press, New York, 1994.

3.10 Stejskal, E.O.; Memory, J.D. High Resolution NMR in the Solid State: Fundamentals of CP/MAS; Oxford University Press, New York, 1994.

3.11 Hore, P.J. Nuclear Magnetic Resonance; Oxford University Press, New York, 1995.

3.12 Axelson, D.E. Solid State Nuclear Magnetic Resonance of Fossil Fuels; Multiscience Publications Ltd: Canadian Government Publishing Centre, Supply and Services Canada, 1985.

3.13 Botto, R.E.; Sanada, Y. Magnetic Resonance of Carbonaceous Solids: Advances in Chemistry Series 229; American Chemical Society, Washington D.C., 1993.

3.14 Parker, C.A. Photoluminescence of Solutions: With Applications to Photochemistry and Analytical Chemistry; Elsevier Publishing Company, New York, 1968.

3.15 Becker, R.S. Theory and Interpretation of Fluorescence and Phosphorescence; John Wiley & Sons, New York, 1969.

3.16 Lumb, M.D. in Luminescence Spectroscopy: Lumb M.D. (ed.); Academic Press, New York, 1978.

3.17 Schulman, S.G. Fluorescence and Phosphorescence Spectroscopy: Physiochemical Principles and Practice; Pergamon Press, New York, 1977.

3.18 Lakowicz, J.R. Principles of Fluorescence Spectroscopy; Plenum Press, New York, 1983.

3.19 Harris, D. C. Quantitative Chemical Analysis: (2nd ed.); W.H. Freeman and Company, New York, 1987, Chapter 20.

3.20 Nanny, M.A.; Minear, R.A.; Leenheer, J.A. Nuclear Magnetic Resonance Spectroscopy in Environmental Chemistry; Oxford University Press, New York, 1997.

3.21 Buffle, J. Complexation Reactions in Aquatic Systems. An Analytical Approach; Ellis Harwood Ltd, Chester, UK, 1988.

3.22 Hayes, M.H.B.; MacCarthy, P.; Malcolm, R.L.; Swift, R.S. Humic Substances II. In Search of Structure; John Wiley & Sons, Toronto, 1989. (1.4)

3.23 Stevenson, F.J. Humus Chemistry. Genesis. Composition. Reactions (2nd ed.); John Wiley & Sons, Toronto, 1994.

3.24 Purcell, E.M.; Torrey, H.C.; Pound, R.V. *Phys. Rev.* **1946**, 69, 37.

3.25 Bloch, F.; Hansen, W.W.; Packard, M. *Phys. Rev.* **1946**, 69, 127.

3.26 Lowe, I.J. *Phys. Rev. Ltters* **1959**, 2, 285.

3.27 Andrews, E.R. *Progr. Nucl. Magn. Reson. Spectrosc.* **1971**, 8, 1.

3.28 VanderHart, D.L.; Garroway, A.N. *J. Chem. Phys.* **1979**, 71, 2773.

3.29 Suwelack, D.; Rothwell, W.P.; Waugh, J.S. *J. Chem. Phys.* **1981**, 74, 2721.

3.30 Rothwell, W.P.; Waugh, J.S. *J. Chem. Phys.* **1980**, 73, 2559.

3.31 VanderHart, D.L.; Earl, W.L.; Garroway, A.N. *J. Magn. Reson.* **1981**, 44, 361.

3.32 Hertzfield, J.; Berger, A.E. *J. Chem. Phys.* **1980**, 73, 6021.

3.33 Levitt, M.H.; Suter, D., Ernst, R.R. *J. Chem. Phys.* **1986**, 84, 4243.

3.34 Marks, D.; Vega, S *J. Magn. Reson. Ser. A* **1996**, 118, 157.

3.35 Hartmann, S.R.; Hahn, E.L. *Phys. Rev.* **1962**, 128, 2042.

3.36 Stejskal, E.O.; Schaefer, J.; Waugh, J.S. *J. Magn. Reson.* **1977**, 28, 105.

3.37 Sardashti, M.; Maciel, G.E. *J. Magn. Reson.* **1987**, 72, 467.

3.38 Wind, R.A.; Dec, S.F.; Lock, H.; Maciel, G.E. *J. Magn. Reson.* **1988**, 79, 136.

3.39 Pruski, M.; dela Rosa, L.; Gerstein, B.C. *Energy Fuels*, **1990**, 4, 160.

3.40 Komorowski, R.A. in High Resolution NMR Spectroscopy of Synthetic Polymers in Bulk : Komorowski, R.A., Ed.; VCH: Deerfield, Fl, 1986; p 42.

3.41 Garroway, A..N.; Moniz, W.B.; Resing, H.A. in Carbon-13 NMR in Polymer Science ; Paski, W.M., Ed.; ACS Symposium Series 103; American Chemical Society; Washington, D.C., 1979; p 67.

3.42 Metz, G.; Wu, X.; Smith, S.O. *J. Magn. Reson. A* **1994**, 110, 219.

3.43 Cook, R.L.; Langford, C.H.; Yamdagni, R.; Preston, C.M. *Anal. Chem.* **1996**, 68, 3979.

3.44 Peersen, O.B.; Wu, X.; Smith, S.O. *J. Magn. Reson. Ser. A.* **1994**, 106, 127.

3.45 Zhang, S. *J. Magn. Reson. Ser. A* **1994**, 111, 73.

3.46 Hediger, S.; Meier, B.H.; Narayanan, D.K. Bodenhausen, G. Ernst, R.R. *Chem. Phys. Letters* **1994**, 223, 283.

3.47 Solomon, I. *Phys. Rev.* **1955**, 99, 559.

3.48 Bloembergen, N. *J. Chem. Phys.* **1957**, 27, 572.

3.49 Lloyd, J.B.F. *Nature* **1971**, 231, 64.

3.50 Lloyd, J.B.F.; Evett, I.W. *Anal. Chem.* **1977**, 49, 1710.

3.51 Vo-Dinh, T. *Anal. Chem.* **1978**, 50, 396.

3.52 Vo-Dinh, T. *Appl. Spectrosc.* **1982**, 36, 576.

3.53 Cabaniss, S.E. *Anal. Chem.* **1991**, 63, 1323.

3.54 Lehrer, S.S. *Biochemistry* **1971**, 10, 3254.

3.55 Guillet, J. Polymer Photophysics and Photochemistry. an Introduction to the Study of Photoprocesses in Macromolecules; Cambridge University Press, New York, 1985, Chapters 7 and 9.

Chapter 4
Experimental

4.1 Materials

This work exploits both the Laurentian fulvic acid (LFA) and Laurentian humic acid (LHA) extracted from a forest podzol from the area controlled by Laval University (Quebec). They were then prepared and purified as described in references [4.1,4.2]. Both LHA and LFA have been the subject of extensive studies, including elemental composition, acid-base and metal titration curves, emission fluorescence, FT-IR, ^{1}H NMR and MCD.[4.3-4.7] The composition of LFA was 45.1% C, 4.1% H, 1.1% N, 49.7% O, < 1ppm Fe, and < 1% Ash; that of LHA was 51.9% C, 5.5% H, 2.3% N, 39.9% O, 6 ppm Na, and 2 ppm Fe (as determined by elemental analysis and atomic absorption).

The metal salts used were nickel chloride (BDH Lot 2733500L), and cupric nitrate (Fisher Lot 874505). The water was 18 MΩ produced by a Barnstead Nanopure system (unless otherwise stated).

4.2 Fluorescence

4.2.1 Equipment

Both the emission and synchronous fluorescence measurements were made on a Photon Technology Inc. Alphascan Fluorimeter, with the photomultiplier tube operating in photon-counting mode using a water cooled 70W Xe arc lamp source. Excitation slits were set at 10 nm, and the emission slits were set at 2 nm. pH dependence measurements were

performed in accordance to methods described in reference 4.8. The picosecond experiments were carried out at the Canadian Centre for Picosecond Laser Spectroscopy (at Concordia University). This apparatus uses a mode locked Nd/Yag producing a third harmonic pulse at 355nm. The half pulse width is 30 ps and the pulses measured had energies of 2.5 ± 0.5 mJ. The emission decay was measured at 455 nm on a Hammamatsu streak camera with a time resolution of 20 ps. The emitted light was viewed through an interference filter. Dr. A. Vlcek conducted quite independent nanosecond laser pulse experiments which can test the assignment of the longer lifetimes. His apparatus used a Lambda Physik excimer laser (308nm, XeCl). The pulse width is 25 ns. The emission was measured at ~455 nm and detected by Applied Photophysics Laser Kinetic Spectrometer LKS20 (the signal was captured by a Philips digital oscilloscope).

4.2.2 Procedure

The pH dependence studies were carried out, by Mr. M Pullin and Dr. S. E. Cabaniss, with a stock solution of 10.0 mg/L of LFA and 10 mM K_2HPO_4 (Fisher) in Milli-Q water. pH adjustment was done with small amounts of HCl and NaOH. The pH emission fluorescence experiments used 340 nm excitation, while the synchronous fluorescence measurements were made with a constant 20 nm offset ($\Delta\lambda$) between the excitation monochromator and emission monochromator.[4.8]

For the metal ion studies a stock solution of LFA was made from 0.175g/L (LFA has been found to have a bidentate complexing capacity of 5.8 mmol/g [18]). 10 mL of this stock solution was then added to a 100 mL volumetric flask and the necessary amount of metal was added to give stoichiometeric ratios of 0.100 to 0.900 (1×10^{-5} M to 9×10^{-5} M) metal ion to bidentate binding sites (M:B.S.) after which the solutions were diluted to

100 mL. The solutions were then adjusted to a pH of either 4.0, 5.0, 6.4, or 8.0, with either NaOH or HCl. Fulvic acid self buffers. The emission fluorescence experiments used 355 nm excitation, while the synchronous fluorescence measurements were made with a constant 20 nm offset ($\Delta\lambda$). The solutions were protected from light and allowed to equilibrate for a minimum of twelve hours.

The same procedure was used for making the stock solution for both the picosecond and nanosecond fluorescence decay experiments except the fulvic acid concentration was 0.25 g/L, and all the tested solutions had a pH of 6.4. These solutions were protected from light and allowed to equilibrate for a minimum of sixteen hours.

4.2.3 Data Treatment

All the steady state spectra were smoothed using a 15-point Savitsky-Golay filter. The fitting of the emission decay was done using a three component exponential decay fit in the following manner;

$$D(t) = \sum a_i \exp(-t / \tau_i) \qquad (4.1)$$

where $D(t)$ is the signal at time t,, a_i is the pre-exponential term, and τ_i is the lifetime of the luminophore. The data was weighted to the relative intensity and the allowable error was 0.1% with the general fit of the KaleidaGraph software package (for the Macintosh platform) which uses the Levenberg-Marquardt algorithm. The nanosecond emission was deconvoluted in a similar method using an exponential decay fit by in house software employing Marquardt's optimisation method.

The average metal ion binding constant, $|\overline{K}_4|$ of reference 4.9, was calculated in the following way. Consider the equilibrium;

$$SH^- + M^{2+} \Leftrightarrow SM + H^+, \tag{4.2}$$

where SH^- represents all singly deprotonated bidentate complexation sites, and SM is a metal ion complexed to these bidentate sites. In terms of concentration, the average equilibrium constant is defined by:

$$|\overline{K}_4| = [SM]\,[H^+]/[SH^-][M^{2+}]. \tag{4.3}$$

This definition corresponds to that used in references 4.10 to 4.12.

4.3 Nuclear Magnetic Resonance

4.3.1 Equipment

All solid-state spectra where obtained on a Bruker AMX2-300 spectrometer, with a Bruker BL4 probe. The rotors used were 4 mm O.D. by 18 mm long zirconia rotors with Kel-F caps. All calibration such as magic angle setting and Hartman-Hahn matching was done on ^{13}C labelled glycine, using the ketonic signal. The liquid state spectrum was obtained on a Bruker MSL-300 spectrometer, with a BB10 probe, and a 10 mm glass NMR tube by Dr. C. M. Preston.

4.3.2 Procedure

4.3.2.1 Instrumental

All solid state spectra were obtained at 75.469 MHz and a 1 s recycle time. A standard contact time experiment (where the contact time is varied) revealed that $T_{1\rho}{}^{1}H >> T_{CH}$, and thus, the cross polarisation experiment does work on this sample (see theory section for explanation). A 1 s recycle time was found to allow complete relaxation of the system (the spectra obtained at longer delays where identical to the spectra obtained with a delay of 1 s), as has been reported by Schnitzer and Preston.[4.13]

The ramp was applied to the proton channel, because the amplifier for the proton channel has higher linearity than that of the X (^{13}C) channel. The ramp was set so that it was centred on the -1 sideband. The reasons for this are twofold: (i) if the ramp had been set on the +1 sideband arcing would have occurred at the probe; (ii) it has been shown that the signal buildup at the -1 sideband is much faster than that at the centerband.[4.14-4.16] The ramp was set, in hertz, at the spinning rate, except where the spinning rate was smaller than the smallest available ramp. In this case, the ramp was set at the 8 kHz minimum (for the spectrometer used in this study).

For the spin rate dependence experiments, the contact time was 1 ms and the number of scans was 25,500 for both LFA and LHA. For all other experiments, except for the contact time experiments, a contact time of 3 ms was used for LFA and a contact time of 2.5 ms was used for LHA. The number of scans for all experiments was 14,400 (except for the two dimensional and metal loading experiments). For the two dimensional experiments the number of scans was 12,000, and for the metal loading experiments the number of scans was 160,000. For the pulse sequences used in the solid state studies see section 4.3.3.

All liquid state spectra were obtained, by Dr. C.M. Preston, at 75.468 MHz using inverse-gated decoupling, acquisition time 100 ms, a 45° degree pulse and a relaxation delay (decoupler off) of 2 s. The number of scans was 98,000 for LHA and 48,000 for LFA. These conditions were chosen to yield reasonably qualitative intensity distributions while maintaining usable signal-to-noise ratios. A full account of the application of this method for humic materials is given by Preston and Blackwell.[4.17]

4.3.2.2 Sample

For all solid state experiments, except the metal loading experiment, the purified protonated form of both LFA and LHA was used. The metal loaded samples were prepared in a similar way to the fluorescence samples, except at much higher concentrations. 300 mg of fulvic acid was dissolved in the appropriate volume of water e.g. 100 ml for the 0.05 M:B.S sample, 150 ml for the 0.10 M:B.S. sample, and 200 ml for the 0.15 M:B.S. sample. The volume was chosen so that the LFA in solution would just start to precipitate after the desired amount of Cu (II) had been added. Once the LFA had fully dissolved (after about an hour of stirring at medium speed) the desired amount of Cu (II) was added. The solution was then allowed to air dry for just over a month, after which it was transferred to a sample vial.

All solid samples, except LFA, were ground with a mortar and pestle before being packed into the rotor. The rotor packing followed standard procedures.

Samples for solution NMR were prepared by adding 2.7 ml D_2O and 0.3 ml NaOH to 175 mg LHA and LFA. Samples were left to dissolve overnight, centrifuged, and filtered through fritted-glass filters into 10 mm NMR tubes.

4.3.3 Solid State ^{13}C NMR Pulse Sequences

In this section the pulse sequences used in the solid state ^{13}C NMR studies are discussed (see Figure 4.1). Since this section and the theory section overlap, the details covered in the theoretical section will not be covered here, however the pulse sequences used to obtain relaxation parameters are discussed in some detail.

4.3.3.1 Ramp-CP

Ramp-CP is a relatively novel approach to cross polarisation, first introduced by Smith and co-workers.[4.15] The Ramp-CP method of cross polarisation can be placed in a family of techniques known as variable amplitude cross polarisation (VACP). The Ramp-CP pulse sequence is the same as the classic CP (single amplitude cross polarisation [SACP]) pulse sequence except one of the spin-lock conditions is varied continuously (Figure 4.1a); in this study it is the proton spin-lock condition. Ramp-CP covers a range of cross polarisation frequencies centred on the Hartmann-Hahn match (HH) frequency. It has been shown that a ramp centred on the -1 sideband gives the best results.[4.15] The scan range of the ramp is set equal to the spinning rate (although it can be made smaller or larger [4.15]). Ramp-CP overcomes the motional modulation of the CH coupling caused by spinning the sample at a high rate, by changing one of the spin-lock conditions to compensate for the high spinning speed. It also allows for more than just one HH condition to be matched for samples which are mixtures. These advantages of Ramp-CP in relation to humic materials are discussed in much greater details in Chapter 5.

Ramp-CP can replace classical cross polarisation in all pulse sequences, without altering the overall result of the pulse sequence.

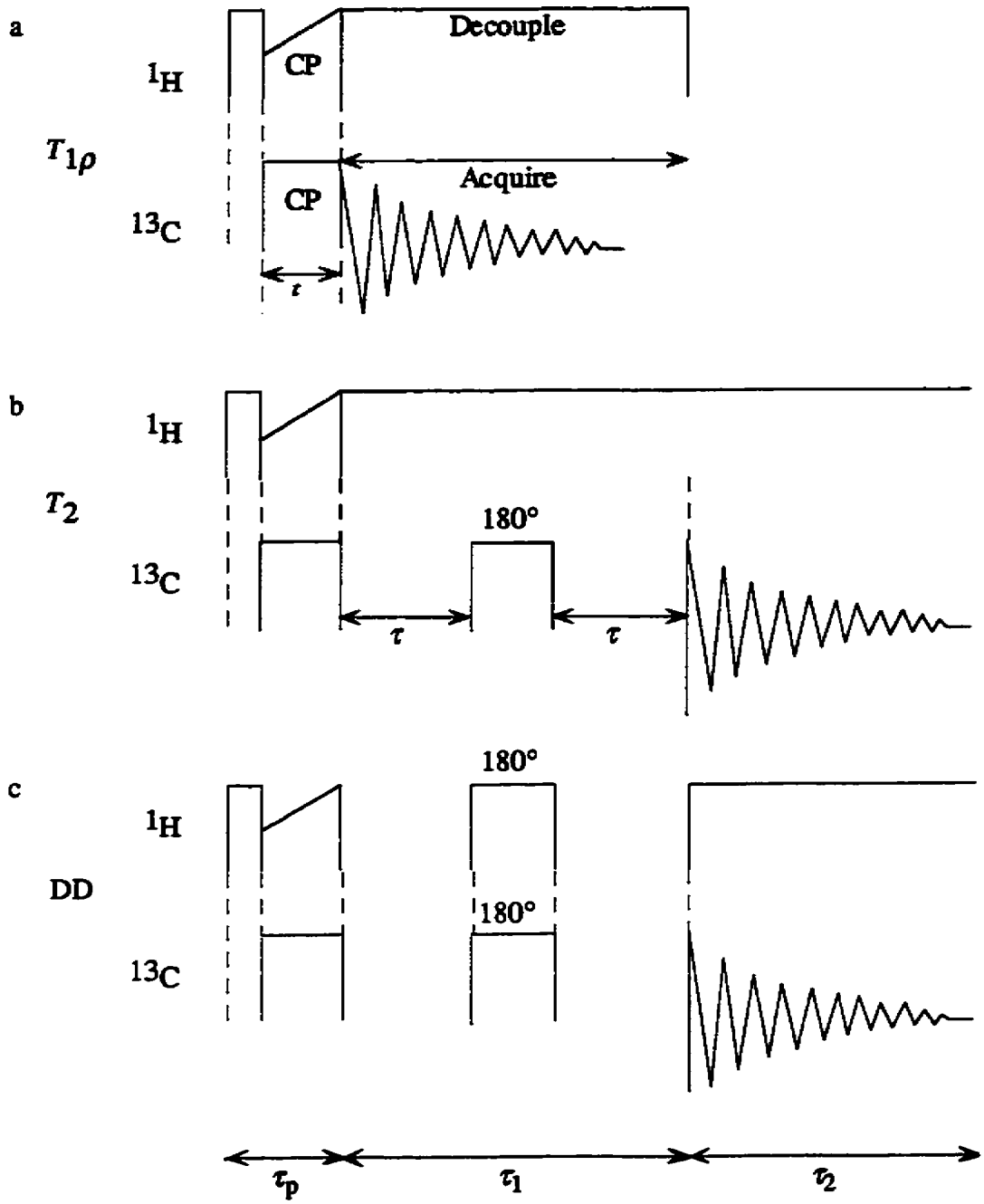

Figure 4.1: The pulse sequences used in this study: a) the Ramp-CP and $T_{1\rho}$ pulse sequence (see Figure 3.5a for SACP pulse sequence); b) the T_2 ^{13}C pulse sequence; c) the two dimensional dipolar-dephasing pulse sequence (see text for details).

4.3.3.2 Chemical Shift Spectra

The chemical shift spectra were obtained using the pulse sequence shown in Figure 4.1a. This is the classic cross polarisation pulse sequence which has been modified to incorporate ramping the ^1H spin-lock condition.

4.3.3.3 Proton Rotating Frame Spin-Lattice Relaxation Time, $T_{1\rho}(^1H)$

There are two possible approaches to measuring $T_{1\rho}(^1H)$ via CPMAS ^{13}C NMR. The more frequently used approach is to vary the length of the CP contact. This is the method used in this study. The alternative approach is to vary the length of the ^1H spin lock condition, and only at the end allow for cross polarisation with a fixed contact time. This second method overcomes some of the disadvantages of the first method, however it does have its own disadvatages. The major disadvantage is at least a 1000-fold decrease in the signal-to-noise ratio.[4.18] Because of this disadvantage, it is almost impossible to apply this method to obtaining $T_{1\rho}(^1H)$ for humic materials.

The experimental data can be plotted as the natural logarithm of signal intensity versus contact time. Initially, the plot rises with a slope equal to rate of cross polarisation (T_{CH}^{-1}), after a certain time the curve falls with a slope equal to $-T_{1\rho}(^1H)^{-1}$. In other words, T_{CH} is determined from the short contact times, and $T_{1\rho}(^1H)$ is determined from the long contact times. This experiment also gives a way of finding the contact time which is optimal and gives the most liquid like spectra (if a comparison liquid state spectrum is available). For a more thorough discussion on $T_{1\rho}(^1H)$ refer to references 4.18-4.21.

4.3.3.4 Carbon-13 Spin-Spin Relaxation Time, $T_2(^{13}C)$

The preferred method of measuring $T_2(^{13}C)$ in solution is via the Carr-Purcell sequence, in which one uses a 90° ($\pi/2$) pulse followed by a series of equally spaced 180° (π) pulses. This method is inappropriate for solids, since there is a slight cross polarisation effect that occurs at each 180° pulse. This is a cumulative effect and thus, after several pulses, the relaxation measurement is meaningless.[4.23]

However, $T_2(^{13}C)$ can be measured in solids via the Hahn spin-echo method, which can be adapted to CP-MAS.[4.23] Figure 4.1b shows this pulse sequence, in the Ramp-CP modification. After CP the transverse carbon magnetisation is allowed to dephase for a time period, τ. A 180° pulse is applied to the carbons at time τ. Another time delay follows, τ, during which the fraction of the carbon magnetisation, which has decayed due to inhomogeneous interactions, is refocused. Thus, the 180° pulse can be considered as a refocusing pulse. Data acquisition starts at the end of the second τ period. The reduction of the signal from the initial signal reveals the loss of carbon magnetisation caused only by the natural T_2 processes. It is important to note that τ must be an integral multiple of the spinning rate, so that it permits an effective time reversal of all inhomogeneous interactions at the 180° pulse. A plot of ln(signal intensity) versus 2τ gives a slope equal to $T_2(^{13}C)^{-1}$.[4.20, 4.23]

4.3.3.5 Two Dimensional Dipolar-Dephasing (DD)

A pulse sequence which produces a two dimensional (2D) spectrum requires three time periods. The first of these periods is the preparation period, τ_p. During this period the spin system is prepared in a coherent nonequilibrium state. During the second time

period, known as the evolutionary period, the system freely evolves under the influence of the Hamiltonian, H^e, which in this case represents dipolar-dephasing. The magnitude of the influence of H^e on the spin system is determined by the length of an evolutionary period, τ_1. The τ_1-evolution must be sampled, and in order to do this a series of experiments with a systematic incrementation of τ_1 must be carried out. The minimium number of τ_1 increments is 32. The third and final time period is the acquisition or detection period, τ_2. Thus, there are two independent time dimensions τ_1 and τ_2 which give a matrix surface(τ_1, τ_2) that can be transformed via a two-dimensional Fourier transform to give a frequency-domain matrix, surface(ω_1, ω_2). The 2D transform can be considered as a succession of two 1D Fourier transforms.[4.23] The intensity is portrayed by a surface in three dimensional space of the two dimensional spectrum. The orthogonal axes ω_1 and ω_2 represent the two independent frequency dimensions.[4.23, 4.24]

The pulse sequence shown in Figure 4.1c, will produce a 2D spectrum. In the pulse sequence the spin system is prepared by cross polarisation, via Ramp-CP, during τ_p. The τ_1-evolution in this experiment is a dipolar-dephasing evolution, with a 180° refocusing pulse in the middle of τ_1. This 180° refocusing pulse is placed in the pulse sequence to reverse the chemical shift dephasing and leads to a refocusing of the chemical shift dephasing. Care must been taken to ensure that during the 180° refocusing pulse no CP takes place. A normal chemical shift spectrum is obtained from τ_2 after the 2D Fourier transform.

The dipolar-dephasing (DD) experiment was first introduced by Opella and Frey.[4.25] It was then extended by Wilson [4.26] to the pulse sequence seen in Figure 4.1c, except SACP was used in τ_p. In a dipolar-dephasing experiment there is a delay between CP and the acquisition, during which the ^1H and ^{13}C radio frequencies are off. During the delay the ^{13}C spins, which are strongly coupled to protons via dipole-dipole interactions,

are efficiently dephased (hence, the name dipolar-dephasing), causing a large loss in the observed ^{13}C signal. The stronger the dipole-dipole interaction, the faster the dephasing. Thus, the weaker the dipole-dipole interaction is, the longer delay becomes before the ^{13}C signal is lost.

It can be seen that the ω_1 axis of the DD spectrum is a measure of the C-H dipole-dipole interaction strength of different carbons i.e.: the further the signal extends on the ω_1 axis the weaker the dipole-dipole interaction, and the ω_1 axis can be used to indicate the functionalisation of different structural moieties. It must be noted that because methyl groups rotate rapidly even in the solid state, the dipole-dipole interactions between the carbons and protons is almost completely destroyed. Hence the methyl carbons will also extend out on the ω_1 axis. The diagnostic point is that the further the moiety's signal extends on the ω_1 axis, the more functionalised that moiety is, and the fewer the protons on the carbons.

4.4.5 Data Analysis

The 1D solid state spectra were processed with the 1D WIN-NMR software package from Bruker. Exponential/Fourier transforms were performed with 60 Hz line broadening. The phase correction was initially done with a 5^{th} order PKNL function and then finely adjusted in the phase correction mode of the software to give the most realistic spectra. The baseline correction was cubic spline, but no forcing of the baseline was done i.e. very little baseline correction was needed. The two dimensional spectra where processed in a manner very similiar to the 1D spectra, except X-WIN NMR software from Bruker was used.

The liquid-state spectra were processed with 50 Hz line broadening, and baseline correction was by curve matching and subtraction.

The intensity distribution was interpreted in terms of the following chemical shift regions:[4.27] unsubstituted aliphatic carbon (0-50 ppm); carbon singly bonded to O or N heteroatoms (50-96 ppm); carbon singly bonded to two O atoms (96-108 ppm); aromatic carbons (108-162 ppm); carboxyl carbons (162-190 ppm); and ketonic carbons (190-220 ppm). For the LHA sample the 50-90 ppm region was subdivided into two regions: aliphatic esters, ethers, methoxyl, and ethoxyl (50-60 ppm); and all other anomeric carbons (60-96 ppm). The uncertainties of these numbers are of the same magnitude as the experimental error.

The solid state spectra peaks were integrated with resets determined by the chemical shift regions discussed above e.g. the carboxyl peak was integrated from 162-190 ppm, and where reported by the 1D WIN-NMR software. The liquid spectra where integrated with no resets. The resets where then done by hand allowing the integration curve to be portions and quantified.

These regions in the solid state spectra where then further quantified in the following manner: first sideband corrections were applied and then the integrated area for each region was expressed as a percentage of the total observable carbons (%TOC). The sideband correction was done by using the sideband of the carboxyl carbons as the reference and then subtracting the appropriate sideband intensity when a sideband underlay a region of interpretation in the spectra. The standard deviation is about ±0.2 or less, unless otherwise stated.

4.4 Gel Filtration

20 grams of Sephadex G-75 was allowed to swell for 7 days in water, after which suction was applied until no air bubbles were visible. The flask was then lightly swirled and allowed to stand for 10 minutes after which the supernatant was poured off to remove the fine particles. 300 mL of water was added to the flask and the above procedure was repeated twice more. The gel was then poured into a 30 cm by 4 cm^2 column and allowed to settle, the final height of the gel after settling was 30 cm. The column was then conditioned by passing water through it for 24 hours.[4.28]

300 mg of LFA dissolved in 15 mL of water was applied to the top of the column and eluted with water under a 1 m hydrostatic head. The flow rate was set at 0.33 ml/min. The volume of each sample collected was 5 mL, and the total volum collected was 150 ml. The samples were stored at 4°C and analysed over a period of 48 hours.

References

4.1 Griffith, S.M.; Schnitzer, M. *Soil Soc.* **1975**, 120, 126.

4.2 Schnitzer, M. Skinner, S.I.M. *Soil Soc.* **1968**, 105, 392.

4.3 Bruccoleri, A.: Pant, B.C.; Sharma, D.K.; Langford, C.H. *Environ. Sci. Technol.* **1993**, 27, 889.

4.5 Wang, Z.D.; Pant B.C.; Langford C.H. *Anal. Chim. Acta.* **1990**, 232, 43.

4.6 Wang, Z.D.; Gamble D.S.; Langford C.H. *Environ. Sci. Technol.* **1992**, 26, 560.

4.7 Wang, Z.D. PhD. Thesis, Concordia University, Montreal, 1989.

4.8 Pullin, M.J.; Cabaniss, S.E. *Environ. Sci. Tech.* **1995**, 29, 1460.

4.9 Gamble, D.S.; Underdown, A.W.; Langford, C.H. *Anal. Chem.* **1980**, 52, 1901.

4.10 Saar, R.A.; Weber, J.H. *Anal. Chem.* **1980**, 52, 2095.

4.11 Ryan, D.K.; Weber, J.H. *Anal. Chem.* **1982**, 54, 986.

4.12 Ryan, D.K.; Weber, J.H. *Environ. Sci. Technol.* **1982**, 16, 866.

4.13 Schnitzer, M.; Preston, C.M. *Soil Sci. Am. J.* **1986**, 50, 326.

4.14 Stejskal, E.O.; Schaefer, J.; Waugh, J.S. *J. Magn. Reson.* **1977**, 28, 105.

4.15 Metz, G.; Wu, X.; Smith, S.O. *J. Magn. Reson. A* **1994**, 110, 219.

4.16 Marks, D.; Vega, S. *J. Magn. Reson. Ser. A* **1996**, 118, 157.

4.17 Preston, C.M.; Blackwell, B.A. *Soil Sci.* **1985**, 139, 88.

4.18 Voelkel, R. *Angew. Chem. Int. Ed. Engl.* **1988**, 27, 1468.

4.19 Wilson, M.A. NMR Techniques and Applications in Geochemistry and Soil Chemistry; Pergamon Press, Oxford, 1987. (and reference cited there in).

4.20 Axelson, D.E. Solid State Nuclear Magnetic Resonance of Fossil Fuels; Multiscience Publications Ltd: Canadian Government Publishing Centre, Supply and Services Canada, 1985. chap 1-3 and 6 (and reference cited there in).

4.21 Stejskal, E.O.; Memory, J.D. High Resolution NMR in the Solid State: Fundamentals of CP/MAS; Oxford University Press, New York, 1994. Chap 2 and 3 (and reference cited therein).

4.22 Earl, W.L.; VanderHart, D.L. *Macromolecule*, **1979**, 12, 762.

4.23 Ernst, R.R.; Bodenhausen, G.; Wokaun, A. Principles of Nuclear Magnetic Resonance in One and Two Dimensions; Oxford University Press, New York, 1994. chapter 6.

4.24 Freeman, R. A. Handbook of Nuclear Magnetic Resonance; Longman Science & Technical, Essex, England, 1988. pp 291-297.

4.25 Opella, S.J.; Frey, M.H. *J. Am. Chem. Soc.* **1974**, 101, 5854.

4.26 Wilson, M.A. *J. Soil Sci.* **1984**, 35, 209.

4.27 Malcolm, R.L. *Anal. Chim. Acta.* **1990**, 232, 19.

4.28 Underdown, A.W. PhD thesis, Carlton University, Ottawa, 1982.

Chapter 5
The Development of a New CP-MAS ^{13}C NMR Procedure for the Study of Humic Materials.

As discussed in chapter 2, the recommended (standard) method of obtaining a CP-MAS ^{13}C NMR spectrum of a humic material is to use the SACP pulse sequence, a low field instrument, and slow spinning rates (less than 5 kHz). Recently, there has been a proliferation of high-field CP-MAS instruments. This proliferation of high-field CP-MAS instruments results mainly from the fact that the same instrument can be used for liquid and solid state measurements. And in liquid NMR the higher the field the higher the sensitivity and resolution one obtains. However, in solid state NMR higher fields also lead to larger linebroadening due to CSA effects (note: the CSA effect is a function of the magnetic field strength). Thus, the proliferation of high-field CP-MAS has led to the commercial availability of MAS probes capable of spinning rates up to 25 kHz. Concurrent with this, modifications have been developed for the CP-MAS pulse to alleviate the CP problem due to high-speed spinning. The most promising pulse sequence for large heterogeneous macromolecular polymeric mixtures such as humic substances is Ramp-CP, as discussed in Chapter 3.

These advances have been addressed in terms of theory in Chapter 3. In this chapter the effects of high fields and high MAS rates when used with Ramp-CP for the study of humic substances are experimentally investigated.

5.1 LFA

In this study it was found that the liquid state spectrum and CP-MAS spectrum

obtained with Ramp CP and a contact of 3 ms are in good agreement with one another. Because of this cross correlation, possible loss of organic matter during filtration is shown to be negligible, and the liquid state ^{13}C NMR spectrum can be considered to be an accurate qualitative and quantitative representation of the carbon distribution of LFA. Thus, the liquid state spectrum of LFA, Figure 5.1, will be considered as the reference spectrum, while the solid spectra obtained via CP-MAS ^{13}C NMR must be compared to it because of the possible biasing in CP. This may not always be the case for humic materials since the liquid sample must be filtered which may lead to loss of organic matter if there is coagulation, and humic materials are known to coagulate.[5.1] Also, the liquid spectrum takes a long period of time (3 to 4 days) to obtain, during this time the dissolved humic material may start to degrade.

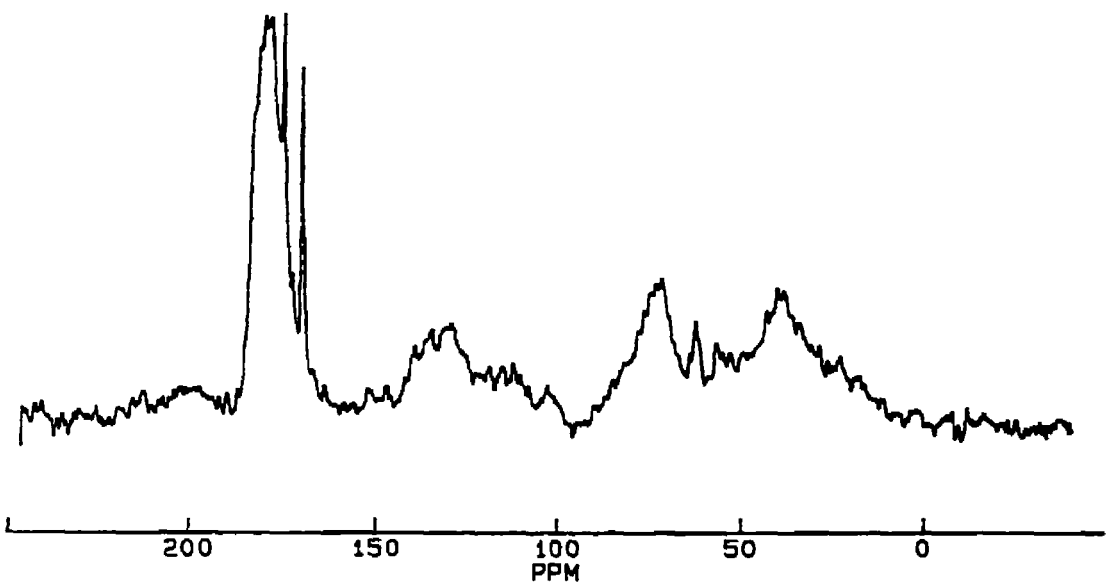

Figure 5.1: Liquid state ^{13}C NMR spectrum of LGA.

5.1.1 Effects of Sample Spinning Speed

5.1.1.1 SACP

Table 5.1 shows the changes in different carbons, via %TOC (percentage of total observed carbon), as a function of spinning rate for the SACP spectra. Representative SACP spectra are shown in Figure 5.3. There are large effects with increasing spinning speed. Figure 5.2 highlights the increase in observable aromatic carbon in terms of %TOC. The largest increase occurs between 5 and 8 kHz (centred at around 6.5 kHz). Since the carboxyl carbons in terms of %TOC are inversely related to the aromatic carbons

Table 5.1: %TOC as a function of spin rate of LFA interrogated with the SACP pulse sequence.

	Spinning rate (/kHz)					
Chemical Shift Assignment(/ppm)	2.5	5.0	7.0	8.0	10.0	14.0
Ketonic (190-220)	2.1±0.5	6.1±0.3	5.0±0.2	3.8±0.2	4.8±0.2	3.3±0.3
Carboxyl (162-190)	23.0±0.3	27.8±0.3	25.3±0.2	21.9±0.2	21.7±0.2	16.3±0.2
Phen./Arom. (108-162)	1.7±0.7	1.9±0.3	6.0±0.2	6.9±0.2	6.9±0.2	7.6±0.3
O-C-O (96-108)	1.6±0.7	1.5±0.6	2.0±0.2	2.4±0.2	2.1±0.2	2.4±0.3
Carbohydrate (50-96)	29.3±0.2	28.2±0.2	28.0±0.2	28.2±0.2	28.6±0.2	31.0±0.2
Aliphatic (0-50)	42.3±0.2	34.5±0.2	33.7±0.2	36.8±0.2	35.9±0.2	39.4±0.2
Signal to noise ratio	19.7±0.2	30.2±0.2	30.3±0.1	40.9±0.1	34.2±0.1	17.2±0.3

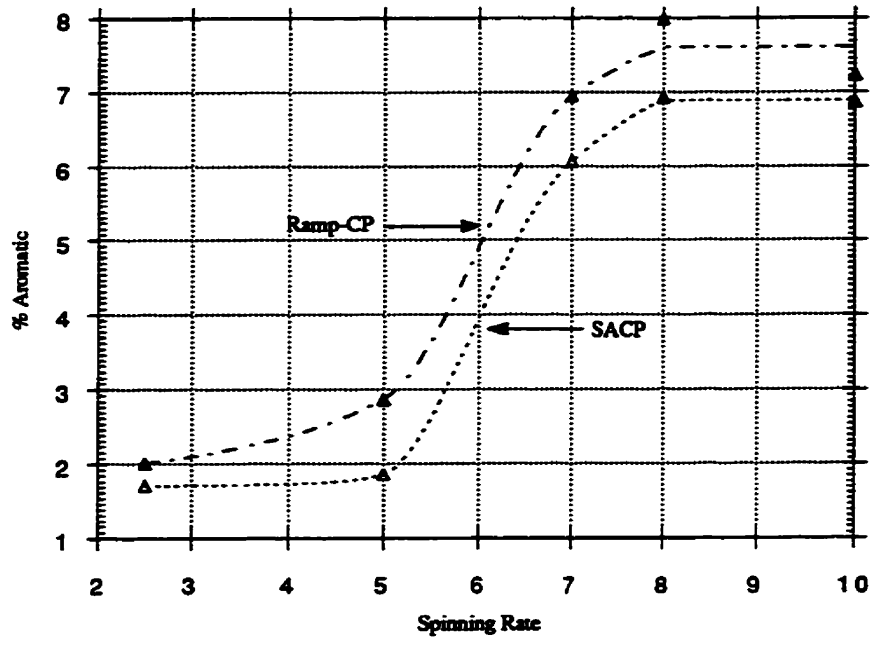

Figure 5.2: Quantity of observable aromatic carbons in terms of %TOC as a function of spinning rate.

(this is also true for LHA, see below). It is likely that excessive broadening of the aromatic region at low spinning speeds is responsible for the low aromaticities observed under those conditions.

Thus, it seems the aromatic signal is always in the spectrum even at sample spinning rates as low as 2.5 kHz, but it can be too broad to be resolved well. This may explain the decrease in the carboxyl peak. If we assume that at low sample spinning rates the aromatic peak is so broad that it underlies the carboxyl peak in significant measure, less of it will lie under the carboxyl peak at higher spinning rates. This will appear in the spectral integrals, but it will also affect the phase and baseline correction in such a manner

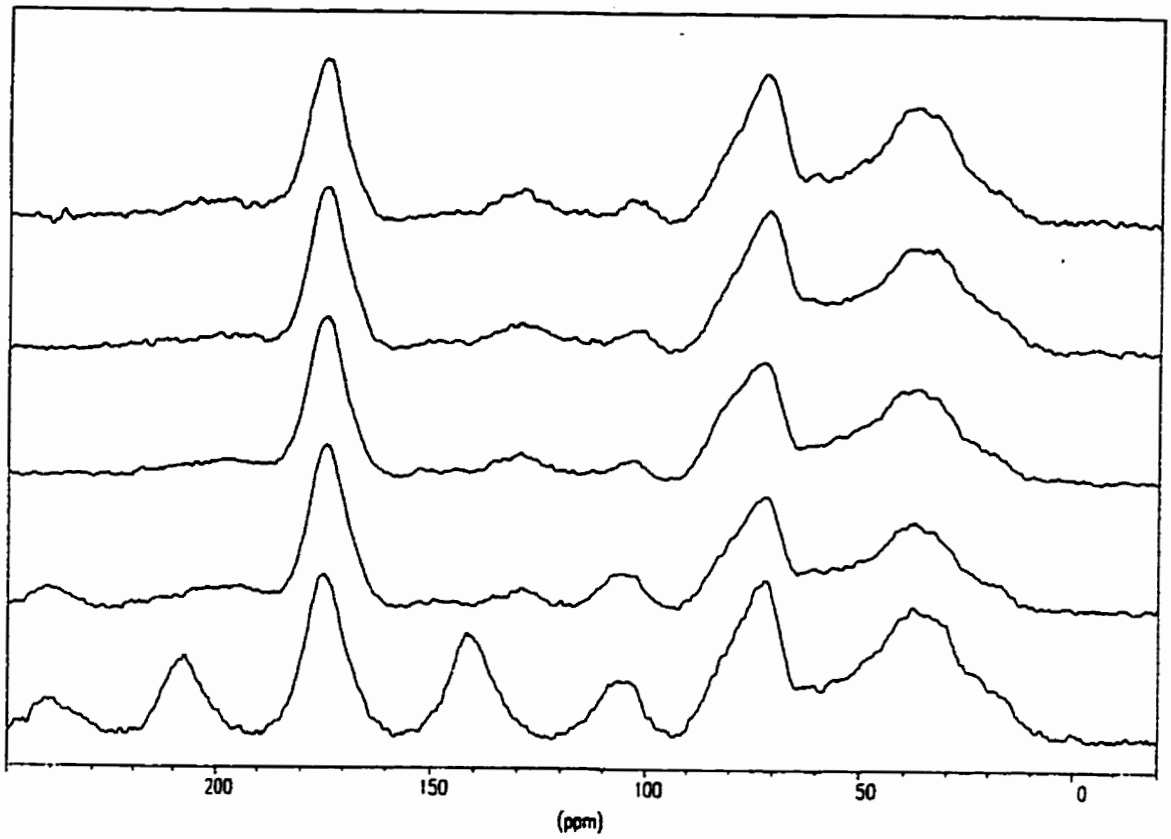

Figure 5.3: SACP pulse sequence spectrum at spinning rates 2.5, 5, 7, 8, 10 kHz, from bottom to top.

as to decrease the effect the broad aromatic peak has on the carboxyl peak as the aromatic peak narrows. This is confirmed by the fact that the percentage of total carbon assigned to carboxyl carbons decreases as a near mirror image to the increase of aromatic carbons as the sample spinning rate increases.

No literature could be found which reports a humic material ^{13}C CP-MAS NMR experiment run at higher sample spinning frequencies than 5 kHz, and as the results above show this is still in the low % aromatic (aromaticity) domain. So the question must be

posed, has the seemingly low aromaticity in many humic materials previously observed in ^{13}C CP-MAS NMR been real or an artefact of a suboptimal spinning rate?

5.1.1.2 Ramp CP

If the Ramp CP sequence is used then the motional modulation of the CH coupling is eliminated, and the spin rate dependence of the carbon distribution observed must arise via chemical shift anisotropy (see Section 3.1.2.2). Representative Ramp-CP spectra are shown in Figure 5.4. Table 5.2 shows the changes in proportional carbon intensities and the total intensity with spinning rate for the Ramp-CP spectra. Once again, there are large effects with increasing spinning speed, Figure 5.2 highlights the increase in aromatic

Table 5.2: Table 5.1: %TOC as a function of spin rate of LFA interrogated with the SACP pulse sequence.

	Spinning rate (/kHz)					
Chemical Shift Assignment (/ppm)	2.5	5.0	7.0	8.0	10.0	14.0
Ketonic (190-220)	1.9±0.4	2.0±0.3	3.4±0.2	4.2±0.2	6.0±0.2	1.4±0.2
Carboxyl (162-190)	12.8±0.2	18.0±0.2	25.5±0.2	29.0±0.2	28.6±0.2	13.2±0.2
Phenolic/Arom. (108-162)	2.0±0.5	2.90.3	7.0±0.2	8.0±0.2	7.2±0.2	12.2±0.3
O-C-O (96-108)	2.4±0.4	2.5±0.3	2.5±0.2	2.9±0.2	2.4±0.2	2.4±0.3
Carbohydrate (50-96)	35.1±0.2	31.3±0.2	25.6±0.2	23.2±0.2	24.5±0.2	30.±0.2
Aliphatic (0-50)	45.8±0.2	43.3±0.2	36.0±0.2	32.7±0.2	31.3±0.2	40.4±0.2
Signal to noise ratio	24.2±0.2	36.0±0.1	49.1±0.1	60.4±0.1	52.5±0.1	12.6±0.2

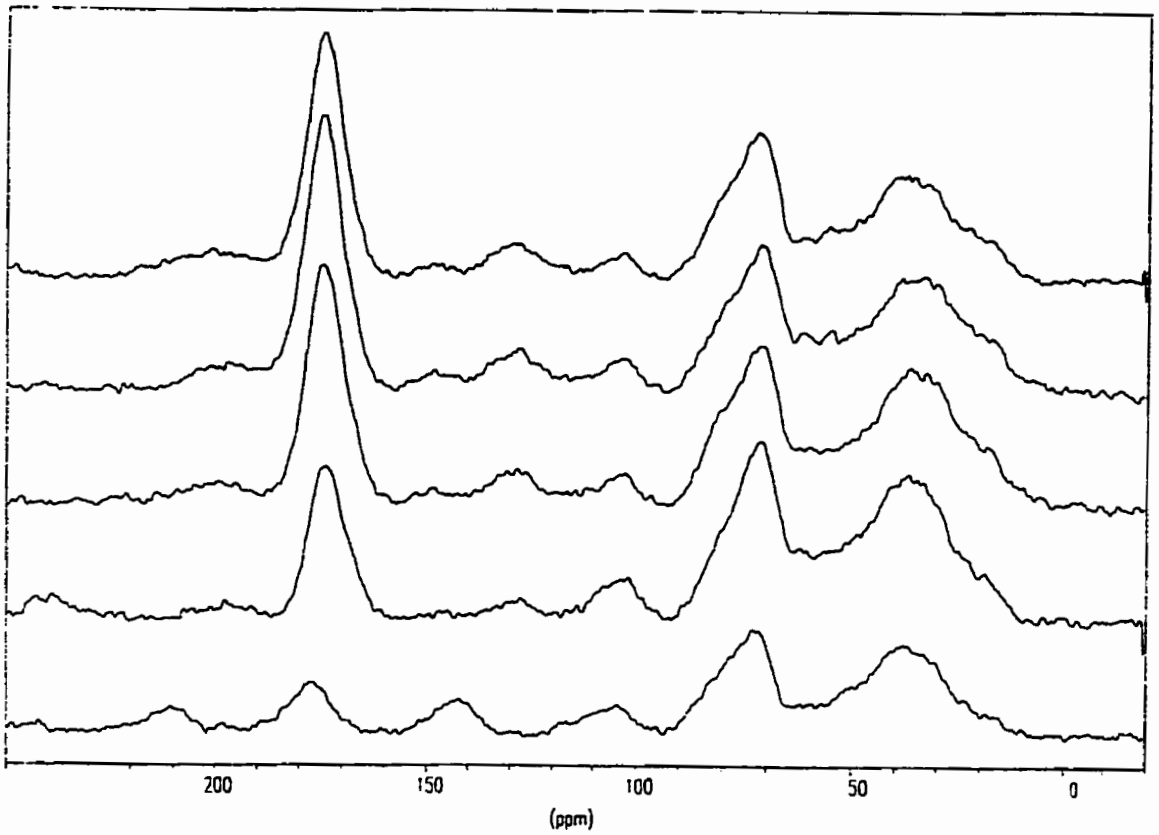

Figure 5.4: Ramp-CP pulse sequence spectrum at spinning rates 2.5, 5, 7, 8, 10 kHz, from bottom to top.

carbon as %TOC. By comparing the results of the two different pulse sequences it can be seen that with the Ramp-CP pulse sequence we are getting identical spinning dependencies for the aromatic carbons as with the SACP pulse sequence.

However, the carboxyl fraction acts very differently with the Ramp-CP pulse sequence than it did with the SACP pulse sequence. Since, the Ramp-CP pulse sequence is expected to sample more types of carbon within the same general type of moiety, it should better sample the carboxylic carbons. This is strongly supported by the way the carboxyl peak increases with spin rate (see discussion below as well as section 3.2.9). As

the carboxyl peak grows in the aromatic peak is narrowing, thus underlying the carboxyl peak much less, giving rise to the steepening of the carboxyl peak on the aromatic side. At the same time the ketonic peak is growing on the ketonic side and starts to overlap with the carboxyl peak. If this is the case, then the increase in carboxyl carbons from a spinning rate of 2.5 kHz to 7 kHz is a result of the line narrowing discussed above for the aromatic carbons.

Because the Ramp CP pulse sequence eliminates variation in spectra due to line broadening by motional modulation of the CH coupling, the only reason for the line broadening that we can identify is the motional modulation of the resonance frequency via CSA. This leads to the conclusion that the CSA for the aromatic carbons is centred between 26 and 28 kHz for LFA. Thus, to obtain quantitative representation, one needs to spin a sample at higher than 7 kHz for LFA when using 7 T solid state NMR spectrometer.

5.1.1.3 Signal to Noise Ratio

If one considers signal to noise ratio (using the carboxyl peak as the signal) and assumes that the greater the value the larger the number of carbons being sampled, a truer representation is obtained for the carbons in the sample for large signal to noise ratio results. It can be seen from Tables 5.1 and 5.2 that for the LFA sample the optimal spinning rate is at approximately 8 kHz.

The signal to noise ratio for the 14 kHz experiments are low in comparison to the rest of the results at spinning rates above 0.25 of the aromatic CSA. It is believed that this spinning rate is beyond the instrumental stability for these samples. Therefore they are not considered in any great detail. The Ramp-CP pulse gives better signal to noise ratios than the SACP pulse sequence in accord with Smith et. al.[5.2]

5.1.2 Contact Time

Both the SACP and Ramp-CP methods give a more quantitatively and qualitatively correct spectrum (considering the liquid state spectrum as the reference, for the reason discussed earlier) using a contact time of 3 ms, as can be seen from Table 5.3. However, a 1 ms contact time gives a better signal to noise ratio with both methods. It must be pointed out that contact time has a very different meaning for SACP than it does for Ramp-CP,

Table 5.3: %TOC of each chemical shift region for LFA under different experimental conditions (note: Ramp-CP takes place on the -1 sideband).

Chemical Shift Assignments (ppm)	Contact time = 1 ms		Contact time = 3 ms			Liquid State
	SACP	Ramp CP	SACP	SACP on the -1 sideband	Ramp CP	
Ketonic (190-220)	1.8%	5.1%	4.6%	4.2%	8.8%	6.9%
Carboxyl (162-190)	17.0%	26.8%	23.4%	27.4%	33.8%	32.4%
Phenolic (145-162)	1.4%	1.5%	1.8%	2.9%	2.1%	1.5%
Aromatic (108-145)	7.5%	7.5%	10.5%	11.4%	12.0%	14.2%
O-C-O (96-108)	2.7%	2.5%	3.9%	3.8%	3.6%	2.9%
Carbohydrate (50-96)	30.7	26.2%	24.2%	22.2%	17.8%	19.1%
Aliphatic (0-50)	38.9%	30.4%	31.6%	28.1%	21.9%	23.0%

since in Ramp-CP the spinlock condition on one of the channels is changing throughout, while on the other channel the condition is held, during Ramp-CP. In Ramp-CP the contact time will depend on the ramp's range of frequencies and scan rate (determined by the contact time).

From the Chapter 3, we can see that for a mixture of different I_NS systems there will be an optimum contact time in which the interplay between T_{SI} and $T_{1\rho}I$ produces a spectrum that is the closest to the "real" spectrum, in our case confirmed by the liquid spectrum. For LFA the optimum contact time has been found to be 3 msec for SACP on both the -1 and central sideband and for Ramp-CP.

5.1.3 Comparing SACP on the -1 Sideband and on the Central Band

As can be seen in Table 5.3, the spectrum obtained on the -1 sideband with a contact time of 3 ms is a more accurate representation of the liquid spectrum than the spectrum obtained on the central band with a contact of 3 ms. This is more apparent if one compares the spectra in Figure 5.5 to the liquid spectrum shown in Figure 5.1. The differences in the two SACP spectra can also be seen in Figure 5.5. The most obvious difference between the two SACP spectra is in the magnitude of the carboxylic carbon signal (162-190 ppm). There is also a difference in the aromatic signal magnitude. In both cases the spectrum obtained on the -1 sideband has a larger signal. This can be explained by the difference in the efficiency of CP on the -1 sideband compared to the central band. This may be due to the fact that T_{SI} (T_{CH} in our case) is too long in comparison with $T_{1\rho}I$ ($T_{1\rho}H$ in our case) on the central band, while on the -1 sideband this is less the case. Put in another way, a contact time of 3 ms is not long enough for full CP to take place if the operation is taking place on the central band. But, a contact time longer than 3 ms will lead

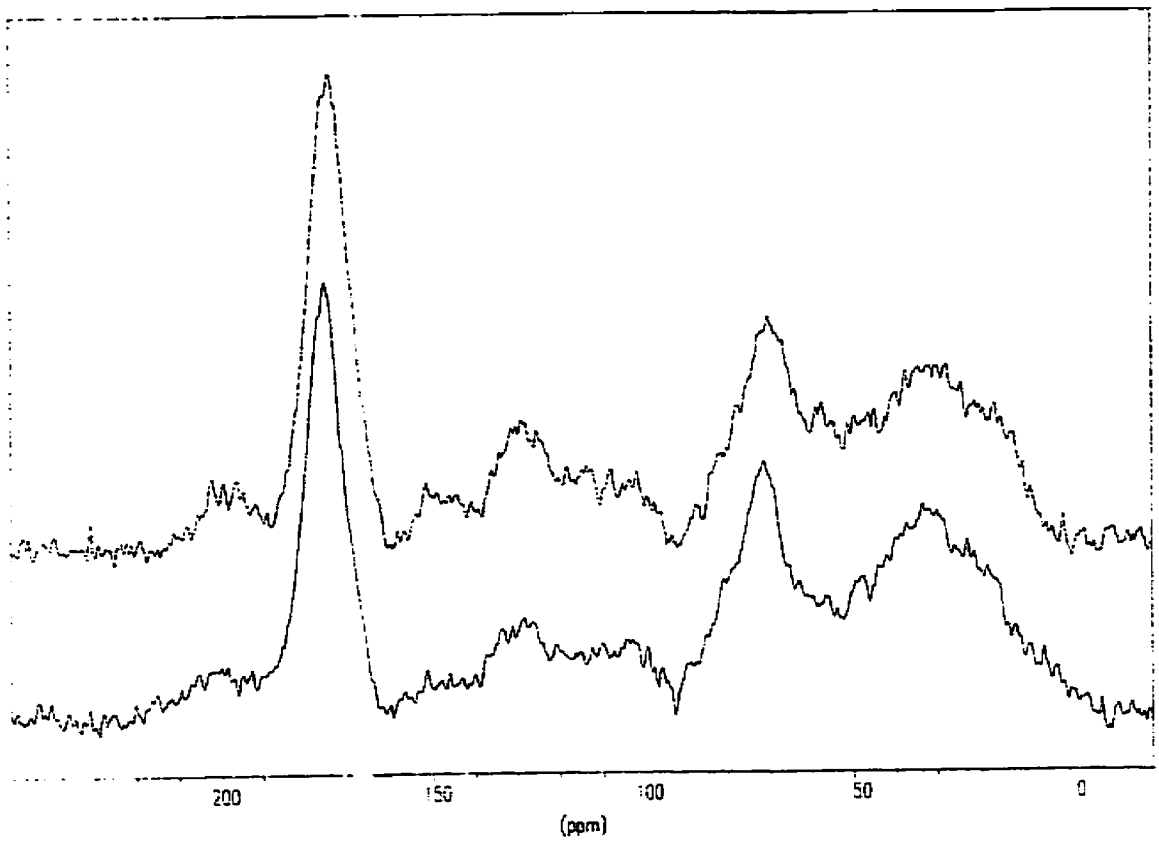

Figure 5.5: The top spectrum was obtained on the -1 sideband, while the bottom spectrum was obtained on the central sideband, see text for further explanation.

to too much signal being lost to spin-lattice relaxation of the protons in the rotating frame. However, a contact time of 3 ms allows for a much fuller CP to take place if the operation is performed on the -1 sideband. This is because the rate of CP is faster on the -1 sideband than on the central band, as discussed above. This explanation is supported by the fact that the aliphatic region is almost identical for the two spectra in question, since the CP rate for aliphatic moieties is faster than the CP rate for carboxylic and aromatic moieties. Thus, for a sample that may have slow CP rates, it is preferable to perform CP on the -1 sideband.

5.1.4 Comparing Ramp-CP and SACP on the -1 Sideband

Ramp-CP in this paper takes place on the -1 sideband, for the reasons discussed in the previous section. This then means that any difference seen between a Ramp-CP spectrum and a SACP spectrum on the -1 sideband is due only to the ramping of one of the channels spin-lock condition. As can be seen in Table 5.3, the spectrum obtained with Ramp-CP is in better agreement with the liquid spectra than the spectrum obtained with SACP on the -1 sideband, using a contact time of 3 ms. This is more apparent if one compares the spectra in Figure 5.6 to the liquid spectrum shown in Figure 5.1. The

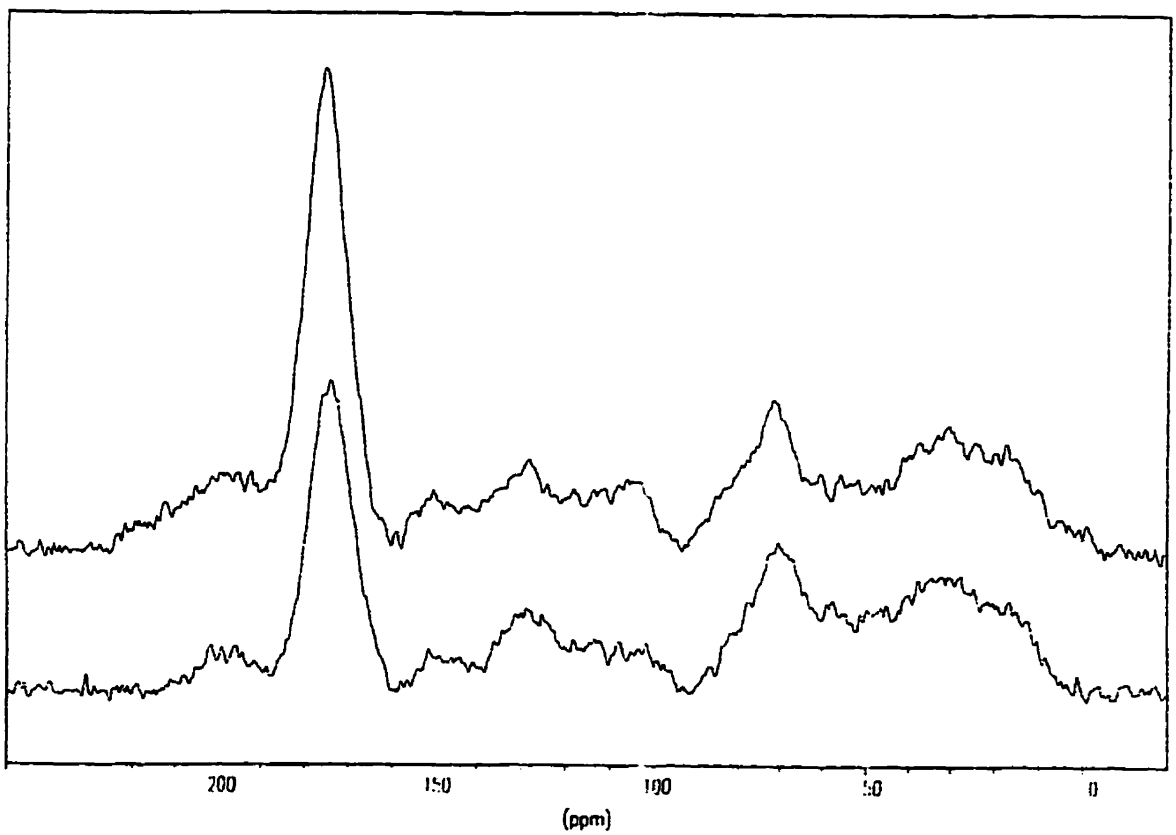

Figure 5.6: The top spectrum was obtained with Ramp-CP, while the bottom spectrum was obtained with SACP, see text for further explanation.

sideband can be seen in Figure 5.6. The major difference between the spectra is that the intensity for the carboxylic carbons is substantially greater in the spectrum obtained via Ramp-CP. The same holds true for the ketonic carbons, phenolic carbons, and carbons singly bonded to two O atoms. All these types of carbons can be expected to give narrow HH sidebands, especially at the spinning speed needed to overcome the CSA broadening effects in this sample. The SACP approach does not allow all the HHs of this sample to be satisfied. The narrower the HH matching sidebands, the more of a problem this becomes. Ramp-CP is able to satisfy multiple HH and thus produces efficient CP for all systems in the sample. Figure 3.9 gives a visual explanation. By combining Table 5.3 and Figures 3.9, 5.1 and 5.6, it can be seen that for complex systems, such as LFA, Ramp-CP will always give the most accurate spectra.

5.1.5 Comparing Ramp-CP and Liquid State

As has been discussed above the Ramp-CP, approach, with a contact time of 3 ms, gives the most liquid-like spectrum for LFA. However there are some differences between the two spectra. These can best be seen by comparing the liquid state spectrum in Figure 5.1 to the Ramp-CP spectrum in Figure 5.6. The first difference is that the liquid state gives better resolution in the carboxylic area. On the other hand, Ramp-CP appears to give better resolution for the ketonic and phenolic carbons. However, on a whole, it appears that the liquid state spectrum is slightly better resolved than the Ramp-CP spectrum is, if the noise level is taken into consideration. Liquid state spectra take more than 10 times the amount of time to achieve the same signal to noise ratio as Ramp-CP spectra. If any NMR characterisation of the sample is needed in which multiple spectra must be obtained Ramp-CP is the superior option. This is especially true for LFA and other humic materials which

may not be stable in some solutions for the length of time needed to do full characterisation in the liquid state. As noted above, to achieve the resolution seen in Figure 5.1 the sample must be filtered and thus there may be some biasing of the liquid spectra, as humic materials are known to coagulate in solution under many circumstances.

5.2 LHA

The same analysis was carried out on LHA from which it was found that the optimal spinning rate is 8 kHz, the optimal contact time is 2.5 ms. The major results of the analysis are shown in Table 5.4, while the ^{13}C NMR liquid spectrum and the optimal ^{13}C

Table 5.4: %TOC of each chemical shift region for LHA under different experimental conditions.

	Contact time = 1 ms		Contact time = 2.5 ms	
Chemical Shift Assignments (/ppm)	SACP	Ramp CP	Ramp CP	LiquidState
Ketonic (190-220)	2.9%	3.1%	6.5%	2.9%
Carboxyl (162-190)	9.5%	15.1%	15.6%	28.2%
Phenolic (145-162)	1.5%	3.0%	2.8%	2.5%
Aromatic (108-145)	14.9%	15.4%	18.7%	25.3%
O-C-O (96-108)	1.5%	0.4%	1.0%.	2.0%
CH_3O-, etc. (60-96)	12.8%	13.3%	11.9%	12.3%
Anomeric (50-60)	9.1%	10.6%	9.1%	4.2%
Aliphatic (0-50)	47.8%	39.1%	34.3%	22.0%

Ramp-CP-MAS NMR spectra are shown in Figures 5.7 and 5.8, respectively. Ramp-CP works better than SACP in terms of qualitative and quantitative sampling of the carbons in the sample. It should be noted that the best CP-MAS ^{13}C NMR spectrum obtained for LHA is not in as good agreement with the liquid spectrum of LHA as the best CP-MAS ^{13}C NMR spectrum of LFA, under optimal conditions, when compared to the liquid spectrum of LFA. There are two possible explanations for this. The first is that the solution spectra is in corrected because of filtration as discussed previously. For LHA this is more of a problem than for LFA, since LHA is less soluble. The second reason is that LHA may have more stable radicals than LFA. This reason is supported by evidence presented in the next section, and is consistent with the aliphatic region being positively biased in the CP-MAS spectra, as this type of moiety is the least likely to be where the stable radicals are located.

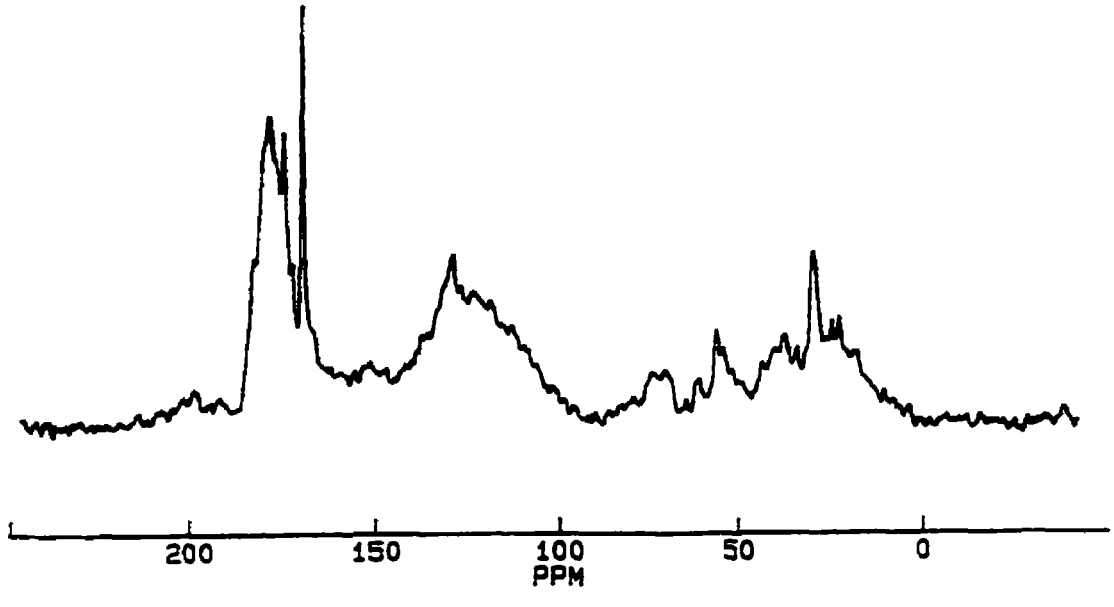

Figure 5.7: Liquid state ^{13}C NMR spectrum of LHA

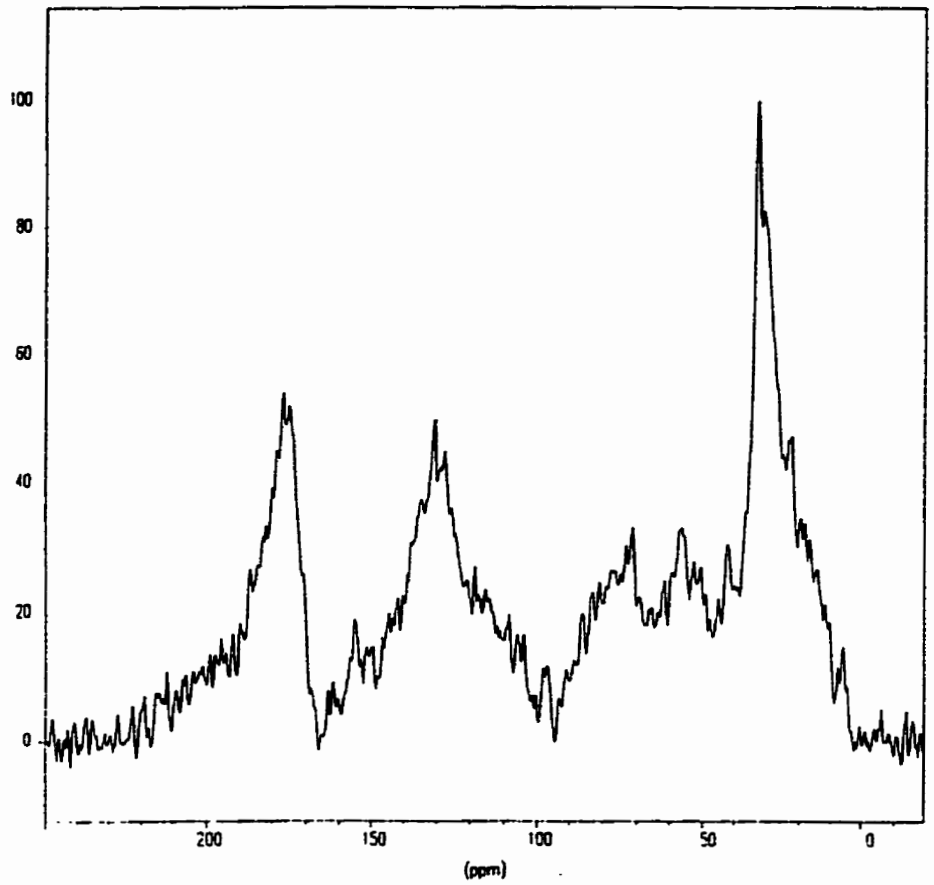

Figure 5.8: Ramp-CP-MAS ^{13}C NMR spectrum of LHA obtained under optimal conditions.

5.3 Implications

The good agreement between the liquid spectra and the solid state spectra obtained at 7 T by Ramp-CP at spinning rates higher than 0.25 of the aromatic CSA of the humic material implies that, for the solid state ^{13}C NMR study of humic materials:

- The sample must be spun at higher rates than 0.25 times its aromatic CSA which must be found for each unique sample.
- The optimal contact time must be found for each unique sample.

- It is preferable to do CP on the -1 matching sideband, or the 1 matching sideband, as T_{CH} is the shortest on these sidebands. The weaker the heteronuclear dipolar interactions, the more important this factor.
- Because of sideband (matching not spinning) narrowing, due to both weak homonuclear dipole interactions and sample spinning, multiple HHs will arise which can be covered by Ramp-CP but not SACP. Thus in terms of sampling the carbons without bias, Ramp CP gives a more realistic spectrum than SACP.
- For complex samples Ramp-CP is a preferable technique to SACP.
- The faster the sample is spun and/or the weaker the homonuclear and/or heteronuclear dipolar interactions the better the Ramp-CP technique will perform in giving both qualitatively and quantitatively accurate spectra.
- The highest resolution and most realistic CP-MAS spectra can be obtained with a high field spectrometer, if the sample is spun at a rate higher than 0.25 the anisotropy of the chemical shift of the aromatic moieties and a Ramp CP pulse sequence is used.
- The percentage aromatic carbons in humic materials may be underestimated by previous CP-MAS ^{13}C NMR methods.

5.4 Summary

High field instruments will give better resolution and sensitivity. However, to take advantages of this, the standard CP-MAS method for humic materials must be altered. The first alteration is higher sample spinning rates at higher fields, since CSA broadening is more problematic the higher the field. The faster one spins the sample, the narrower the HH gets, and the larger the probability of Hartmann-Hahn mismatches. This situation can

be overcome by using Ramp-CP. Thus, by the combination of high field, fast sample spinning, and Ramp-CP the CP-MAS approach can deliver spectra that are almost the equal of liquid state NMR. This allows for the cross checking of spectrum obtained by the two methods. This agreement also allows for the use of the CP-MAS approach in the qualitative and quantitative characterisation of humic material and other complex heterogeneous mixtures.

References

5.1 Buffle, J. Complexation Reactions in Aquatic Systems. An Analytical Approach; Ellis Harwood Ltd, Chester, UK, 1988, pp 184-87.

5.2 Metz, G.; Wu, X.; Smith, S.O. *J. Magn. Reson. A* **1994**, 110, 219.

5.3 Cook, R.L.; Langford, C.H.; Yamdagni, R.; Preston, C.M. *Anal. Chem.* **1996**, 68, 3979.

Chapter 6
Characterisation of the Protonated Form of LFA and LHA

This chapter will deal with structural information from ^{13}C NMR and luminescence studies. As discussed in chapter 2, luminescence has become a very useful tool in the characterisation of humic materials. In this chapter steady state emission and synchronous luminescence as well as time resolved luminescence along with size exclusion chromatography have also been used to characterise the protonated form of LFA.

^{13}C NMR, in particular CP-MAS ^{13}C NMR, has become the preeminenent tool for the investigation of humic materials. However, there has always been concern as to the quantitative nature of CP-MAS based techniques. In Chapter 5 these concerns have been addressed, and it was shown that high field, high sample spinning speed and Ramp-CP-MAS when combined overcome the quantitative limitations of CP-MAS NMR. With this new method in hand, a series of experiments were carried out on the protonated forms of LFA and LHA via Ramp CP-MAS ^{13}C NMR to characterise these samples. The following chapter discusses these results in terms of functionality and structure along with the luminescence and size exclusion results.

6.1 Characterisation of LFA by Luminescence

6.1.1 Characterisation of LFA by Steady State Luminescence and Its pH Dependence

In Figures 6.1 and 6.2 the luminescence spectra for LFA are shown. In the emission luminescence spectrum (Figure 6.1) a single broad band is evident. This broad,

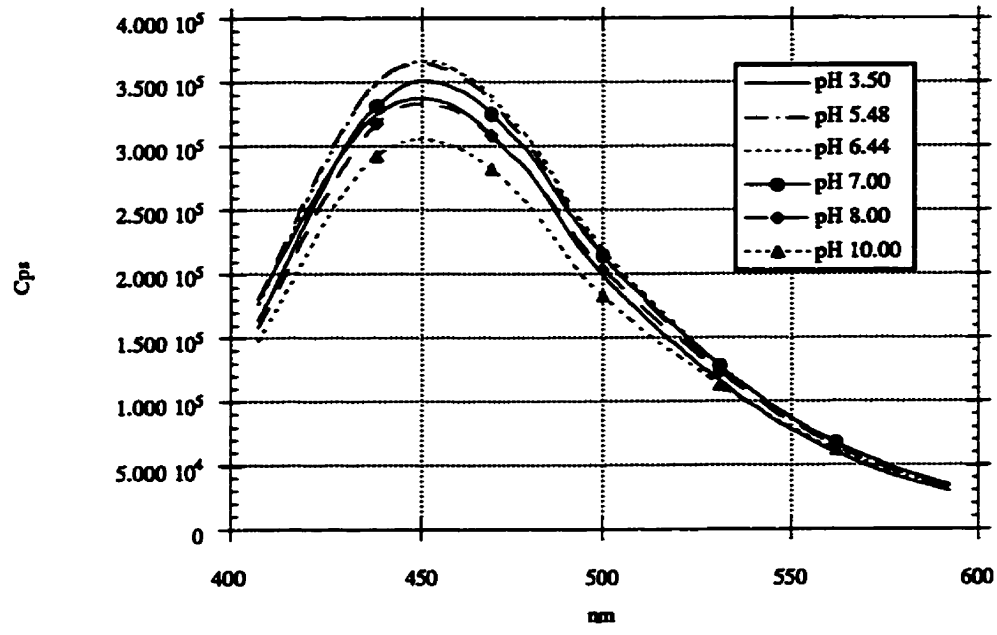

Figure 6.1: The effect of pH on LFA's fluorescence monitored by emission luminescence (Cps = counts per second).

asymmetrical, band has a maximum at ~456 nm. The asymmetry is evident from the slope in the region from ~490 nm to ~550 nm, which is indicative of another spectral feature, called from here on as the ~512 nm shoulder. All emission spectra could be fitted by a sum of two gaussians centred at 456 nm and 512 nm, confirming the generality of the 512 nm shoulder. It was found that the shape of the emission spectrum altered very little from pH 4.0 to 8.0, and a maximum signal was obtained at a pH around ~5.5. These findings are very similar to some reported previously for other fulvic acids.[6.1-6.6] The synchronous spectra of the same fulvic acid sample show much more structure as can be seen by

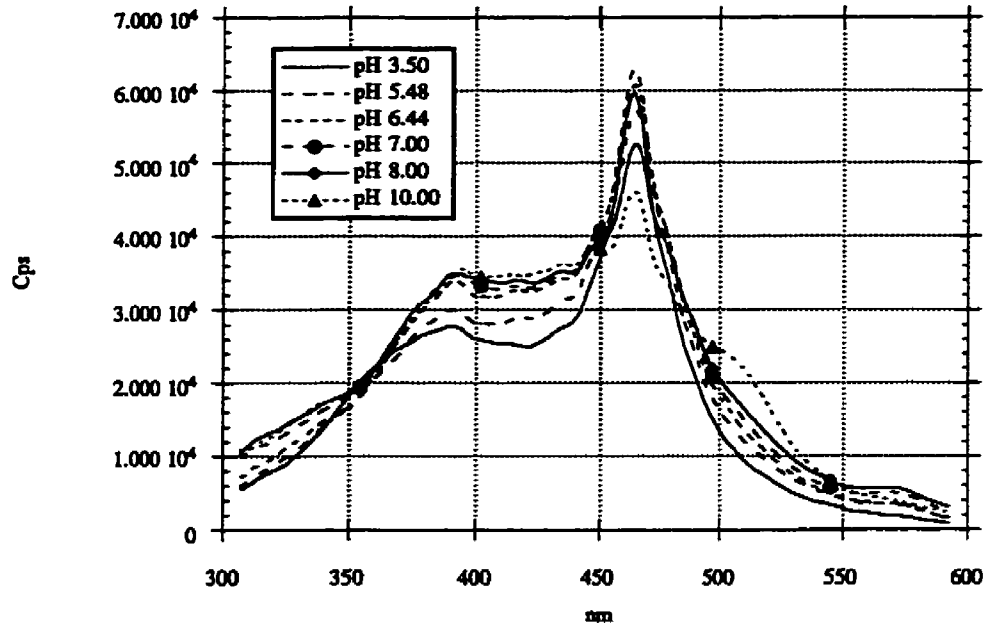

Figure 6.2: The effect of pH on LFA's fluorescence monitored by synchronous luminescence.

comparing Figures 6.1 and 6.2. First, it can be seen that the synchronous signal is ~4.5 times less intense than the emision signal, as is expected since the excitation wavelength is not chosen for optimum emission intensity. There are two peaks in the synchronous spectra at ~392 nm and ~465 nm, and a shoulder at ~512 nm. The pH dependence is more complex. The maximum signal was obtained at pH 5.5 for the 465 nm peak while the maximum for the 392 nm feature was found to be at pH 10 (the highest pH studied). As well the shoulder at 512 nm grew in as the pH increased. There was some change in the shape of the 465 nm peak as pH increased. There is evidence of shoulder growth on either

side of that peak (~447 nm and ~478 nm). It should also be noted that the maximum quantum yield is very likely occurring at pH 5.5.

The dependence of the synchronous luminescence spectra on pH can be interpreted in terms of four distinct features. (i) The first of these is a luminescence increase between pH 3.5 and 5.5. This change can be correlated with the deprotonation of type A carboxylic groups (defined in reference 6.7 as the more acidic carboxylates). (ii) Between pH 5.5 and 6.5 there is a very gradual decrease in luminescence, as well as the growth of a shoulder on both sides of the 465 nm peak, and a simultaneous large increase in the 392 nm peak. This can be related to the deprotonation of type B carboxylic groups (defined in reference 6.7 as the less acidic carboxylates). (iii) From pH 7.0 to 8.0 the 465 nm feature decreases drastically. This change may correlate to deprotonation of acidic -OH groups (previously these groups have been interpreted as phenolic groups, but the NMR results discussed below contradict this interpretation and favour -OH on carbohydrate structures). (iv) The final aspect is an increase in the 512 nm shoulder from pH 8.0 to 10.0. This can be correlated with deprotonation of -OH groups with pK_as in this region. In this pH range a weak peak to the blue of the 465 nm has developed at ~447 nm. From this study it can be seen that synchronous luminescence resolves distributions of luminophores that emission luminescence does not distinguish.

6.1.2 Characterisation of LFA by Luminescence Lifetimes

It was found that a minimum of three components were required to fully describe the emission decay of this sample of fulvic acid. The Chi-square tests (χ^2 [the lower the better]) of the one, two, and three component fits are 1.354, 0.241, and 0.232 (as given by Kaleidagraph), respectively, while the correlation coefficient values (the closer to 1.0000

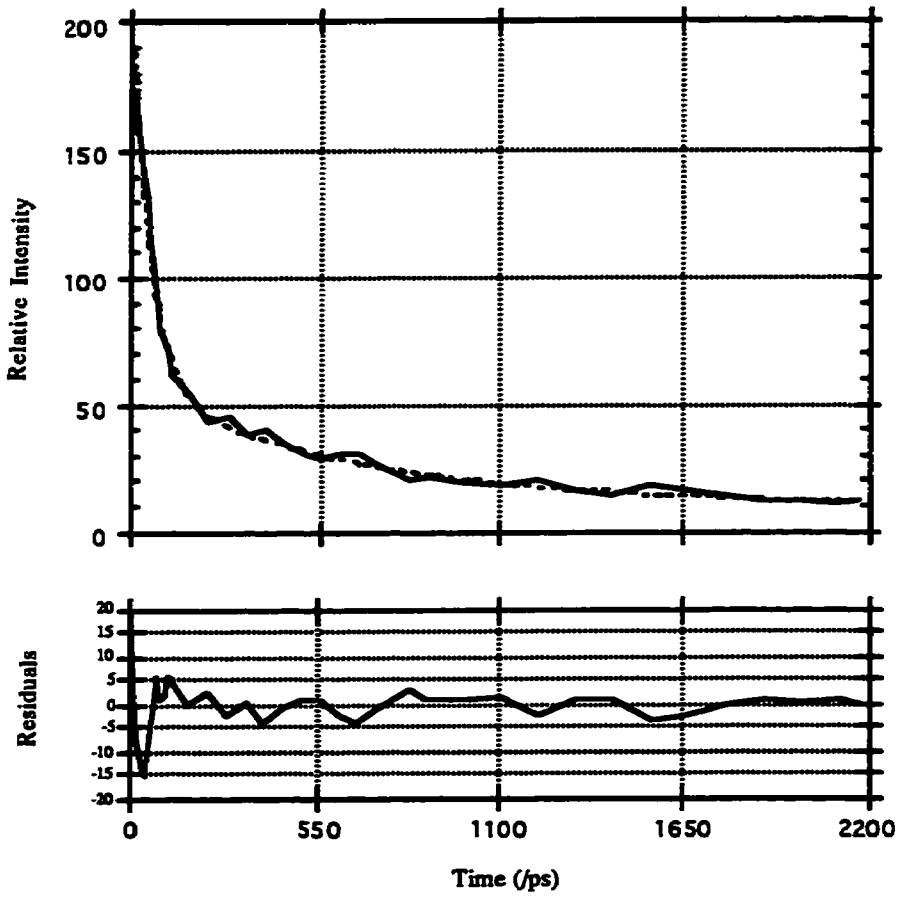

Figure 6.3: LFA's time resolved fluorescence fitted with three components, and residuals for this fit, where the solid line in the upper figure is the fit and the broken line the data.

Table 6.1: Lifetime components of two fulvic acids.

	Laurentian Fulvic Acid		Armadale Fulvic Acid	
Component	Preexponential term*	Lifetime	Preexponential term*	Lifetime
1	0.66	~50 ps	0.86	200 ps
2	0.20	~430 ps	0.11	2 ns
3	0.14	4.2 ns	0.03	7 ns

* - sum of the components are normalised to 1

the better), r, for the one, two, and three component fits are 0.9926, 0.9985, 0.9986 (as given by Kaleidagraph), respectively. Figure 6.3 shows the three component fit to the picosecond data with residuals. The lifetimes and quantities of the three components are tabulated in Table 6.1. The subnanosecond components were obtained from a series of picosecond time resolution emission experiments, while the nanosecond time component was found from both the picosecond time resolution studies and independent nanosecond resolution emission experiments. It should be noted that in the nanosecond experiments the two picosecond components will not contribute, because they will have died out, but this third component must be included to maximally fit the picosecond time resolved LFA emission decay. In short, the picosecond results require two components. The nanosecond result demands a third which the picosecond results accommodate. Thus, there must be no fewer than three components. It is reassuring that a minimum of three components were also found by Power and co-workers [6.8] to fully describe the emission decay of an Armadale fulvic acid (AFA) sample as, tabulated in Table 6.1. The most important result to note from Table 6.1 is that for two different fulvic acid samples a minimum of three lifetimes were needed to describe the emission decay curve. *Caution should be exercised when considering these lifetimes, as they are a minimum set of parameters to fit the decay curves within the experimental error. There may well be a more complicated distribution of lifetimes, as the synchronous luminescence results strongly suggest.*

6.2 Characterisation of LFA by Size Exclusion

The results from monitoring a size exclusion chromatogram by both the absorbance measurements and emission luminescence are shown in Figure 6.4. From these results it

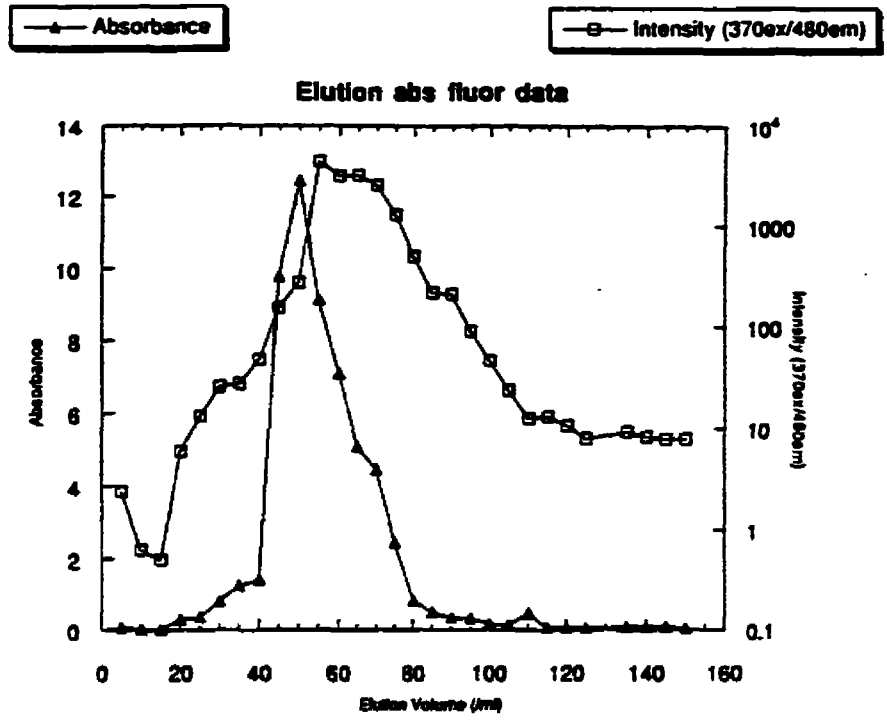

Figure 6.4: Absorbance and emission luminescence of LFA as a function of elution volume.

can be seen that the photoactive molecules are small. It can also be seen that the molecules responsible for luminescence are smaller than the molecules responsible for absorbance. Very similar results for Armadale fulvic acid (AFA) where found by Underdown et. al.[6.9] It was found that synchronous luminescence spectroscopy gave a much more detailed characterisation of the fractions than emission luminescence spectroscopy or absorption spectroscopy did. The emission luminescence spectra show a broad featureless peak, like the ones presented in Figure 6.1, for all elution volumes. The absorption spectra also show a broad featureless decay curve for all elution volumes. The synchronous luminescence spectra, on the other hand, show continual change with elution volume, as

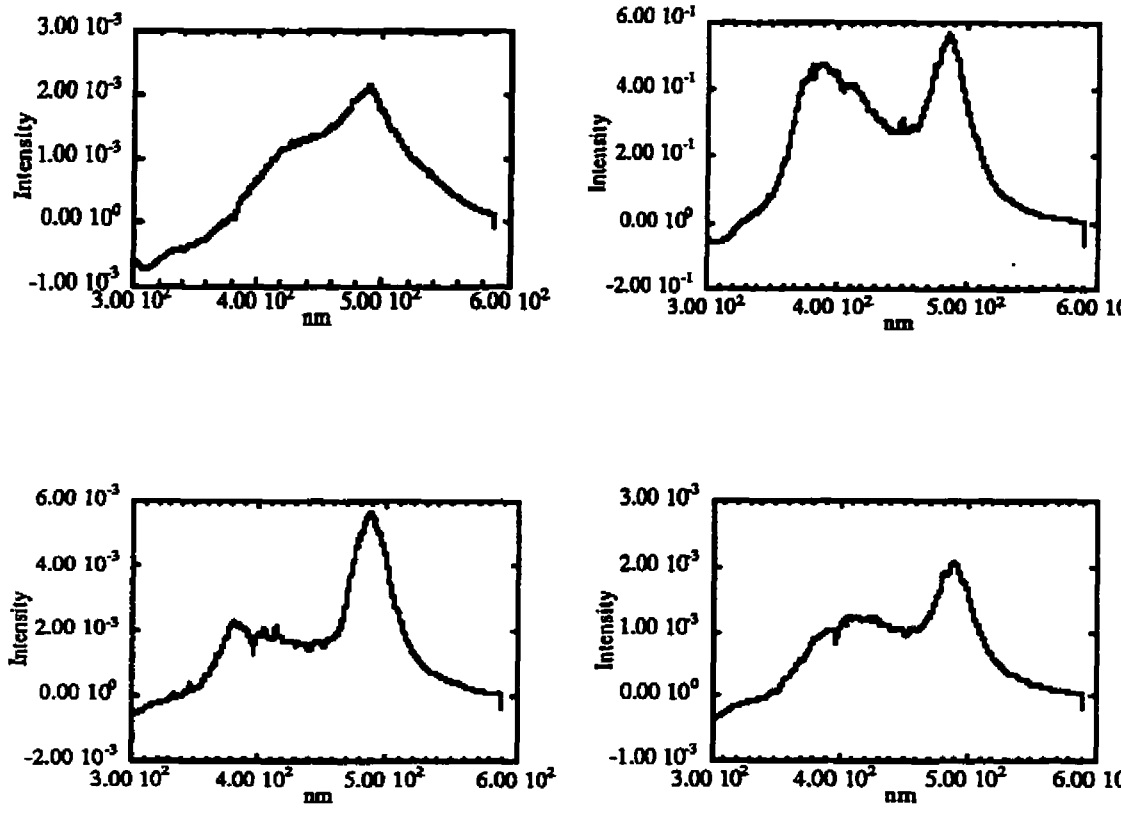

Figure 6.5: Synchronous luminescence spectra at different elution volumes in the size exclusion experiment 15-20 ml fraction (top left), 60-65 ml fraction (top right), 105-110 ml fraction (bottom left), and 135-140 ml fraction (bottom right).

can be seen in Figure 6.5. This finding suggests that there is a continual change in luminescent molecules with elution volume. But to detect these differences a high resolution technique such as synchronous luminescence must be used. This finding is further evidence that there is a complicated distribution of luminophores in LFA and probably for most, if not all, fulvic acids.

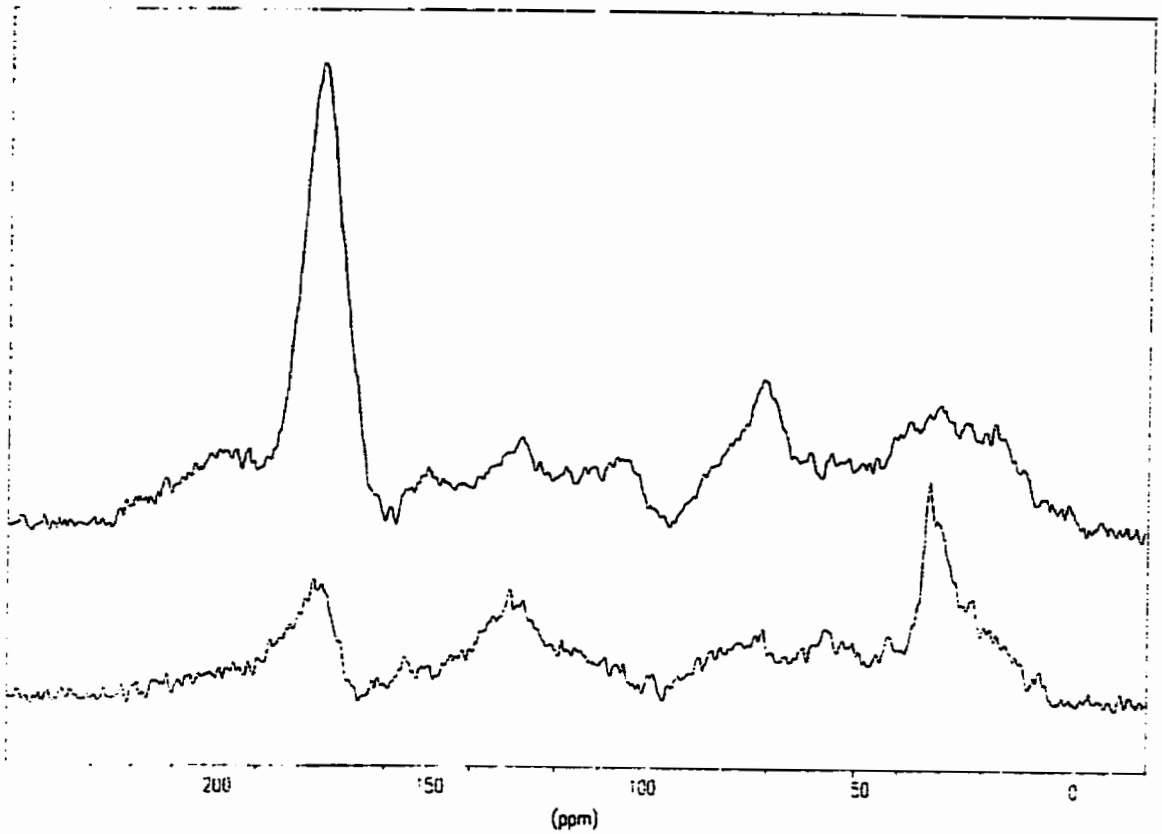

Figure 6.6: Ramp-CP-MAS ^{13}C NMR spectra of LFA (top) and LHA (bottom).

6.3 Characterisation of LFA and LHA by CP-MAS ^{13}C NMR

Consider first chemical shift evidence, Figure 6.6 shows the 1D chemical shift spectra of LFA and LHA. The integrated area of each region in the LFA and LHA spectra is expressed as a percentage of the total observable carbons (%TOC), as shown in Tables 6.2 and 6.3. From these results it can be seen that LFA is predominantly aliphatic/carbohydrate, while LHA is substantially aliphatic/aromatic in terms of structural units. The fact that aliphatic units play a major role in the molecular structures of LFA is in no way unexpected, since previous fulvic acid NMR data [6.10-6.12] have shown that the

aliphatic moieties of fulvic acid are of great importance. The fact that aliphatic moieties also play an important role in LHA is less expected, and indicates that the aliphatic moieties may deserve more attention in considering humic substance structure. For LFA, the importance of the carbohydrate moieties in structure is emphasised, since it has often been assumed that aromatic moieties play the dominant functional role in humic substances.

Further evidence of structure comes from $T_2(^{13}C)$ relaxation times. These times are reported in Tables 6.2 and 6.3 for both LFA and LHA. In general, shorter relaxation times reflect reduced mobility.[6.13] The $T_2(^{13}C)$ in all regions are shorter for LHA than for LFA. Thus, LHA's structural units appear to be less mobile and larger, dynamic units as expected. If the $T_2(^{13}C)$s of LFA moieties are compared, it can be seen that the aliphatic moieties are the least mobile and probably the largest, while the carbohydrate and aromatic moieties are significantly smaller. This finding is also supported by the size exclusion results, which emphasise the separability of some of these "functional" components. For LHA the $T_2(^{13}C)$ times suggest that the aliphatic, ester, ether, and carbohydrate moieties are the largest, while the aromatic moieties are somewhat smaller. These data once again underline that aliphatic and carbohydrate moieties play an important structural role in polymeric networks.

The spectra in Figure 6.6 and the %TOC data in Tables 6.2 and 6.3 show that LFA is more extensively functionalised than LHA is, and that the carboxyl groups constitute the majority of groups in both LFA and LHA. Although phenolic groups are present in both LFA and LHA, it is unlikely they are sufficiently abundant to account for all weak acid (pK_a=8-10) functionality. This is particularly the case for LFA. This leads to the new conclusion that much of the weak acid functionality must be located on the aliphatic/carbohydrate moieties. This is supported by the major peak in the chemical shift

Table 6.2: Ramp-CP-MAS ^{13}C NMR characterisation of LFA.

Chemical Shift Assignments (/ppm)	LFA		
	%TOC	$T_{1\rho}{}^{1}H$ (/ms)	$T_2{}^{13}C$ (/ms)
Ketonic (190-220)	8.8	7.3	11.9
Carboxyl (162-190)	33.8	4.9	13.1
Phenolic (145-162)	2.2	6.0	22.7
Aromatic (108-145)	12.0	5.5	11.4
O-C-O (96-108)	3.6	3.6	10.4
Carbohydrate (50-96)	17.8	2.6	12.3
Aliphatic (0-50)	21.8	2.8	8.0

Table 6.3: Ramp-CP-MAS ^{13}C NMR characterization of LHA

Chemical Shift Assignments (/ppm)	LHA		
	%TOC	$T_{1\rho}{}^{1}H$ (/ms)	$T_2{}^{13}C$ (/ms)
Ketonic (190-220)	6.5	2.4	7.8
Carboxyl (162-190)	15.6	3.2	8.3
Phenolic (145-162)	2.8	4.6	9.1
Aromatic (108-145)	18.7	4.1	7.8
O-C-O (96-108)	1.0	3.6	5.1
CH_3O-, etc. (60-96)	11.9	2.3	6.0
Anomeric (50-60)	9.1	2.8	5.1
Aliphatic (0-50)	34.3	3.0	6.9

range between 65-80 ppm which can be assigned to carbohydrate -OH groups. This interpretation is not contradicted by results of potentiometric titration.[6.14] Originally, weak acid pK_a's were assigned to phenolic groups, but hydroxyl groups located on carbohydrate moieties may also be responsible.

The data in Table 6.2 also shows that the content of carboxylic carbons is approximately three times that of aromatic carbons. From these data it can be inferred that LFA is highly functionalised and the majority of this functionality is not on the aromatic moieties, but on the aliphatic/carbohydrate moieties. This inference is supported by the dipolar dephased (DD) spectrum of LFA, shown in Figure 6.7. From this spectrum it can be seen that the CH coupling is much weaker for the aliphatic and carbohydrate moieties than it is for the aromatic moieties. The explanation for this is that the aliphatic and carbohydrate carbons are highly functionalised carrying few protons, while the aromatic moieties are not. The interpretation is further supported by the fact that the CH coupling of the carboxyl carbons is very weak, while the CH coupling of the phenolic carbons is somewhat stronger. The weakness of the carboxyl carbons CH coupling indicates few neighbouring protons. This has also been found for Suwannee River fulvic acid by Leenheer and co-workers.[6.15, 6.16] The relative strength of the CH coupling of the phenols also indicates that the aromatic rings bearing the phenolic -OH groups are protonated. The $T_2(^{13}C)$ values for the carboxyl carbons also support the inference that the carbohydrate carbons are highly functionalised. The $T_2(^{13}C)$ values of the carboxyl carbons are seen to be most comparable to the $T_2(^{13}C)$ values of the carbohydrate carbons (Table 6.2). There is also evidence from the $T_2(^{13}C)$ values that the more mobile carbohydrate moieties are also the most functionalised. The $T_{1\rho}(^{1}H)$ values are consistent with the interpretations just given.

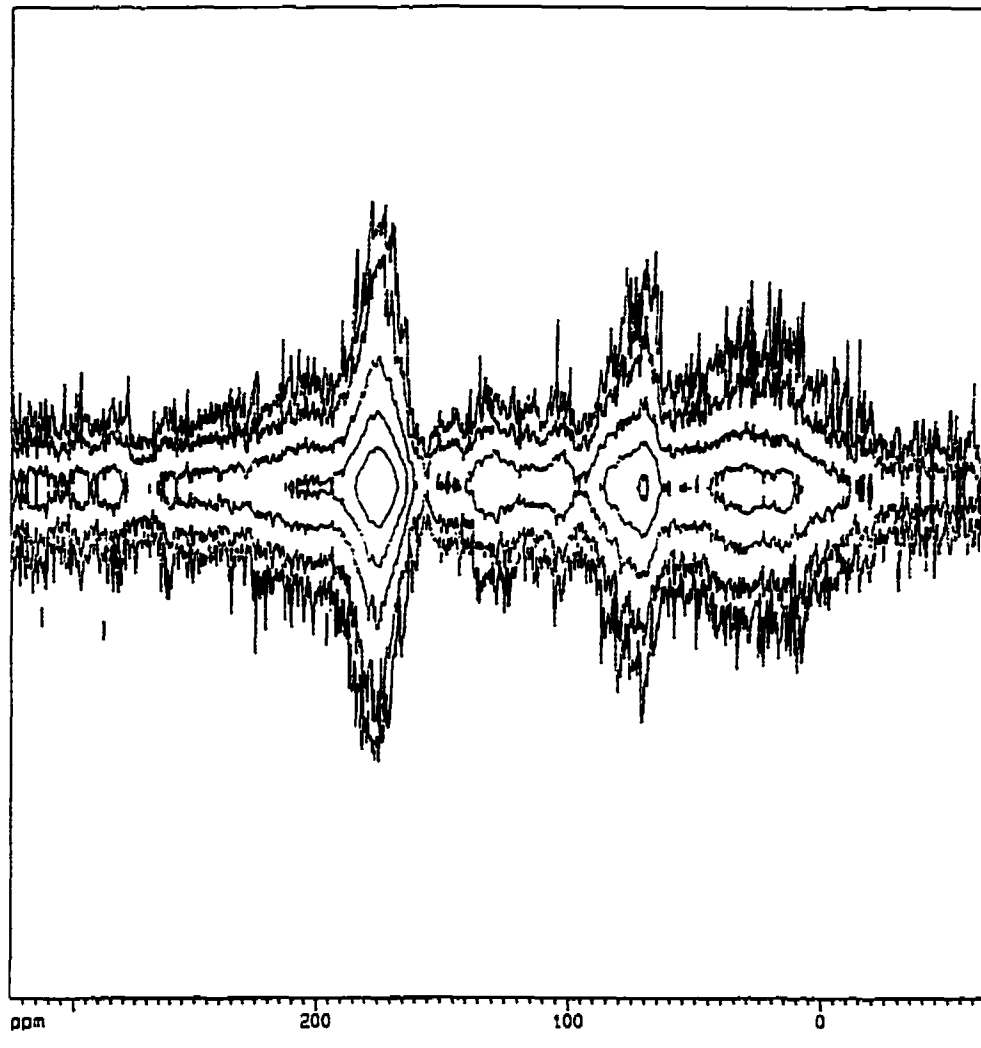

Figure 6.7: The two dimensional dipolar-dephasing spectrum of LFA. The vertical axis, which is in arbitrary units, represents dipolar-dephasing, and the horizontal axis represents chemical shift (see section 4.3.3.5 for details).

Turning to LHA, the data in Table 6.3 indicates enough aromatic carbons in LHA to support all the carboxyl groups. Thus, there is no evidence contrary to the common view that the majority of the acid functionality of humic acid is on the aromatic moieties. This

finding is supported by the DD spectrum of LHA, shown in Figure 6.8. From this spectrum it can be seen that the CH coupling in the aromatic domain is very weak, almost of the same order as that of the carboxyl carbons. The weakness of this CH coupling can be explained if the aromatic moieties are highly functionalised. The weakness of the phenolic CH coupling (recall the LFA phenolic CH coupling strength) supports this view. The carbohydrate/aliphatic region of the spectrum reveals strong CH coupling, indicating less substitution in these regions. The weak CH coupling in the aliphatic region of the spectrum can be explained by the methyl groups (-CH_3 groups have very weak CH couplings, due the high rate of free rotation). Apparently, the aliphatic region is highly -CH_3 substituted.

The LHA $T_2(^{13}C)$ values support the interpretation. The $T_2(^{13}C)$ of the carboxyl carbons are most comparable to the $T_2(^{13}C)$ of the aromatic carbons (Table 6.3). Again, it appears that the aromatic rings are highly functionalised. The $T_{1\rho}(^1H)$ values of LHA, are shorter than those of LFA for the carboxyl, phenolic, and aromatic carbons by about 1.5 ms (or 28%). A shorter $T_{1\rho}(^1H)$ can come about by three mechanisms: molecular motion; a paramagnetic impurity; or the presence of radicals. The first mechanism is very unlikely since the aromatic moieties, because of ring rigidity, are the least likely to be affected by motional effects. A paramagnetic impurity (e.g. Fe (III)) is possible, but because of the method by which this sample was purified, rather unlikely. This leads to the conclusion that the reduction in $T_{1\rho}(^1H)$ of the carboxyl, phenolic, and aromatic moieties of LHA, in comparison to LFA, is due to stable organic radicals on the aromatic moieties. This conclusion is also supported by the poorer signal to noise ratio for LHA in comparison to LFA, even though the same amount of material was loaded into the rotor. This is consistent with EPR (electron paramagnetic resonance) results on similar humics,[6.17] and again implies that aromatic ring functionalities allow for stable radicals.

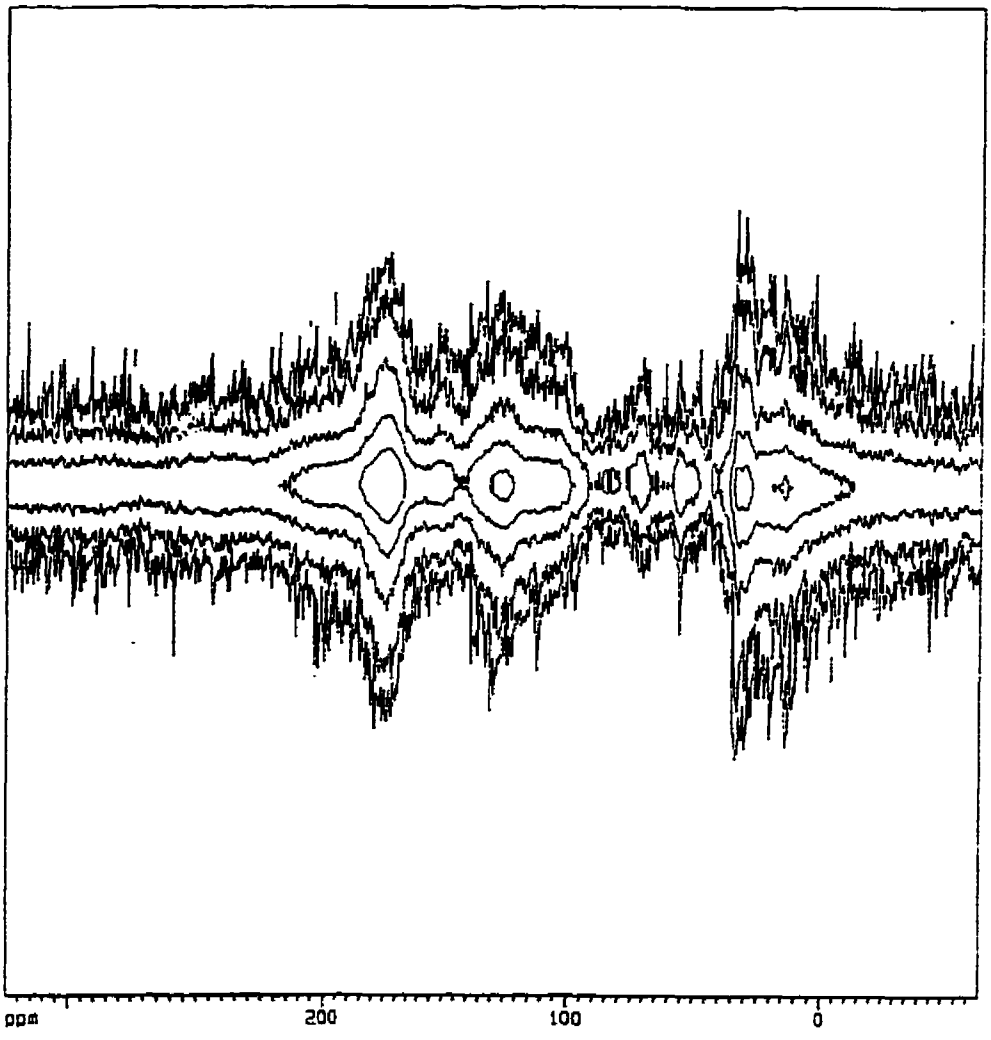

Figure 6.8: The two dimensional dipolar-dephasing spectrum of LHA. The vertical axis, which is in arbitrary units, represents dipolar-dephasing, and the horizontal axis represents chemical shift (see section 4.3.3.5. for details).

6.4 Implications

The NMR data suggests the majority of the LFA's weak acid protons may be aliphatic/carbohydrate -OH and not phenolic -OH, as assigned earlier. In terms of

structure, the above characterisation leads to the following structural description of LFA and LHA.

LFA: A structural model for LFA emerges in which there appear to be three major components. These are: (i) a group of large relatively immobile structural units; (ii) some mobile unfunctionalised units; and (iii) some highly substituted functionalised units. The large relatively immobile units are mainly aliphatic and unfunctionalised. The unfunctionalised mobile units are mainly aromatic, while the functionalised mobile units are mainly carbohydrate in nature. The mobile carbohydrate units have both carboxyl and hydroxyl functionality, with pK_a's of 3.5-6.5 and 7-10, respectively. This structural model raises an important question as to the relative importance of functionality on carbohydrate moieties and aromatic moieties in metal binding, as addressed in the next section.

LHA: The structural model for LHA that emerges consists of one type of major immobile unit, associated with slightly more mobile units that are mainly aromatic in nature. These slightly smaller and more mobile units are highly substituted and expected to be the major players in metal and acidic proton binding.

6.5 Summary

In conclusion, the models suggest significantly different composition for LFA and LHA. The LFA structural model is less like previously proposed structural models for fulvic acid. The LHA structural model is evolved from earlier proposed structural models for humic acid, and is consistent with some of the more recent structural proposals, such as

the Donnan gel model put forward by Benedetti, Van Riemsdijk, and Koopal.[6.18] It is especially important that all results emphasise the mixture of different size fragments in humic materials. Thus, no effort is made to show a "typical structural formula" as has often been done, since such structures can be highly misleading. Dynamic models are needed.

References

6.1 Senesi, N.; Miano, T.M.; Provenzano, M.R.; Brunetti, G. *Soil Sci.* **1991**, 152, 259.

6.2 Miano T.M.; Senesi N. *Sci. Total Environ.* **1992**, 117/118, 41.

6.3 Power, J.F. PhD thesis, Concordia University, Montreal, 1986

6.4 Lavigne, J.A. PhD thesis, Concordia University, Montreal, 1988

6.5 Cabaniss, S.E. *Environ. Sci. Technol.* **1992**, 26, 1133.

6.6 Cabaniss, S.E.; Shuman, M.S. *Marine Chemistry* **1987**, 21, 37.

6.7 Gamble, D.S.; Underdown, A.W.; Langford, C.H. *Anal. Chem.* **1980**, 52, 1901.

6.8 Power J.F.; Lesage R.; Sharma D.K.; Langford C.H. *Environ. Tech. Lett.* **1986**, 7, 425.

6.9 Underdown A.W.; Langford C.H.; Gamble D.S. *Environ. Sci. Technol.* **1985**, 19, 132.

6.10 Wilson, M.A. NMR Techniques and Applications in Geochemistry and Soil Chemistry; Pergamon Press, Oxford, 1987. (and references cited therein).

6.11 Hatcher, P.G.; Schnitzer, M.; Dennis, L.W.; Maciel, G.E. *Soil Sci. Soc. Am. J.* **1981**, 45, 1089.

6.12 Stevenson, F.J. Humus Chemistry, Genesis, Composition, Reactions (2nd ed.); John Wiley & Sons, Toronto, 1994. Chap. 12.

6.13 Axelson, D.E. Solid State Nuclear Magnetic Resonance of Fossil Fuels; Multiscience Publications Ltd: Canadian Government Publishing Centre, Supply and Services Canada, 1985, Chap 1-3 and 6 (and references cited therein).

6.14 Wang Z.D. PhD. Thesis, Concordia University, Montreal, 1989.

6.15 Leenheer, J.A.; Wershaw, R.L.; Reddy, M.M. *Environ. Sci. Technol.* **1995**, 29, 393.

6.16 Leenheer, J.A.; Wershaw, R.L.; Reddy, M.M. *Environ. Sci. Technol.* **1995**, 29, 399.

6.17 Senesi, N.; Schnitzer, M. in Environmental Biogeochemistry and Geomicrobiology: Krumbein, E. W., Ed.; Ann Arbor Science, Ann Arbor, MI, 1978, pp. 467-481.

6.18 Benedetti, M.F.; Van Riemsdijk, W.H.; Koopal, L.K. *Environ. Sci. Technol.* **1996**, 30, 1805.

Chapter 7
Cu(II) Binding Studies of LFA

Due to the importance of fulvic acids in metal speciation, discussed in Chapter 1, a study which combined luminescence and NMR spectroscopy was undertaken and is discussed in this chapter. The reason for using these two different spectroscopic techniques is that both give information by themselves, but when combined, a much clearer picture emerges. The advantage of luminescence over NMR is sensitivity. The high sensitivity of luminescence allows one to study metal binding at natural water concentrations. Also, luminescence provides evidence of environmental effects, e.g. pH, as well as the nature of the binding site. NMR paramagnetic relaxation, on the other hand, allows one to determine directly what types of carbons are involved in paramagnetic metal ion binding. This determination is very site specific due to the $1/r^6$ distance dependence discussed in Chapter 3. It should also be noted that this is the first systematic metal binding study which uses NMR as a monitor. Luminescence and NMR results combined should provide insight into both the metal binding sites and aggregation effects caused by metal binding.

7.1 Cu(II) Quenching of Luminescence

7.1.1 Steady State

In the emission scan luminescence, the broad main band is quenched, by Cu(II), as shown in Figure 7.1. In the synchronous scan luminescence (Figure 7.2), the quenching is greater on the 465 nm peak than on the 392 nm one, and there seems to be much less

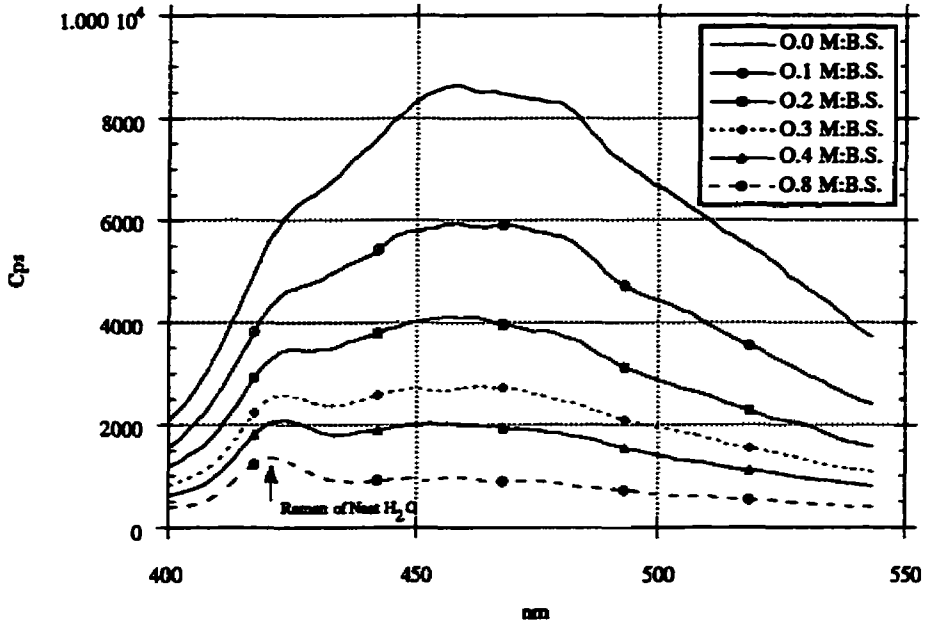

Figure 7.1: Cu (II) quenching of LFA's luminescence at pH 6.4 monitored by emission luminescence (M:B.S. = metal: bidentate complexing sites [bidentate complexing sites=1]).

quenching of the 512 nm shoulder. This is evident in the emergence of the 392 nm peak and of the 512 nm shoulder as the metal ion quenching increases as illustrated in Figure 7.2. Figures 7.1 and 7.2 confirm the earlier observation that synchronous luminescence resolves a broader distribution of luminophores than emission luminescence does. In fact, it appears that the broad peak centred at ~456 nm may be sampling mainly the same set of luminophores as sampled by synchronous luminescence in the two peaks at ~392 nm and ~465 nm.

Figures 7.3 and 7.4 show curves representing the decrease in luminescence with the increase in ratio of Cu (II) to binding sites at different pHs for both types of steady state

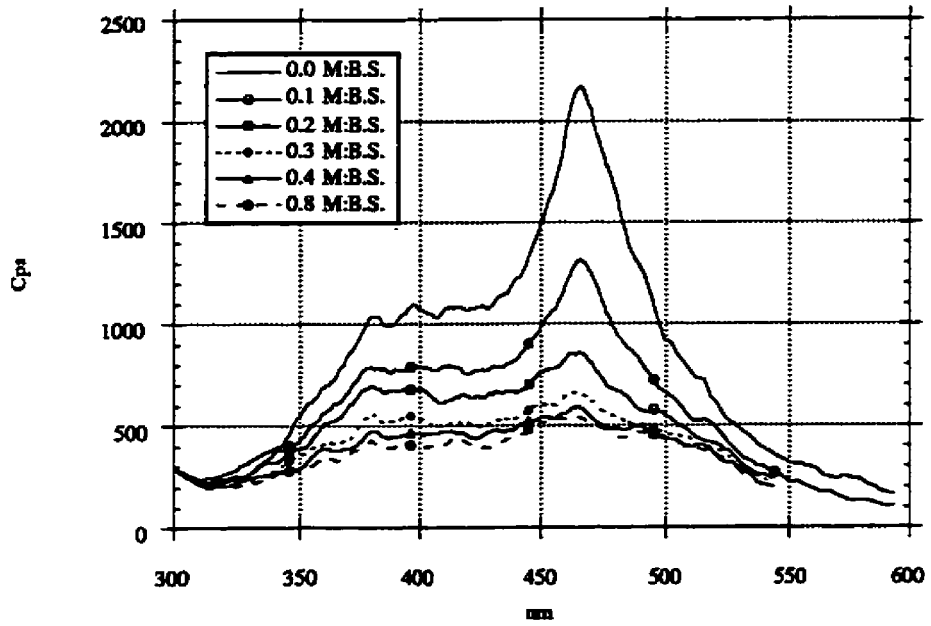

Figure 7.2: Cu (II) quenching of LFA's fluorescence at pH 6.4 monitored by synchronous luminescence.

luminescence measurements used in this study. The ratio of metal to binding site (M:B.S.) was established based on the report that LFA has a bidentate complexing capacity of 5.8 mmol/g i.e. $1x10^{-4}$ mole of Cu (II) is the minimum needed to occupy all the bidentate complexing sites of 17.5 mg LFA.[7.1] The synchronous luminescence curves were obtained by monitoring the quenching of the 465 nm maximum, while 456 nm was monitored for the emission luminescence curves. The first observation is that at pH 4.0 the quenching curves are approximately linear for both cases. Since Cu (II) has been shown to compete only weakly with protons for the binding sites at this pH [7.2], this probably indicates dynamic collisional quenching. Quenching due to Cu (II) complexation,

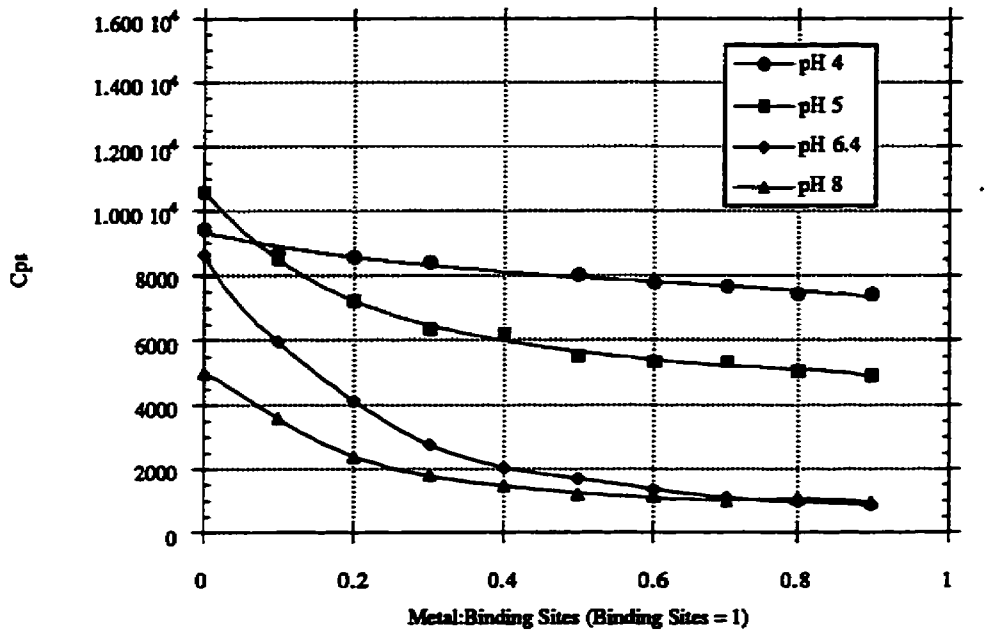

Figure 7.3: Emission luminescence quenching curves, monitoring the 450 nm peak, of LFA by Cu (II) at different pHs (Binding Sites = bidentate complexing sites).

occurring at pHs above 4.0, will be over and above this collisional quenching. One can presume (see time resolved for confirmation) that quenching induced by complexation is static, and that this is by far the major quenching that occurs at pH's above 4.0. In other words, dynamic quenching takes place when Cu (II) is not complexed, at pH 4.0. On the other hand, static quenching takes place when Cu (II) is complexed along with the dynamic quenching of uncomplexed Cu (II), above pH 4.0. However, when one is dealing with macromolecules that can trap but not complex ions (outer sphere complexes), static quenching could be possible even though the metal ion has not been complexed (inner sphere complexes). The major part of the synchronous signal quenching, due to

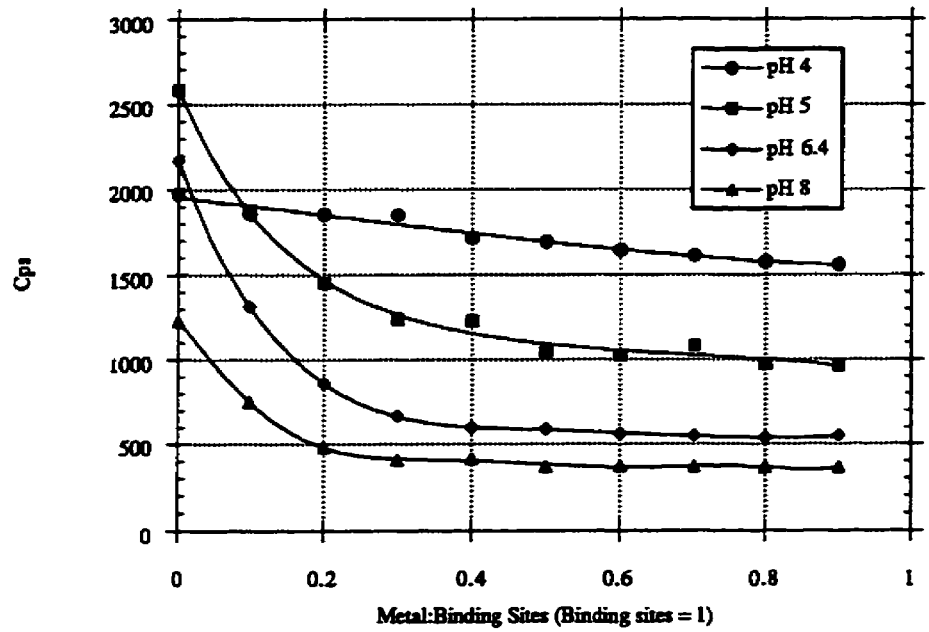

Figure 7.4: Synchronous fluorescence quenching curves, monitoring the 465 nm peak, of LFA by Cu (II) at different pHs.

complexation, seems to occur over a narrower range of Cu (II) concentrations than for the emission signal. This can be understood from Figures 7.1 and 7.2, recalling that the 465 nm peak is more affected by metal quenching than the 392 nm peak. In emission measurements, the signal is a mixture of these two features. The largest difference in curve shapes between the two methods is observed at pH 6.4. This observation leads to the suggestion that the 392 nm component is quenched over a wider Cu (II) concentration range than the 465 nm component is (see Figure 7.2).

From figures 7.3 and 7.4 it can be seen that as the pH is increased the amount of quenching increases, up to pH 6.4 and then at pH 8.0 quenching is reduced again. There

are two elements in the explanation for this, the first being that at lower pH the Cu(II) binding sites are less accessible because of proton competition. The second is an extension

It is clear from the results in Table 7.1 and 7.2 that the linear quenching assumption of references 7.3-7.5 cannot be maintained, as there is more metal available to bind than was added to the system! This despite the smooth quenching curves shown in Figure 7.3 and 7.4. Application of references 7.3 to 7.5 method to humic substances in general, as reported in references 7.6 to 7.9, must be viewed with great reservations. This seems to confirm that there is more than one type of luminophore, Lo, within the fulvic acid system, and that the luminescence of these different luminophores is quenched differently. This point of view is also supported by the fact that the synchronous measurements showed a greater deviation from the linear assumption than the emission luminescence measurements $|\overline{K}_4|$ values were calculated when possible but gave no meaningful results.

Table 7.1: Amount of Cu(II) ion bound in accordance with Weber and co-workers' (ref. 7.3 to 7.5) linear assumption at different pHs (results based on three experiments).

pH	Cu(II) added ($/10^{-5}M$)	Synchronous luminescence ($/10^{-5}M$)	Emission luminescence ($/10^{-5}M$)
4.0	1.00	0.85±0.12	0.98±0.11
5.0	1.00	3.27±0.55	2.16±0.27
6.4	1.00	5.53±0.38	3.17±0.23
8.0	1.00	5.04±0.16	3.07±0.04

Table 7.2: A comparision of the amount of Cu (II) added to how much is bound according to the Weber and co-workers' (7.3 to 7.5) assumption.

Cu (II) added as a fraction of available binding sites	Cu (II) bound calculated by the Weber and co-workers' assumption	Luminscence intensity Cps (counts per second)
0.0	0	2174.0
0.1	0.586	1314.7
0.2	0.812	860.6
0.3	0.908	665.1
0.4	0.943	597.1
0.5	0.947	590.0
0.6	0.960	563.6
0.7	0.966	551.8
0.8	0.967	541.0
0.9	0.968	535.5

7.1.2 Stern-Volmer Plots

Stern-Volmer plots [7.10] and modified Stern-Volmer plots which allow for more than one quenchable Lo [7.11] were plotted for both emission (456 nm and 512 nm components) and synchronous (392 nm, 465 nm and 512 nm components) luminescence measurements, and are shown in Figures 7.5-7.8. Once again the components showed unique behaviour. Both types of luminescence measurements showed linear Stern-Volmer behaviour at pH 4.0. This is consistent with the idea that the important quenching taking place at this pH is collisional. But, at pH 5.0 and higher, where complexation takes place, the Stern-Volmer plots deviated from linearity towards the x axis, indicating the presence

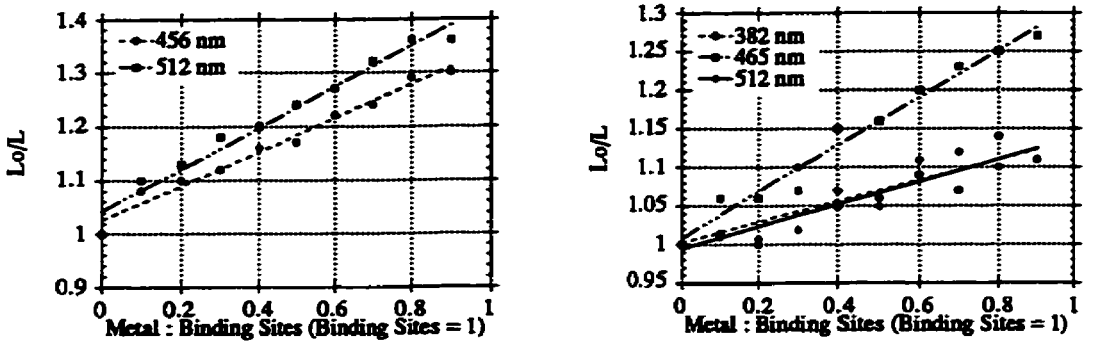

Figure 7.5: pH 4.0 Stern-Volmer plots from emission (left) and synchronous (right) fluorescence monitoring.

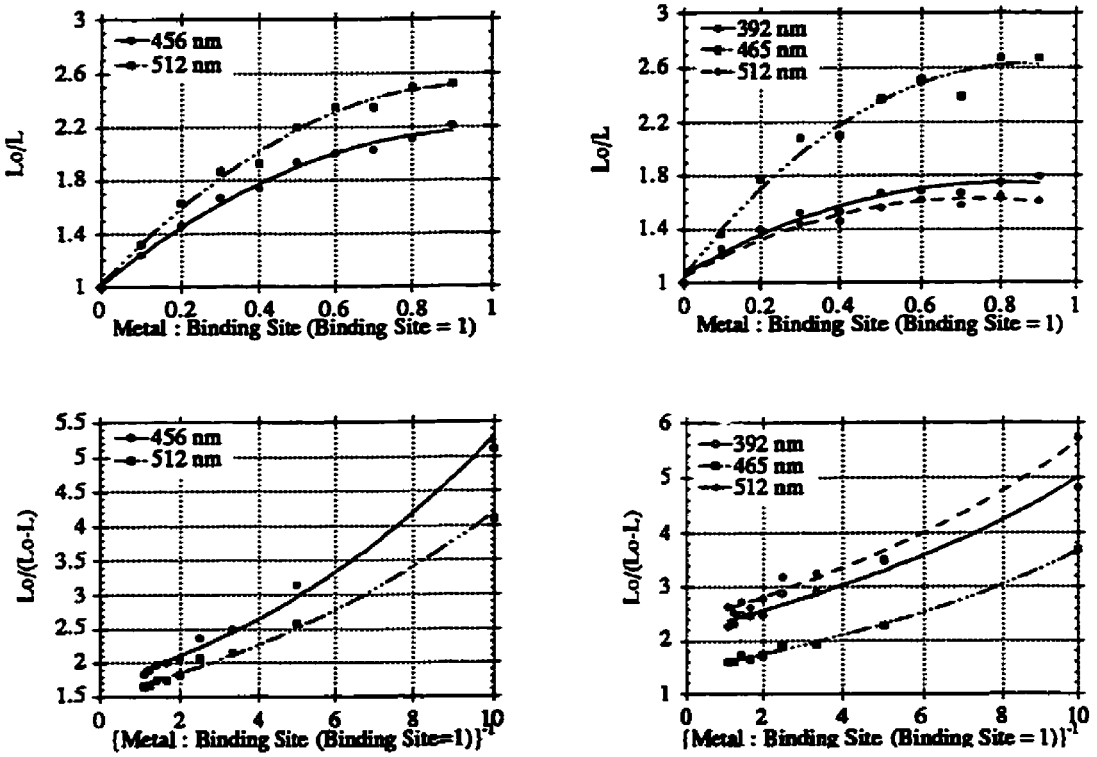

Figure 7.6: pH 5.0 Stern-Volmer plots. The top plots are classic Stern-Volmer plots from emission (left) and synchronous (right) fluorescence monitoring. The bottom plots are two component Stern-Volmer plots from emission (left) and synchronous (right) fluorescence monitoring.

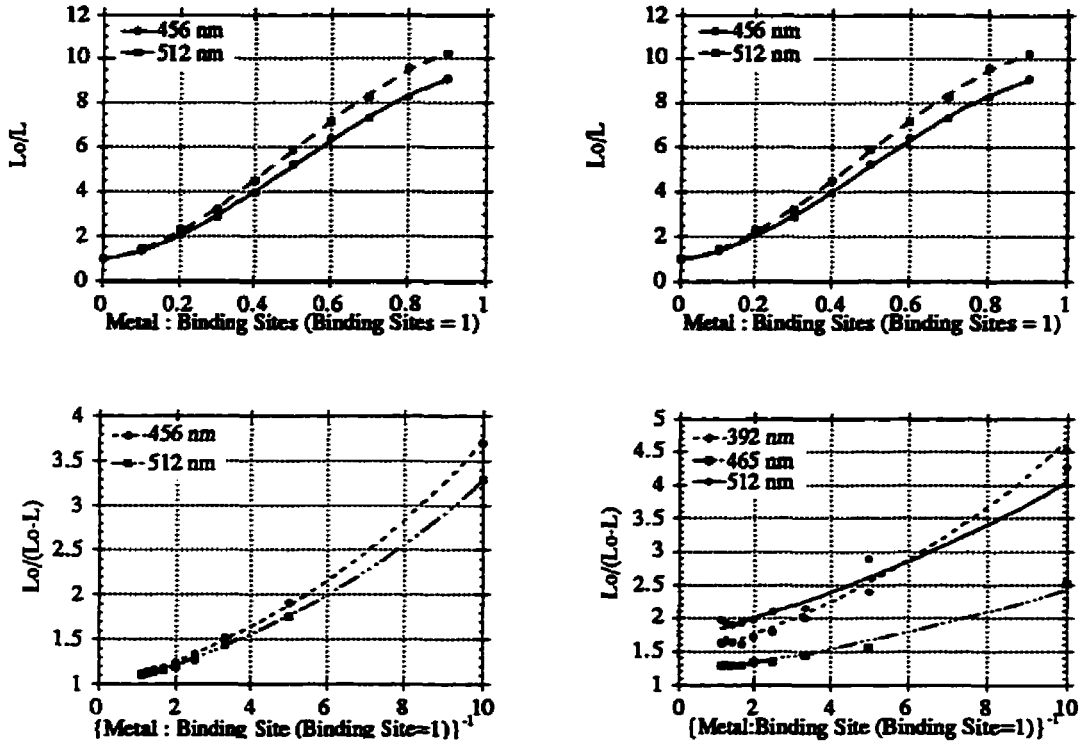

Figure 7.7: pH 6.4 Stern-Volmer plots. The top plots are classic Stern-Volmer plots from emission (left) and synchronous (right) fluorescence monitoring. The bottom plots are two component Stern-Volmer plots from emission (left) and synchronous (right) fluorescence monitoring.

of two or more luminophores that are not equally accessible to complexation. Modified Stern-Volmer plots, which accommodate two component luminophores, deviated from linearity towards the y axis, for pH 5.0 and higher, indicating that there are more than two luminophores responsible. Thus, it would seem that the Stern-Volmer plots also indicate that there are at least three components in the luminescence signal of our fulvic acid.

An approach to confirm the above conclusion, that there is a distribution of

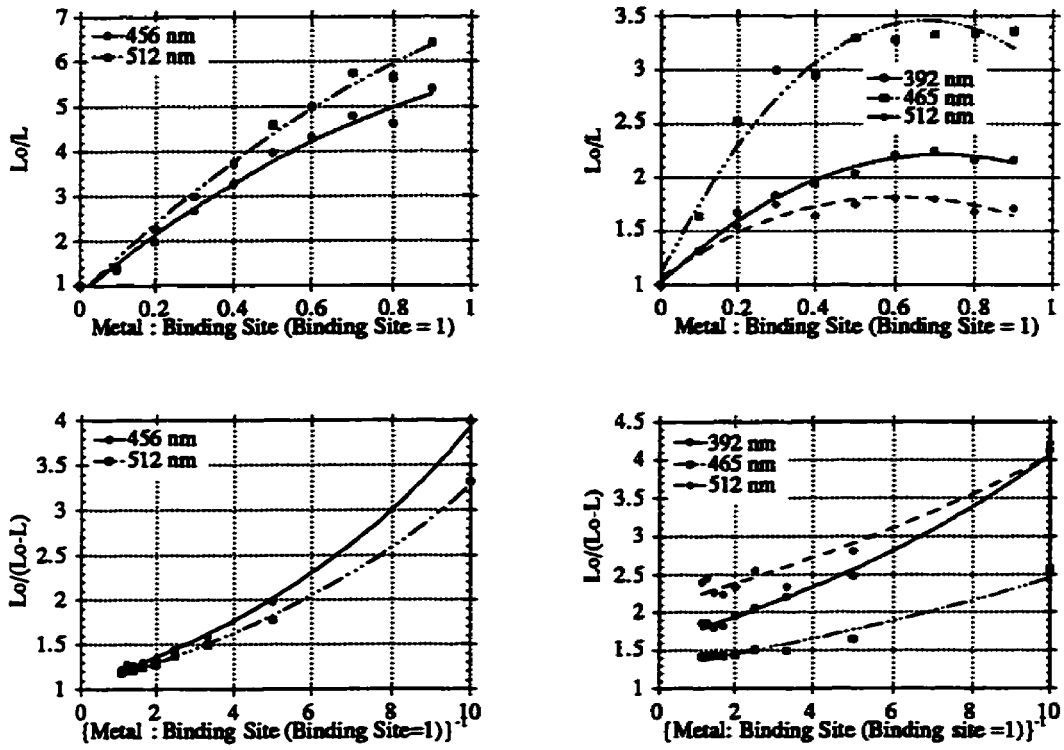

Figure 7.8: pH 8.0 Stern-Volmer plots. The top plots are classic Stern-Volmer plots from emission (left) and synchronous (right) fluorescence monitoring. The bottom plots are two component Stern-Volmer plots from emission (left) and synchronous (right) fluorescence monitoring.

differentially quenched luminophores, is to examine the distribution of luminescence lifetimes.

7.1.3 Time Resolved Experiments

A series of experiments was carried out in both the picosecond and nanosecond time domains in which the fulvic acid luminescence was quenched by Cu(II) ions. The

results for the picosecond experiments for Cu (II) are shown in Figure 7.9. The nanosecond results showed no clear quenching of the 4.2 ns component, even at metal ion to binding site ratio (M:B.S.) up to 0.8. Because of this, only two components are required to describe the emission quenching, the ~50 ps and the ~430 ps components. The quenching of these components is shown in Table 7.3. The results in Table 7.3 indicate that these two distinguishable sets of Lo are being quenched. It also appears that the ~430 ps component is quenched to a greater extent at lower metal to binding site ratios than is the ~50 ps component. Comparing these results to the synchronous luminescence metal quenching study, the following lifetime assignments can be proposed. The 392 nm peak is associated with the ~50 ps component, the 465 nm component is associated with the ~430 ps peak, and the 512 nm peak, which is not quenched measurably is associated with is the 4.2 ns component.

It is important that luminescence quenching affects subnanosecond lifetimes, i.e. these processes are faster than collision rates in solution. This is strong evidence that mainly static quenching is occurring, and there is little dynamic quenching at pH 5.0 or higher. This is a very important observation because it implies that the non linear Stern-Volmer quenching behaviour noted above results from only one quenching mechanism, and thus the deviation from linearity must come from the fact the separate luminophores quench differentially.

7.1.4 Combining the Synchronous Luminescence and Time Resolved Quenching Results

It can be seen that monitoring the luminescence of this fulvic acid sample (and the AFA sample) involves monitoring more than one Lo. In fact, there may be a very complex distribution of luminophores. But, when one combines the synchronous and time resolved

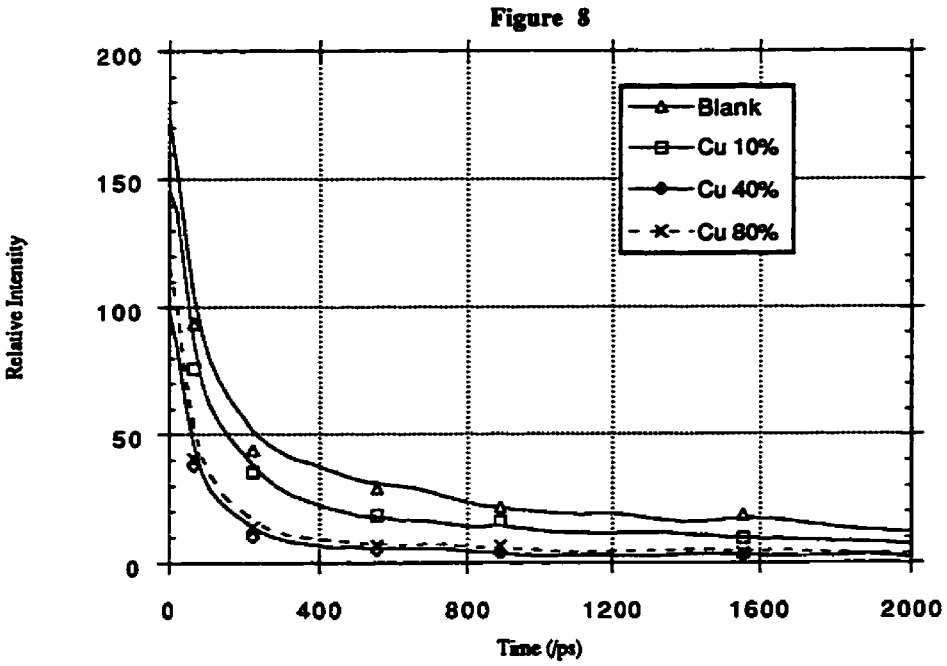

Figure 7.9: Cu(II) quenching of LFA's luminescence monitored by time resolved fluorescence (Blank = LFA with no metal ion added). Where 10%, 40% and 80% correspond to 0.10 M:B.S., 0.40 M:B.S., and 0.80 M:B.S..

Table 7.3: Cu(II) concentration effect on the 50 ps and 430 ps preexponential terms.

M:B.S.	50 ps	430 ps
0.00*	0.75 ± 0.06	0.25 ± 0.02
0.20	0.77 ± 0.06	0.14 ± 0.01
0.40	0.59 ± 0.11	0.07 ± 0.02
0.50	0.68 ± 0.07	0.07 ± 0.01

* - normalised to 1.00

luminescence quenching results, there is an emerging case for a physically meaningful three component first approximation model of fulvic acid. Thus for LFA, we propose to assign the three component groupings found in the synchronous spectra, the following lifetimes: the 392 nm component ~50 ps, the 465 nm component ~430 ps, and the 512 nm component 4.2 ns. Thus, there cannot be a linear relationship between the amount of metal bound to the fulvic acid and the quenching of that fulvic acid's luminescence.

7.2 Cu(II) Line Broadening of CP-MAS ^{13}C NMR

Although metal binding to humic materials has been an active area of research for some time, no study has found on what moieties metal ions bind. There have been attempts to elucidate this by methods such as EPR,[7.12] Mössbauer,[7.13] and EXAFS [7.14, 7.15] spectroscopies. However, to date they have only provided information on what types of functional group are involved in the binding, and their number. As discussed previously, ^{3}C NMR is a more promising approach, especially CP-MAS ^{13}C NMR.

Spectra were recorded at 0.00 M:B.S. (ratio of metal to bidentate bind sites), 0.05 M:B.S., 0.10 M:B.S. and 0.15 M:B.S. Cu(II) loadings in terms of total bidentate sites of Laurentian fulvic acid (LFA). Thus, the spectra study the earlier parts of the titration curve and focus on the stronger metal ion binding sites in the LFA complex mixture. Figure 7.10 shows the LFA spectra at the four different metal loadings. As would be expected, all regions of the spectra experience signal loss under the influence of the paramagnetic ions, and no nucleus is absolutely "remote" (isolated from the effects of the paramagnetic centres). Thus, it is not possible to compare the spectra to each other in absolute terms as some paramagnetic effects weaken all signals. However, it is possible to compare the spectra to each other in relative terms as the overall effects of paramagnetic loading

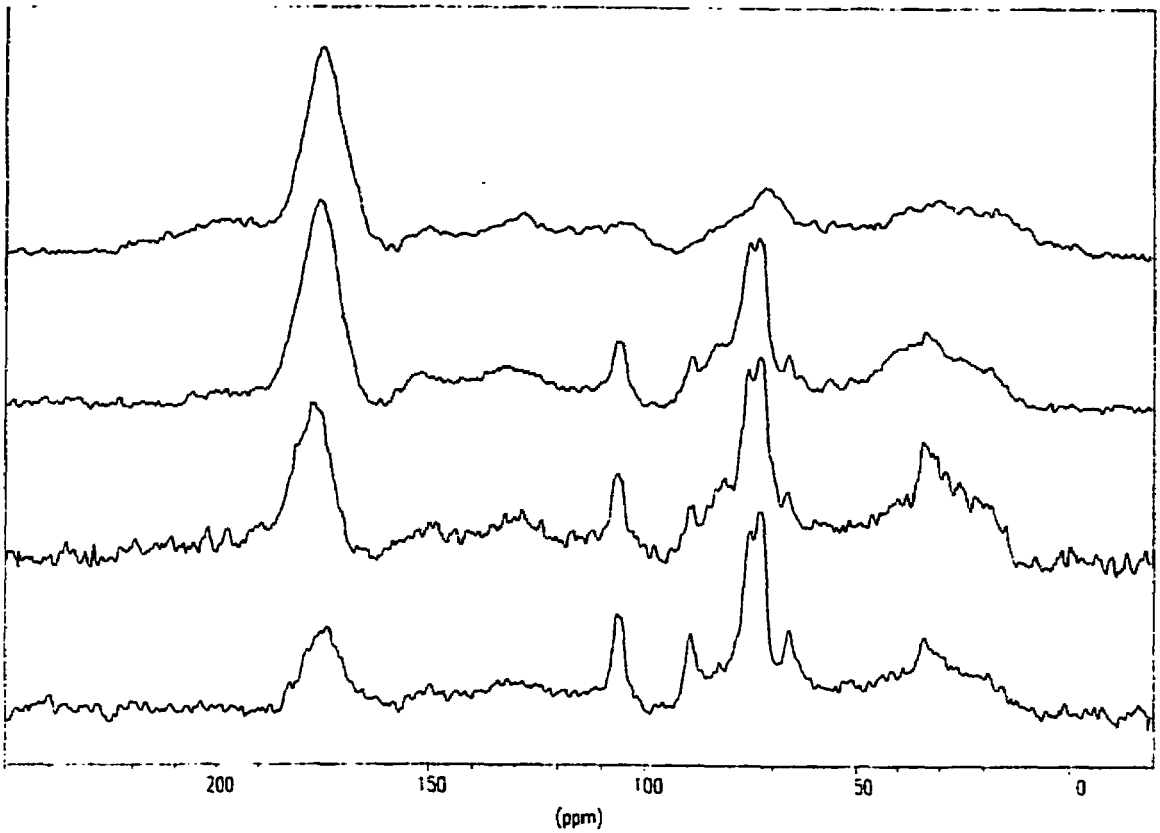

Figure 7.10: LFA chemical shift spectra at different Cu(II) loadings. The top spectrum is with no Cu(II) loaded, followed by (going down) 0.05 M:B.S., 0.10 M:B.S., and 0.15 M:B.S. Cu(II) loaded spectra.

influences the spectral regions differently.

It has commonly been assumed that the majority, and the strongest, of the metal binding sites are phenol-carboxylate or phthalic type functionalities where two carboxyl groups are adjacent to each other on an aromatic ring. This is evident from the fact that a large number of studies intended to shed light on the binding of metal ions by organic matter in soils and fresh water have exploited aromatic model compounds including, notably, salicylic acid and phthalic acid. Perhaps this is a bias from degradation and fragmentation results. An examination of Figure 7.10 immediately reveals the limitation of

this concept. The most striking feature of the Figure 7.10 is the broadening in the carbohydrate region (50-92 ppm) induced by metal loading. Even at 0.05 M:B.S loading this perturbation is very pronounced, and becomes even more pronounced at higher loading. In contrast, it is difficult to detect any perturbation of the phenol (145-162 ppm) and aromatic (108-162 ppm) signals up to 0.10 M:B.S. loading. As expected, the other major region of perturbation is the carboxylate region (162-195 ppm). It appears that the strongest binding sites are associated with carboxylate groups and quite possibly acidic -OH groups on the carbohydrate structures. Almost certainly, these are bidentate and multidentate sites. Recall that the data presented in Chapter 6 strongly indicate that the majority of functionality (-COOH and -OH groups) is on carbohydrate moieties and not on the aromatic moieties in LFA. This is especially important for natural water chemistry, where heavy metal concentrations are small compared to humic carboxylate concentrations. In this geochemically important limit, carbohydrate moieties are the major moieties involved in metal binding, and thus metal speciation.

By 0.15 M:B.S loading we see clear evidence that the phenolic and aromatic regions of the spectra are being specifically perturbed by the paramagnetic ion. These spectra do suggest that the phenolic groups can, and do, participate in metal ion complexation. It should also be noted that the aliphatic region (0-50 ppm) experiences significant and specific paramagnetic perturbation throughout. Either aliphatic side chains are neighbours to complexation sites or metal ion complexation induces a conformational change which brings the complexation site and aliphatic moieties into closer proximity. The dipolar dephasing results (e.g. CH coupling strength), discussed in Chapter 6, strongly indicate that the aromatic moieties are highly substituted and not rich in aliphatic sidechains. Consequently, effects on the aliphatic region also tend to de-emphasise the role

of aromatic moieties in the structure of the stronger metal binding sites, and further emphasise the importance of the carbohydrate moieties.

It is interesting to note that the NMR signature in the region between 50 ppm and 108 ppm, which becomes more apparent at higher loading, is that of cellulose. The cellulose signature is consistent with the fact that one does not expect cellulose to be a strong metal ion binding moiety. Although there has been little attention paid to cellulose in the literature on humics, these results suggest that cellulose may be a more important component of fulvic acids than previously thought.

7.3 Linking the Luminescence and CP-MAS ^{13}C NMR Metal Binding Results

It is interesting to link the NMR observation to Cu (II) quenching of LFA luminescence, since quenching has been proposed as a monitor of metal ion complexation, and aromatic functionality is a good candidate for a Lo. Above, it has been shown that Cu (II) quenching of LFA luminescence does not follow a linear Stern-Volmer relationship, even assuming two components. The relationship of Cu (II) to the Lo site may not be simple. If an aromatic Lo is important, there are three ways that quenching by Cu (II) bound at functional group distant from the luminophore may arise. Figure 7.11 illustrates these well known phenomena in polymer photophysics.[7.16] Mechanism (i) is the simplest case where the metal ion is bound directly to the luminophore, while mechanism (ii) is an extension of mechanism (i), where the quenching effect of the metal ion is transferred via a conjugated bond system to the luminophore. The remaining mechanisms are more complicated. Mechanism (iii) is a Förster resonance excitation transfer mechanism between an excited state to a luminophore. Mechanisms (iv) and (v) are Donor/Acceptor complex

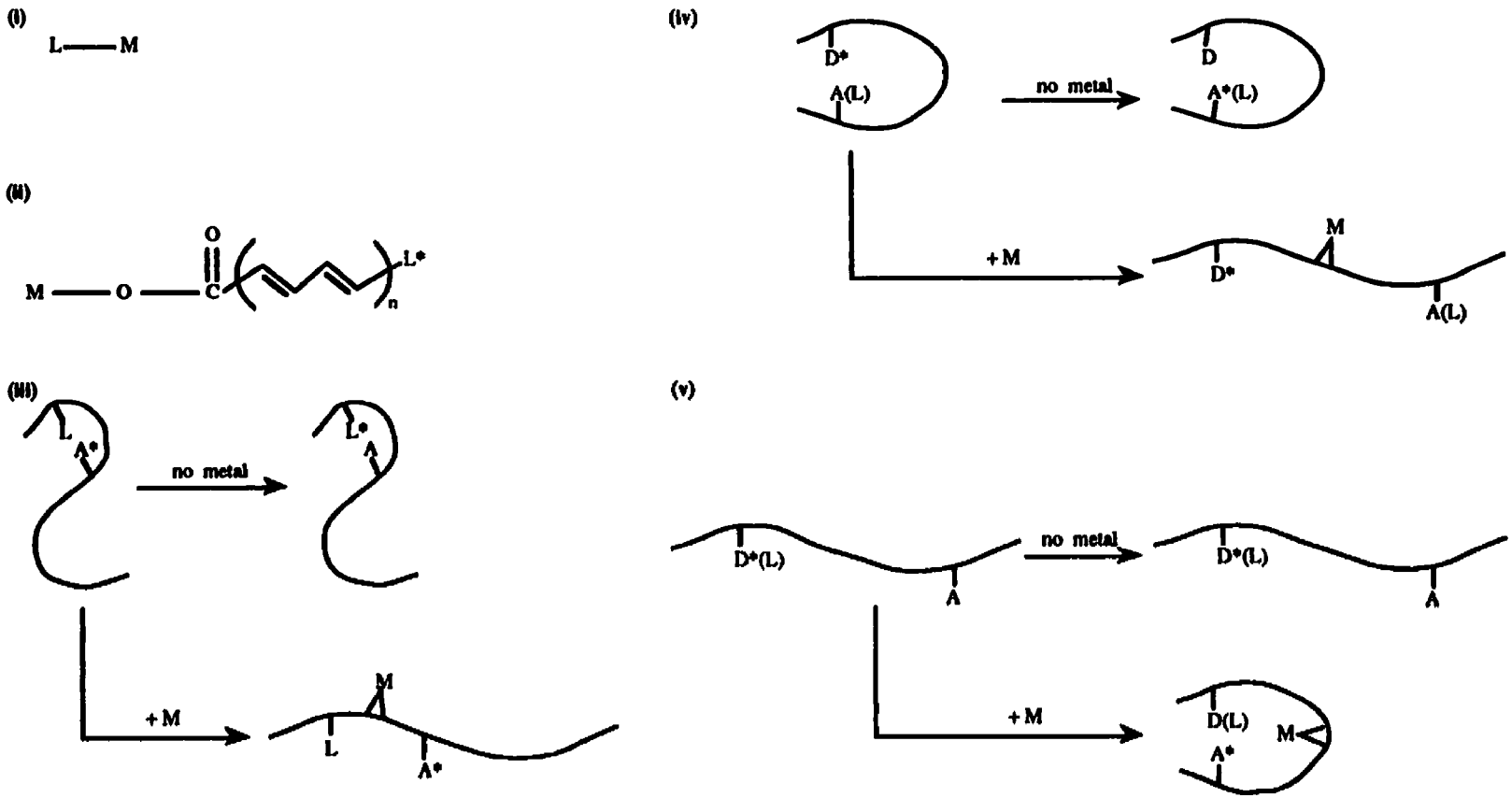

Figure 7.11: Possible mechanisms for luminiscence quenching by metal ions. M represents a metal ion which causes luminescence quenching, L represents a luminophore, and * represents an excited state.

mechanisms. Mechanism (iv) is where the acceptor is a luminophore, while in mechanism (v) the acceptor is not a luminophore. Thus in mechanisms (iii) and (iv) the binding of a metal ion will cause a conformational change which separates the luminophore from the excited state moiety so that no transfer can take place. Thus the luminophore remains in its ground state, hence no luminescence. In mechanism (v) the binding of a metal decreases the distance between a donor and acceptor to allow for a transfer, but in this cases the donor is a luminophore while the acceptor is not, hence once again there will be no luminescence. However, if there is no metal bound, for all cases there will be luminescence. Clearly, Cu (II) binding can interfere with emission from a donor/acceptor complex or Förster resonance excitation transfer without binding at the Lo site.

7.4 Implications

The above results lead to the following metal binding (in particular Cu (II)) implications:

- The predominant metal binding sites are not mainly aromatic in nature as previously believed, but are in fact carbohydrate (at least for LFA).
- Metal binding causes aggregation changes in which the carbohydrate moieties are most drastically affected, but the aliphatic moieties are also affected to a certain extent.
- The strongest metal binding sites may be multidentate, and thus the bidentate site prediction of available metal binding sites in terms of moles of divalent metal that can be bound is questionable.

7.5 Summary

The strongest metal binding sites exploit carboxylate and other oxygen donor functionality on the carbohydrate moieties. The involvement of the aliphatic moieties in the Cu (II) binding sites strongly suggests that the aggregation equilibria among mixture components and/or conformational changes are a factor in the behaviour of the strongest metal binding sites. Commonly exploited models for metal binding sites such as salicylic and phathalic acid may be quite misleading.

References

7.1 Wang, Z.D. PhD. Thesis, Concordia University, Montreal, 1989

7.2 Gamble, D.S.; Underdown, A.W.; Langford, C.H. *Anal. Chem.* **1980**, 52, 1901.

7.3 Saar, R.A.; Weber, J.H. *Anal. Chem.* **1980**, 52, 2095.

7.4 Ryan, D.K.; Weber, J.H. *Anal. Chem.* **1982**, 54, 986.

7.5 Ryan, D.K.; Weber, J.H. *Environ. Sci. Technol.* **1982**, 16, 866.

7.6 Ventry, L.S.; Ryan, D.K.; Gilbert, T.R. *Microchem. J.* **1991**, 44, 201.

7.7 Grimm, D.M.; Azarraga, L.V.; Carreira, L.A.; Susetyo, W. *Environ. Sci. Technol.* **1991**, 25, 1427.

7.8 Sposito, G.; William, S. *Soil Sci Soc. Am. J.* **1990**, 54, 933.

7.9 Luster, J.; Llyod, T.; Sposito, G.; Fry, I.V. *Environ. Sci. Technol.* **1996**, 30, 1565.

7.10 Lakowicz J.R. Principles of Fluorescence Specroscopy; Plenum, Press, New York, 1983, Chapter 9.

7.11 Lehrer, S.S. *Biochem.* **1971**, 10, 3254.

7.12 McBride, M.B. *Soil Sci.* **1978**, 126, 200.

7.13 Lakatos, B.; Korecz, L.; Meisel, J. *Geoderma* **1977**, 19, 149.

7.14 Xia, K.; Bleam, W.; Helmke, P.A. *Geochim. Cosmochim. Acta* **1997**, 61, 2211.

7.15 Xia, K.; Bleam, W.; Helmke, P.A. *Geochim. Cosmochim. Acta* **1997**, 61, 2223.

7.16 Guillet, J. Polymer Photophysics and Photochemistry, an Introduction to the Study of Photoprocesses in Macromolecules; Cambrideg University Press, New York, 1985, Chapters 7 and 9.

Chapter 8
Conclusion

Just as with any investigation on a complex system, both direct and indirect conclusions may be drawn from this work. The direct conclusions are derived from the experiments in black and white terms, with very little grey. On the other hand, the indirect conclusions are based on what the data is hinting at, and this is the very grey area. This work has answered some questions, but the answers have led to many more questions. These questions will need new experiments to answer them, but naturally each answer will lead to many more questions. In this chapter the direct and indirect conclusions from this work will be examined (it must be remembered that these conclusions are in the eye of the writer). Following this, possible future work will be suggested, and finally some of the author's personal thoughts will be given.

8.1 Direct Conclusions

8.1.1 Instrumental Techniques

From the data presented it can be seen that both Ramp-CP-MAS ^{13}C NMR and synchronous luminescence spectroscopy are better at resolving humic materials than their more traditional counterparts. The main reason for this is that, in both techniques, the interrogating, or probing, parameter is being scanned rather than being locked, and when one thinks of the complexity of humic materials, this makes perfect sense as shown in chapter 3. This conclusion can be extrapolated to the interrogation of any complex mixture.

the carbohydrate moieties and not on the aromatic moieties, as previously believed. This finding also brings into question the use of model compounds such as salicylic and phthalic acid for metal binding studies. From a functional group distribution point of view these model compounds may not be at all appropriate for fulvic acids, but are not ruled out as inappropriate for humic acid.

This work also shows that metal binding is a dynamic process in which aggregation is very important.

The NMR data also indicates that, at least for LFA, cellulose may be a more important component in fulvic acid than previously thought.

8.2 Indirect Conclusions

The structural information, from the NMR evidence, hints at a fractal dimensionality between 1 and 2 for LFA and 2-3 fractal dimensionality for LHA. In terms of physical entities LFA consist of more or less linear chain type entities, while LHA is three dimensional gel like entity. This then leads to the conclusion that LFA is a less ordered system than LHA. This is supported by the T_2 results. Thus, it could be said that LFA has a higher entropy than LHA. This finding is supported by the fact that the mathematical modelling of humic acid behaviour, especially in terms of metal binding, has been more successful than the mathematical modelling of fulvic acids. Because LHA is a more ordered system it may be a simpler system to study, with the long term goal of being able to computer model the system to some level of satisfaction.

From the metal binding study it appears that, upon metal binding, LFA becomes a more ordered system due to the aggregation. When a metal ion is bound there is communication within the fulvic acid network which leads to the apparent order via

aggregation one sees. Put in another way, the binding of a metal ion makes the fulvic acid system less complex. The long distance communication paths in a fulvic acid are via Förster resonance or donor/acceptor complexes. When a metal is bound the system becomes less complex and in closer proximity. Hence, long distance communication is no longer needed. This loss of long distance communication becomes visible by the loss of fluorescence. An analogous situation is when people are in close proximity, say at a social gathering, they communicate with each other directly. On the other hand, if everyone is at home, the communication is via the telephone. Thus, if one were to monitor the phone lines of everyone when they are at a social gathering it would seem to us as if no communication was taking place.

If this is so, then there may be much more order in humic materials and in their response to other chemical species than previously thought. This should come as no surprise, since not long ago it was believed that cloud formation was a completely random situation. Since, the introduction of chaos theory this is no longer the case. The above discussion of humic material system is just an extension of complexity theory.

8.3 Future Work

Table 8.1 shows possible paths for future work. Further metal binding studies would be performed by the approach developed in this work. Since the data indicates that LHA's functionality is predominantly on the aromatic moieties, and that these moieties are relatively mobile, it would be of great interest to examine if these are the moieties with the strongest metal binding sites. It would also be of great interest to study metals other than Cu(II) to see if the conclusions drawn from the Cu(II) binding studies could be more

Table 8.1: Possible future research

Studies	Methods
NMR characterisation	- NMR characterisation of humic materials from other sources
Metal binding	- Ramp-CP-MAS ^{13}C NMR on LFA and LHA with Cu(II) and other metal ions - TEM and EELS studies on the above samples - Computer modelling of results
Structural	- ^{17}O and ^{2}H liquid state NMR hydration studies on LFA and LHA - Computer modelling of results
Pesticide interactions	- ^{19}F and ^{31}P both dynamic and static liquid and solid state NMR studies - TEM and EELS studies on the above samples - Computer modelling of results
A whole soil and its organic fractions	- ^{13}C, ^{31}P, and paramagnetic relaxation NMR studies of metal and pesticide binding
Biodegradation of petroleum products	- ^{13}C solid and liquid state and ^{1}H liquid state NMR

general. Due to its very high resolution, transmittance electron microscopy (TEM) along with electron energy loss spectroscopy (EELS) would appear to be a very promising, and complementary technique to NMR.

Pesticide interactions studies would be carried out by ^{19}F and ^{31}P NMR chemical shift, heteronuclear correlation, and heteronuclear coherence transfer spectra as well as dynamic relaxation and kinetic experiments. The reason for choosing ^{19}F and ^{31}P is that they are very sensitive NMR nuclei, they both have large chemical shift ranges, and there is an extensive biological literature on them. This biological literature addresses similar problems to pesticide interactions with humic materials. The experiments would be performed in water and water/organic mixtures. This would allow one to understand the hydrophobic/hydrophilic nature of these interactions, as well as the time involved for the system to reach a quasi-equilibrium. It may also be interesting to conduct variable temperature studies. There are two reasons for the variable temperature studies. The first is to see if the quasi-equilibrium after each temperature fluctuation will be similar or different. The variable temperature experiments may also allow one to determine an activation energy or activation energies, if there are any, for these interactions.

In the research presented here, ^{13}C solid state NMR has been used to get some insight into the mesostructure of LFA and LHA. However, a more promising technique for mesostructural investigations is via the water interacting with the polymeric network. The technique which has shown the most promise in biochemistry is ^{17}O and ^{2}H liquid state relaxation studies at different temperatures and magnetic fields. The same approach is also promising for humic materials, where via the relaxation measurements different types of bound water can be determined which, in turn, give mesostructural information.

All three NMR experiments mentioned above will provide valuable information which can be compared, and act as reference data, to computer modelling results. The way in which this would work is as follows. First one would select the most plausible structural units for humic materials and combine them into a reasonable model, and then optimise it via molecular mechanics. Once this has been done, hydrate the molecule and compare

computational results to the ^{17}O and ^{2}H NMR results on the real system. If the results are with in an acceptable error then proceed to the next step, which is to take the hydrated model and react it with the same pesticides or pesticides on which the ^{19}F and ^{31}P NMR experiments were performed. If this is successful, then do a similar type of calculation but replace the pesticide with a metal ion.

8.4 Personal Thoughts

As can be seen from above I believe that only by the combination of sophisticated tools and methods can the advancement in our understanding of humic materials and the environment continue to break new ground. However, this point of view is very expensive and the techniques are by no means trivial. Thus, highly qualified professionals have to lead new and bright minds into the field. This means that more multidisciplinary collaboration is needed as well as more funding. At the moment the funding that environmental research receives is by no means proportional to the value of what the earth's environment gives us, i.e. $33 trillion (U.S.) per annum.[8.1] As natural resources such as fresh clean water become more and more scarce, their value will increase substantially. This should on pressure on improving the funding situation.. I only hope that this change in the funding situation (not the environmental situation) comes soon, as it is much easier and cheaper in the long run to prevent than to cure.

Reference

8.1 Costanza, R.; d'Arge, R.; de Groot, R.; Farber, S.; Grasso, M.; Hannon, B.; Limburg, K.; Naeem, S.; O'Neill, R.V.; Paruelo, J.; Raskin, P.G.; Sutton, P.; van den Belt, M. *Nature*, **1997**, 387, 253.

Appendix A
Setting Up The Ramp for Ramp-CP

The first step in setting up Ramp-CP is to calibrate the amplifier on which the ramp will be set in terms of frequency (kHz) versus power (dB). This was accomplished by changing the amplifier's power output and measuring the amount of time it took to establish a 90_y° pulse. The time domain was then converted into the frequency domain taking into consideration that the pulsed used was a 90° pulse and not a 360° pulse. An example of this is; $10kHz \rightarrow 100\mu s(90°/360°) \rightarrow 25\mu s$. Figure A.1 shows the calibration curve for the proton channel of the Bruker AMX2-300 at the University of Calgary.

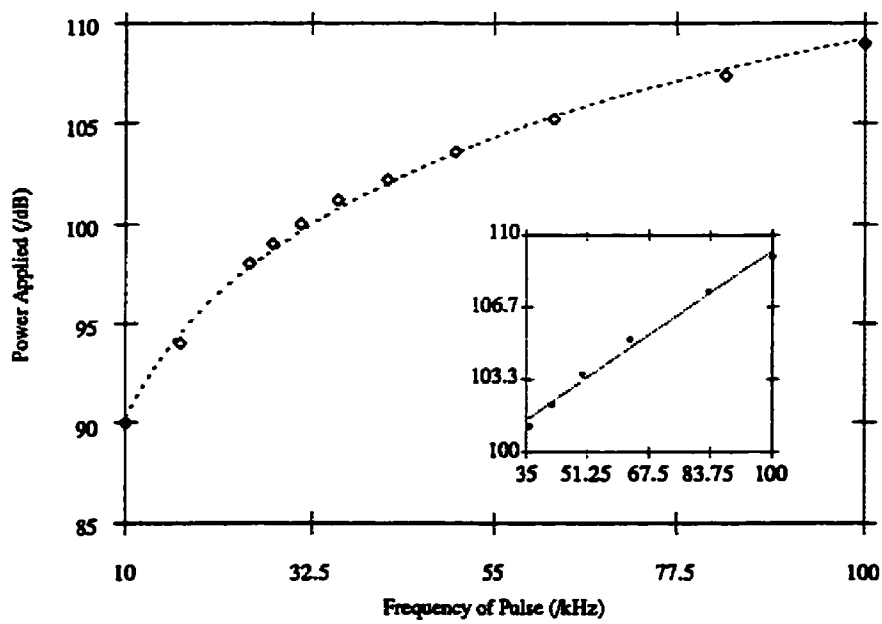

Figure A.1: A plot of the power versus frequency of the applied pulse (the axis on the inset are identical to those of the main plot).

Although the curve is not linear, in fact it is best described as a log function with a correlation coefficient of r=0.998, it does tend to linearity at the higher frequencies. From about 35 kHz, the curve can be considered linear as the insert in Figure A.1 shows, the correlation coefficient for the linear fit is r=0.994. The two curve fittings that produced the correlation values are the standard logarithmic and linear curve fits in KaleidaGraph. The X channel amplifier was not as linear, and thus the proton channel was used for ramping.

The next step was to set the ramp up on the -1 sideband match. The ramp is set up so its centre is at the -1 sideband match, as determined by the ketonic group of glycine. The size of the ramp is determined by the sample spinning speed used, as is the -1 sideband match. Although this may sound to be a very daunting task, it is in fact quite simple if the NMR spectrometer has a pulse programmer and allows for triangular pulses, as the Bruker AMX2-300 does. The first step is to choose the triangular pulse, and then choose the appropriate slice, as shown in Figure A.2. It is mandatory to know the frequency of the HH (Hartmann-Hahn match). From Figure A.2 it can be seen that the first half of the triangular pulse is a linear ascending ramp, while the second half is a linear descending ramp. This is true in terms of both amplitude and frequency because of the amplifier's linearity for the power ranges of interest. For the remainder of the discussion only the ascending half will be considered. Due to the digital nature of pulse shape programmer, this ascending ramp is truly made up of 128 points as shown in Figure A.2 (in reality there are 256 points, but 128 of these are in the imaginary domain). Each of the 128 points can be considered as a step, once again because of the digital nature of the pulse programmer. The HH for the ketonic centre of glycine, on the instrument used in this work, was found to be 60 kHz, and is the maximum of the triangular pulse, as shown in Figure A.2. If we now want to set up a ramp for a sample that is spinning at 10 kHz, then the centre of the

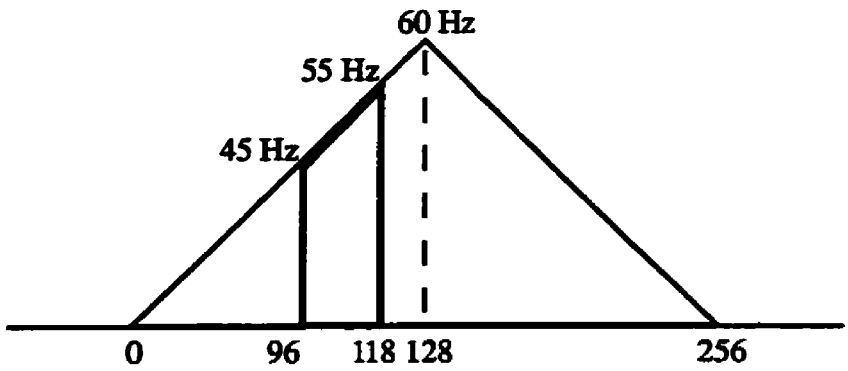

Figure A.2: Turning a triangle pulse into a Ramp-CP pulse.

ramp will be at 50 kHz and the ramp will cover the range of 45 to 55 kHz. If we convert this into point format, the centre of the ramp will be at point 107, and the ramp covers from points 96 to 118. In reality all that has been done is that a slice has been taken out of the triangular pulse, and this slice is a frequency ramped pulse. By applying this on the proton channel during CP one obtains Ramp-CP.

Appendix B
Pulse Programs

The programs for the ramped pulse sequences used in this experiments are given below. The SACP pulse program is not given as it is the same pulse program as supplied by Bruker.

Ramp-CP pulse sequence, stored as cp2levva.ry

```
; set:
; p3=90 degree 1H pulse
; p15=contact time pulse
; dp1 to have HH match with available X power
; dl0 for proton 90
; dl1 to decouple with highest available 1H power

define pulse 90=p3+p17          ; p17 correction pulse
define pulse pct=p15

1 ze
2 d1 tlo dl0 d0
  10u:c4 dl0                    ; unblank AMT
3 p90:d:c4 ph1                  ; 90 degree 1H pulse
4 (pct ph3):dp1 (pct ph2):t:c4  ; cross polarization with shaped
                                ; pulse on proton
```

```
  2u cw dl1
  go=2 ph31
  2m do                          ; decoupler off
5 wr #0
6 exit

ph1=1 3
ph2=0 0 1 1 2 2 3 3
ph3=0
ph31=0 2 1 3 2 0 3 1

; TL(0) set to drive HP X amplifier
; rd=pw=0
; ns=8*n
```

Ramp-CP $^{13}CT_2$ pulse sequence, stored as cp2levxt2va.ry

```
; set:
; p3=90 degree 1H pulse
; p15=contact time pulse
; dp1 to have HH match with available X power
; dl0 fro proton 90
; dl1 to decouple with highest available 1h power
; td1=number of delays in VDLIST
; l0=1 if VDLIST has to be executed as is
```

```
;     the delays in the list are multiplied by 10

define pulse 90=p3+p17        ; p17 correction pulse
define pulse pct=p15
p2=p3*2.0

1 ze
2 d1 tl0 dl0 do
  10u:c4 dl0                  ; unblank AMT
3 p90:d:c4 ph1                ; 90 degree 1H pulse
  (pct ph3):dp1 (pct ph2):t:c4 ; cross polarization
  vd:c4 cw dl1                ; switch to higher power for decoupling
  (p2 ph4) :t:c4              ; X-nucleus pi pulse
  vd:c4
4 go=2 ph31
  2m do                       ; decoupler off
5 100m wr #0 if #0 iv
  go to 1 times td1           ; set td1 to #0 of delays in list
6 exit

ph1=1 3
ph2=0 0 1 1 2 2 3 3
ph3=0
ph4=1 1 2 2 3 3 0 0 0 0 1 1 2 2 3 3
ph31=0 2 1 3 2 0 3 1 2 0 3 1 0 2 1 3
```

```
; p2=180 degree X-pulse, set by the program
; TL(0) set to drive HP X amplifier
; rd=pw=0
; ns=8*n
```

Two dimensional dipolar dephasing pulse sequence, stored as cp2dddpvar5.ry

```
; set:
; p3=90 degree 1H pulse
; p15=contact time pulse
; dp1 to have HH match with available X power
; dl0 for proton 90
; dl1 to decouple with highest available 1h power
; parmode = 2D
; td1=32 or 64
; nd0=2
; p20=180 degree 1H pulse (with dl1 power level)

p2=p3*2.0
define pulse 90=p3+p17          ; p17 correction pulse
define pulse pct=p15

1 ze
2 d1 tl0 dl0 do
```

```
  10u:c4 dl0                    ; unblank AMT
3 p90:d:c4 ph1                  ; 90 degree 1H pulse
  (pct ph3):dp1 (pct ph2):t:c4  ; cross polarization
4 d0                            ; delay #1, equalt to 1/2 t1
  dl1                           ; switch to higher power for decoupling to avoid HH below
  (p20 ph4):d (p2 ph4):t:c4     ; H(180) refocussing pulse and X(180)-CS refocusing pulse
5 d0 dl1                        ; delays #2 equalt to delay #1, and thus equalt to 1/2 t1
6 go=2 ph31
  2m do                         ; decoupler off
7 100m wr #0 if #0 id0 zd
  go to 1 times td1
8 exit

ph1=1 3
ph2=0 0 2 2 1 1 3 3
ph3=0
ph4=0 0 2 2 1 1 3 3
ph31=0 2 2 0 1 3 3 1

; TL(0) set to drive HP X amplifier
; rd=pw=0
; ns=8*n
;nd0=2
;d0=2 us
```

Appendix C
Fluorometric Approach to the Study of Metal Ion Complexation Kinetics

Although, all the work reported in the body of this thesis are equilibrium studies, kinetic studies are very pertinent to speciation studies as life processes are dynamic. The need for both highly sensitive and better probes led to the following work. Luminescence (especially fluorescence) is a probe that offers excellent sensitivity, and humic substances luminesce with lifetime suggesting fluorescence. Many studies have attempted to monitor binding of metal ions by humic materials via observing the quenching of the humic materials luminescence by the bound metal ion. The majority of this work has used the assumption that luminescence quenching and metal ion binding are related linearly. However, as shown in Chapter 7 for LFA, this linear assumption fails badly! Thus, the luminescence of humic materials themselves and the quenching of it by metal ions would not appear to be a promising approach to studying metal complexation and speciation by humic materials.

Recently Kalsbeck and Thorpe have describe a very intriguing fluorescence probe technique to study metal binding by deoxyribonucleic acid (DNA).[C.1] The technique uses a polyanionic Pt complex known as $Pt_2(pop)_4^{4-}$, where pop is a phosphorus bridging ligand, as the fluorescent probe which is quenched dynamically by the metal ions. Since $Pt_2(pop)_4^{4-}$ is coordination saturated it does not complex the metal, and will not strip the metal ions from the DNA polyanion. Also, due to the large negative charge of $Pt_2(pop)_4^{4-}$ it is unlikely to encounter the DNA and DNA-metal polyanions. Thus, the metal ions complexed to the DNA polyanion will not quench the fluorescence of $Pt_2(pop)_4^{4-}$. With these two properties, $Pt_2(pop)_4^{4-}$ is the perfect spectator of free metal in solution. The

DNA/metal ions situation is very similar to the humic material/metal ion situation at natural (intermediate) pH values. Thus, it is quite plausible that a fluorescence probe anion that has little tendency to bind metal ions and a low probability of collision with the humic polyelectrolyte can be found.

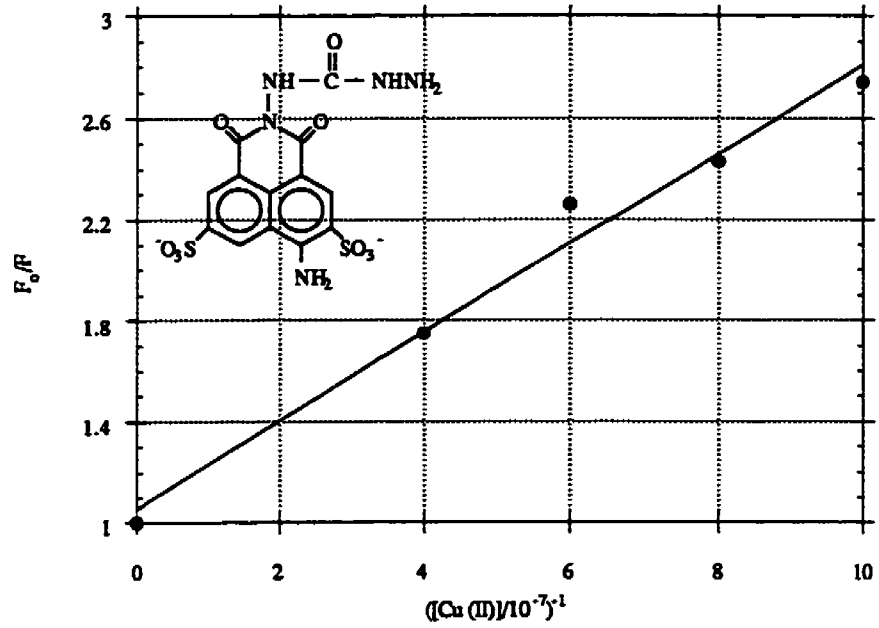

Figure C.1: Stern-Volmer plot of Cu (II) quenching of Lucifer Yellow (10^{-6} *M*).

A most promising anionic fluorescent probe for this type of work is Lucifer Yellow. The Stern-Volmer quenching plot of Lucifer Yellow together with the structure of the probe are shown in Figure C.1. From Figure C.1 it can be seen that the probe is sensitive to suitably low Cu (II) concentration. The $Cu(edta)^{2-}$ complex does quench Lucifer Yellow's fluorescence even at much higher concentrations, as is shown in Figure C.2. The fluorescence of Lucifer Yellow is intense in a region where humic materials have

little absorbance. It is proposed that kinetic experiments would proceed in the following manner: add a small concentration of Lucifer Yellow (approximately 10^{-6} *M*) to the complexant solution; then spike the solution with a small addition of M_{aq} (II), where M is a metal ion that will quench the fluorescence of Lucifer Yellow; and observe fluorescence as a function of time to monitor the reaction of free metal ions with complexants.

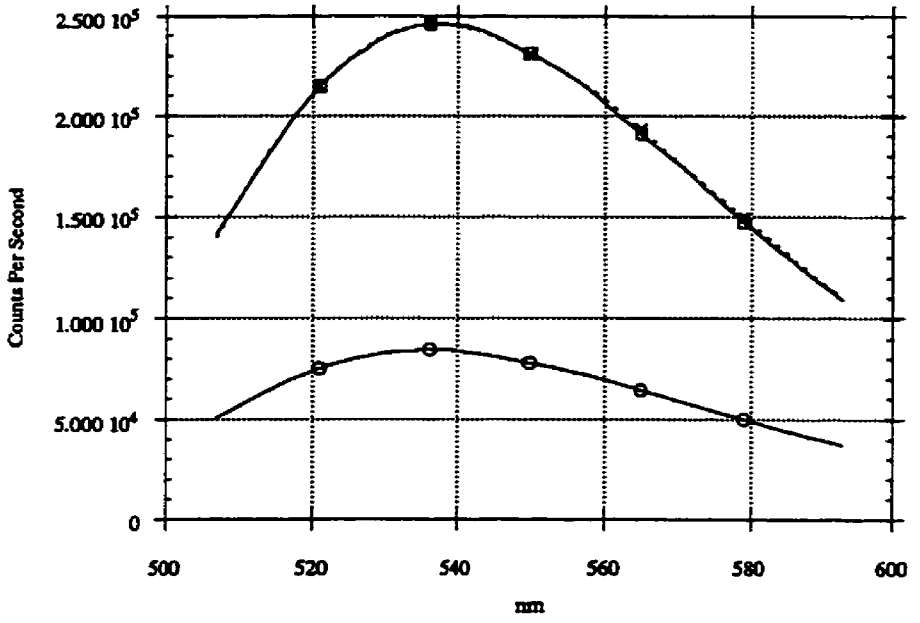

Figure C.2: The upper two spectra are a 10^{-6} *M* solution of Lucifer Yellow (solid curve) and the same solution in the presence of $5*10^{-5}$ *M* $Cu(edta)^{2-}$ (dashed curve). The lower curve is the Lucifer Yellow solution in the presence of 10^{-6} *M* Cu (II).

This approach avoids the ambiguities which arise in the ligand exchange approach, because the fluorescent probe will not interact with humic/metal complex, it will only monitor the free metal ions. This approach allows for the direct examination of features

pertinent to mechanism elucidation of complex formation by the naturally occurring polyelectrolyte ligand systems, e.g. LFA. Due to the fact that this technique uses very simple instrumentation, it should allow for the development of an instrument that can be used in the field in remote locations.

Reference

C.1 Kalsbeck, W.A.; Thorpe, H.H. *J. Am. Chem. Soc.* **1993**, 115, 7146.

Appendix D

A Fluorimetric Method for Detecting Trace Metal Ions In "Clean Glassware", and Procedure for Producing "Clean Glassware"

From Appendix C it can be seen that the glassware used for kinetic studies at natural concentration, e.g. 10^{-7} *M* must be very clean. In terms of metal speciation studies this cleanliness is of paramount importance with respect to metal ions. To obtain glassware with metal ion impurities lower than 10^{-7} *M* is a rather tricky procedure, especially proving that the glassware does indeed have less than 10^{-7} *M* metal ions. It should be pointed out that a simple water wash and then flame atomic absorption (AA) or inductively coupled plasma absorption (ICP) measurement on the wash will not show all metal ion impurities. The reason for this is that some of the metal ions will adsorb onto the glass and only come off by complexation. This leads to another point as well. A simple acid washing of the glass may not be a satisfactory cleaning method for natural water concentration work. As the results below will show, a procedure which uses a three step washing processes gives cleaner glassware. This three step procedure is as follows: the first step is an acid wash after which the glassware is rinsed five times with 18 MΩ water; the glassware is then cleaned with an ethylenediaminetetraacetic acid (edta) solution at neutral pH; a triple wash with very warm 18 MΩ; five washes with 18 MΩ water. The reason for the use of edta is that it is a strong metal ion binding ligand and will out compete the glass surface for metal ions. This is very important step as a similar competition between the humic material and glass will also take place.

Thus, once this cleaning is done one has to check to see if the glassware is clean enough. If one now recalls the finding in Appendix C that the $Cu(edta)^{2-}$ complex does not

quench the fluorescence of Lucifer Yellow at concentration much greater than 10^{-7} *M*, a simple and very sensitive method of detecting trace metal ions in "clean glassware" becomes apparent. The method is as follows: take the "clean glassware" and add a Lucifer Yellow fluorescence dye solution into the glassware and measure the fluorescence intensity. Then add edta to the solution and measure the fluorescence intensity. If the fluorescence intensity stays the same, then the glassware is clean. However, if the fluorescence increases then the glassware is not clean. The increase comes about because the edta is complexing metal ions which are quenching the fluorescence of the Lucifer

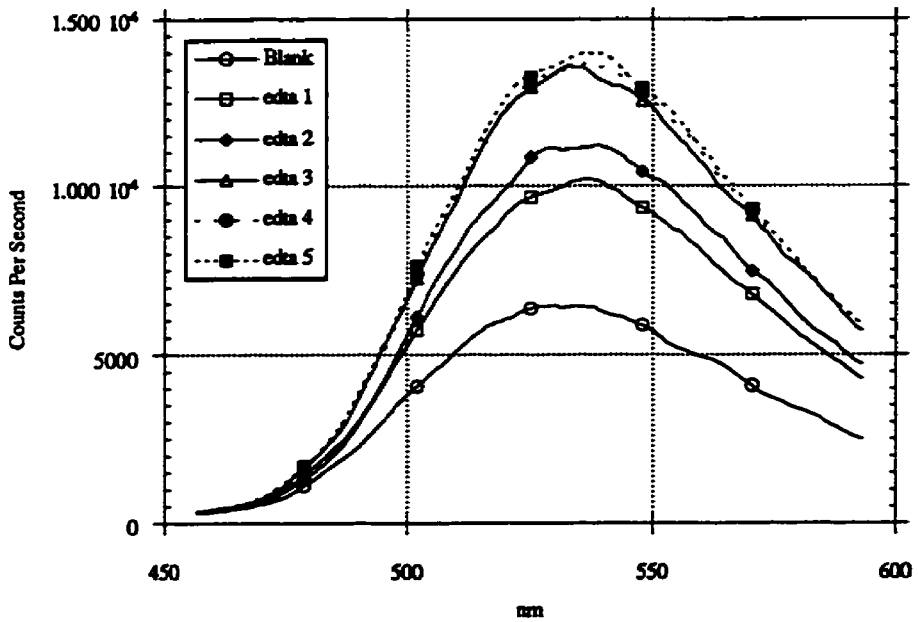

Figure D.1: Results for a volumetric flask washed three times with HNO_3 and then washed ten times with 18 MΩ water. The blank sample is just a 10^{-6} *M* Lucifer Yellow solution in the flask, while edta 1 to edta 5 are the same solution but with $2 \cdot 10^{-7}$ to 10^{-6} *M* edta added.

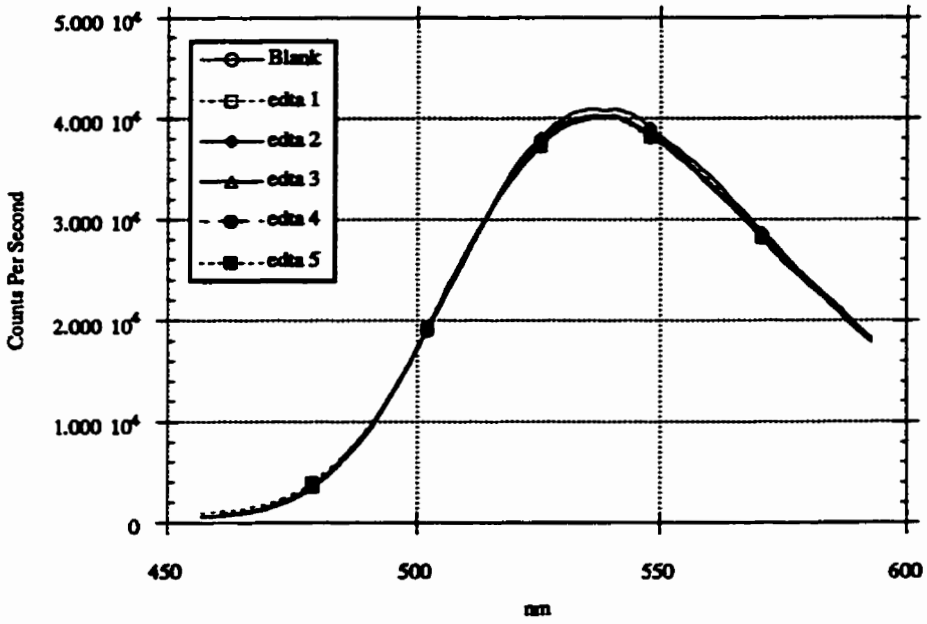

Figure D.2: Results for a volumetric flask washed once with HNO_3 after which the glassware is rinsed five times with 18 MΩ water the glassware is then cleaned with an edta solution at neutral pH this is then followed by a wash with very warm 18 MΩ water three times and the glassware is by a wash with 18 MΩ water five times. The blank sample is just a 10^{-7} *M* Lucifer Yellow solution in the flask, while edta 1 to edta 5 are the same solution but with $2 \cdot 10^{-7}$ to 10^{-6} *M* edta added.

Yellow dye, and thus there are metal ion impurities in the system. Experimental results of this are shown in Figures D.1 and D.2. The reason for the greater intensity in Figure D.2 is that the gain on the photomultipler tube was increased, to allow for better sensitivity to any intensity differences.

From Figures D.1 and D.2 it can be seen that this fluorimetric monitoring is a very sensitive method, and in all probability, this sensitivity can be increased if dyes with higher quantum yields are used. Also, it can be seen that the classic method of acid washing did not yield glassware clean enough for natural water metal speciation studies. This may be from the possible presence of metal ions in the acid itself. However, if one includes an edta wash after the acid wash, one does obtain glassware clean enough for natural water metal speciation studies.

It should also be noted that all glassware should be cured with a 10^{-9} *M* solution of the metal ion being studied after the cleaning, so that any strong glass binding sites are occupied. This curing should be repeated five times for a week each time.

Appendix E
Unsuccessful Experiments

In this section two unsuccessful spectroscopic methods which were investigated are discussed. The two methods that were tried are Raman spectroscopy and X-ray diffraction (XRD) spectroscopy.

E.1 Raman

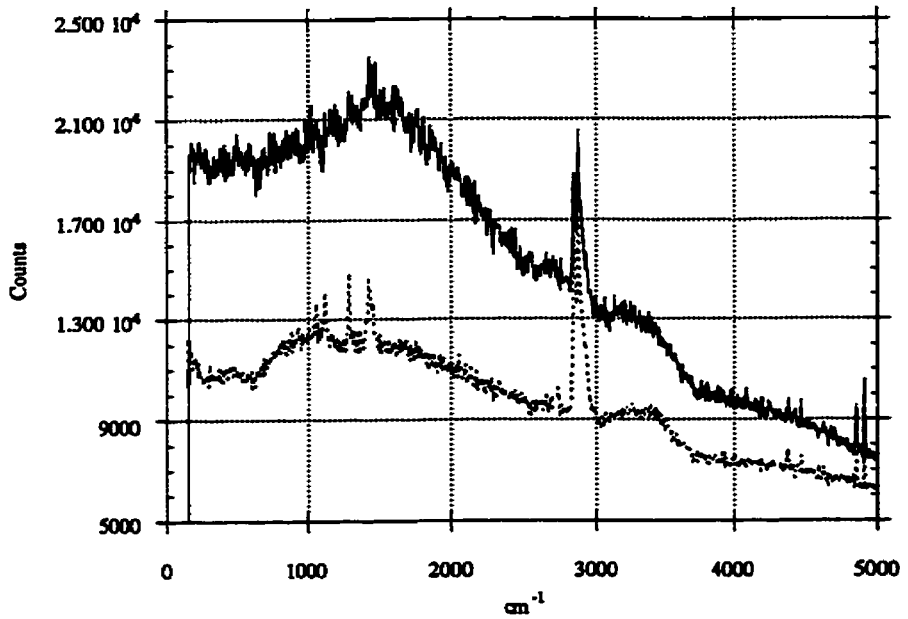

Figure E.1: The bottom scan is an aqueous solution of Cu(II), while the top scan is a solution of Cu (II) and LFA in a 2:1 ratio. It should be noted that the spectrum has been red shifted by 19440.5 cm^{-1}, since the argon laser source emits at that wavenumber.

Raman spectroscopy is a vibration mode based technique that is complimentary to infrared (IR) spectroscopy. Raman is more sensitive to vibrations involving homonuclear bonds compared to IR, but it is not as useful as IR to study oxygen-containing groups. Because of this, Raman is a useful technique for studying polymeric backbones, especially in terms of aggregation. However, due to the fluorescence of LFA Raman spectroscopy was not successful, thus not pursued any further. An example of the results obtained are shown in Figure E.1. However, a new technique known as FT-Raman is able to remove most, if not all, of the fluorescence interference as the laser frequencies used in this technique are in the near IR region. Since, in the near IR region, humic materials fluoresce extremely weakly if at all, it may be worthwhile to conduct a FT-Raman investigation on LFA and LHA.

E.2 XRD

XRD spectroscopy is a method which gives information on medium to long range order in comparison with the short range order information NMR spectroscopy gives. Both LFA and LHA were analysed by XRD, but the resolution was very poor. However, it seemed that LFA had two components and LHA had only one. Due to the poor resolution, this experimental path was not pursued any further. However, small angle XRD may be a useful technique for the study of humic materials.

Bibliography

Abragam, A. The Principles of Nuclear Magnetism; Oxford University Press, New York, 1961. (3.1)

Alemany, L.B.; Grant, D.M.; Pugmire, R.J.; Alger, T.D.; Zilm, K.W. *J. Am. Chem. Soc.* **1983**, 105, 2133. (2.62)

Alemany, L.B.; Grant, D.M.; Pugmire, R.J.; Alger, T.D.; Zilm, K.W. *J. Am. Chem. Soc.* **1983**, 105, 2142. (2.63)

Anderson, A.G.; Hartmann, S.R. *Phys. Rev.* **1962**, 128, 2023. (2.98)

Andrews, E.R. *Progr. Nucl. Magn. Reson. Spectrosc.* **1971**, 8, 1. (2.51, 3.27)

Aschan, O. *J. Prakt. Chem.* **1909**, 77, 172. (2.7)

Axelson, D.E. Solid State Nuclear Magnetic Resonance of Fossil Fuels; Multiscience Publications Ltd: Canadian Government Publishing Centre, Supply and Services Canada, 1985. (1.13, 2.64, 3.12, 4.20, 6.13)

Banerjee, S.K.; Mukherjee, S.K. *J. Indian Soc. Soil Sci.* **1972**, 20, 13. (2.16)

Barbara, T.M.; Williams, E.H. *J. Magn. Reson.* **1992**, 99, 439. (2.85)

Barron, P.F.; Wilson, M.A. *Nature* **1981**, 289, 275. (2.60)

Barron, P.F.; Wilson, M.A.; Stephens, J.F.; Cornell, B.A.; Tate, K.R. *Nature* **1980**, 286, 585. (2.59)

Bartuska, V.J.; Maciel, G.E.; Schaefer, J.; Stejskal, E.O. *Fuel* **1977**, 56, 354. (2.54)

Becker, R.S. Theory and Interpretation of Fluorescence and Phosphorescence; John Wiley & Sons, New York, 1969. (3.15)

Benedetti, M.F.; Van Riemsdijk, W.H.; Koopal, L.K. *Environ. Sci. Technol.* **1996**, 30, 1805. (6.18)

Black, A.P.; Christman, R.F. *J. Am. Water Works Assoc.* **1963**, 55, 753. (2.9)

Bloch, F.; Hansen, W.W.; Packard, M. *Phys. Rev.* **1946**, 69, 127. (3.25)

Bloembergen, N. *J. Chem. Phys.* **1957**, 27, 572. (3.48)

Botto, R.E.; Sanada, Y. Magnetic Resonance of Carbonaceous Solids: Advances in Chemistry Series 229; American Chemical Society, Washington D.C., 1993. (3.13)

Botto, R.E.; Wilson, R.; Winans, R.E. *Energy Fuels* **1987**, 1, 173. (2.73)

Bruccoleri, A.: Pant, B.C.; Sharma, D.K.; Langford, C.H. *Environ. Sci. Technol.* **1993**, 27, 889. (4.3)

Buffle, J. Complexation Reactions in Aquatic Systems. An Analytical Approach; Ellis Harwood Ltd, Chester, UK, 1988. (1.2, 1.29, 3.21, 5.1)

Cabaniss, S.E. *Anal. Chem.* **1991**, 63, 1323. (3.53)

Cabaniss, S.E. *Environ. Sci. Technol.* **1992**, 26, 1133. (6.5, 2.34)

Cabaniss, S.E.; Shuman, M.S. *Anal Chem.* **1990**, 62, 1526. (2.31)

Cabaniss, S.E.; Shuman, M.S. *Anal. Chem.* **1986**, 58, 398. (2.28)

Cabaniss, S.E.; Shuman, M.S. *Anal. Chem.* **1988**, 60, 2418. (2.29)

Cabaniss, S.E.; Shuman, M.S. *Marine Chemistry* **1987**, 21, 37. (6.6)

Cline, J.T.; Holland, J.F. *ERDA Symp. Ser.* **1977**, 42, 264. (2.19)

Cline, J.T.; Holland, J.F. in Biological Implications of Metals in the Environment: Proc. Fifteenth Hanford Life Sci Symp.; Richland, WA, 1975, Tech. Info. Ctr. Energy Res. Developement Admin., 1977. (2.18)

Cook, R.L.; Langford, C.H. *Anal. Chem.* **1995**, 67, 174. (2.26)

Cook, R.L.; Langford, C.H.; Yamdagni, R.; Preston, C.M. *Anal. Chem.* **1996**, 68, 3979. (3.43)

Costanza, R.; d'Arge, R.; de Groot, R.; Farber, S.; Grasso, M.; Hannon, B.; Limburg, K.; Naeem, S.; O'Neill, R.V.; Paruelo, J.; Raskin, P.G.; Sutton, P.; van den Belt, M. *Nature*, **1997**, 387, 253. (1.1, 8.1)

Datta, C.; Ghosh, K.; Mukherjee, S.K. *J. Indian Chem. Soc.* **1971**, 48, 279. (2.13)

Dienert, F. *Compt. Rend.* **1910**, 150, 487. (2.8)

Dudley, R.L.; Fyfe, C.A. *Fuel* **1982**, 61, 651. (2.67)

Dwek, R.A. Nuclear Magentic Resonance (N.M.R.) in Biochemistry: Apllications to Enzyme Systems; Oxford University Press, New York, 1973. (3.2)

Earl, W.L.; VanderHart, D.L. *Macromolecule*, **1979**, 12, 762. (4.22)

Earl, W.L.; Wershaw, R.L.; Thorn, K.A. *J. Magn. Reson.* **1987**, 76, 264. (2.76)

Ernst, R.R.; Bodenhausen, G.; Wokaun, A. Principles of Nuclear Magnetic Resonance in One and Two Dimensions; Oxford University Press, New York, 1994. (2.102, 3.9, 4.23)

Fish, W.; Morel, F.M.M. *Can. J. Chem.* **1985**, 63, 1185. (2.27)

Framer, V.C. *Nature* **1985**, 316, 658. (2.104)

Framer, V.C.; Pisaniello, D.L. *Nature* **1985**, 313, 474. (2.103)

Fraústo da Silva, J.J.R.; Williams, R.J.P. The Biological Chemistry of the Elements: The Inorganic Chemistry of Life; Oxford University Press, New York, 1991. (1.33)

Freeman, R. A. Handbook of Nuclear Magnetic Resonance; Longman Science & Technical, Essex, England, 1988. (3.8, 4.24)

Fründ, R.; Guggenberger, G.; Haider, K.; Knicker, H.; Kögel-Knabner, I.; Lüdemann, H.-D.; Luster, J.; Zech, W.; Spiteller, M. *Z. Pflanzenernähr. Bodenk.* **1994**, 157, 175. (2.5)

Fründ, R.; Lüdemann, H.-D. *Sci. Total Environ.* **1989**, 81/82, 157. (1.14, 2.65)

Gamble, D.S.; Underdown, A.W.; Langford, C.H. *Anal. Chem.* **1980**, 52, 1901. (4.9, 6.7, 7.2)

Garroway, A..N.; Moniz, W.B.; Resing, H.A. in Carbon-13 NMR in Polymer Science: ACS Symposium Series 103: Paski, W.M., Ed.; American Chemical Society, Washington, D.C., 1979. (3.41)

Ghassemi, M. Christman, R.F. *Limnol. Oceanogr.* **1968**, 13, 583. (2.12)

Ghosh, K.; Schnitzer, M. *Can. J. Soil Sci.* **1980**, 60, 373. (2.14)

Ghosh, K.; Schnitzer, M. *Soil Sci.* **1980**, 129, 266. (2.15)

Green, H.; Titman, J.J.; Spiess, H.W. *Chem. Phys. Letters* **1993**, 213, 145. (2.86)

Griffith, S.M.; Schnitzer, M. *Soil Soc.* **1975**, 120, 126. (4.1)

Grimm, D.M.; Azarraga, L.V.; Carreira, L.A.; Susetyo, W. *Environ. Sci. Technol.* **1991**, 25, 1427. (7.7)

Guillet, J. Polymer Photophysics and Photochemistry, an Introduction to the Study of Photoprocesses in Macromolecules; Cambrideg University Press, New York, 1985. (3.55, 7.16)

Harris, D. C. Quantitative Chemical Analysis: (2nd ed.); W.H. Freeman and Company, New York, 1987. (3.19)

Harris, R.K. Nuclear Magnetic Resonance Spectroscopy: A Physiochemical View; Longman Science & Technical, Essex, England, 1986. (3.6)

Hartmann, S.R.; Hahn, E.L. *Phys. Rev.* **1962**, 128, 2042. (2.49, 3.35)

Hatcher, P.G.; Maciel, G.E.; Dennis, L.W. *Org. Geochem.* **1981**, 3, 43. (2.106)

Hatcher, P.G.; Rowan, R.; Mattingly, M. *Org. Geochem.* **1980**, 2, 113 (2.41).

Hatcher, P.G.; Schnitzer, M.; Dennis, L.W.; Maciel, G.E. *Soil Sci. Soc. Am. J.* **1981**, 45, 1089. (2.105, 6.10)

Hatcher, P.G.; Vanderhart, D.L.; Earl, W.L. *Org. Geochem.* **1980**, 2, 87. (2.58)

Hatcher, P.G.; Wilson, M.A. *Org. Geochem.* **1991**, 17, 293. (2.77)

Hayes, M.H.B.; MacCarthy, P.; Malcolm, R.L.; Swift, R.S. Humic Substances II. In Search of Structure; John Wiley & Sons, Toronto, 1989. (1.4, 3.22)

Hediger, S.; Meier, B.H.; Ernst, R.R. *Chem. Phys. Letters* **1993**, 213, 627. (2.90)

Hediger, S.; Meier, B.H.; Ernst, R.R. *Chem. Phys. Letters* **1995**, 240, 449. (2.100)

Hediger, S.; Meier, B.H.; Narayanan, D.K. Bodenhausen, G. Ernst, R.R. *Chem. Phys. Letters* **1994**, 223, 283. (2.99, 3.46)

Hediger, S.; Signer, P.; Tomaselli, M.; Ernst, R.R.; Meier, B.H. *J. Magn. Reson.* **1997**, 125, 291. (2.101)

Hertzfield, J.; Berger, A.E. *J. Chem. Phys.* **1980**, 73, 6021. (3.32)

Hing, A.W.; Vega, S.; Schaefer, J. *J. Magn. Reson.* **1992**, 96, 250. (2.96)

Hing, A.W.; Vega, S.; Schaefer, J. *J. Magn. Reson. A* **1993**, 103, 151. (2.97)

Hore, P.J. Nuclear Magnetic Resonance; Oxford University Press, New York, 1995. (3.11)

Jurkiewicz, A.; Maciel, G.E.; *Anal. Chem.* **1995**, 67, 2188. (1.16)

Kalsbeck, W.A.; Thorpe, H.H. *J. Am. Chem. Soc.* **1993**, 115, 7146 (C.1)

Kinchesh, P.; Powlson, D.S.; Randall, E.W. *Eur. J. Soil. Sci.* **1995**, 46, 125. (1.15, 2.66)

Knowles, P.F.; Marsh, D.; Rattle, H.W.E Magnetic Resoance of Biomolecules: An Introduction to the Theory and Practice of NMR and ESR in Biological Systems; John Wiley & Sons, New York, 1976. (3.3)

Kolbert, A.C.; Bielecki, A. *J. Magn. Reson. Ser. A* **1995**, 116, 29. (2.89)

Komorowski, R.A. in High Resolution NMR Spectroscopy of Synthetic Polymers in Bulk : Komorowski, R.A., Ed.; VCH: Deerfield, Fl, 1986. (3.40)

Kononova, M.M. Soil Organic Matter; Pergamon Press, Oxford, 1966. (2.11)

Lakatos, B.; Korecz, L.; Meisel, J. *Geoderma* **1977**, 19, 149. (7.13)

Lakowicz J.R. Priciples of Fluorescence Specroscopy; Plenum Press, New York, 1983. (3.18, 7.10)

Lavinge, J.A. PhD thesis, Concordia University, Montreal, 1988. (6.4)

Lee, Y.K.; Helmle, M.; Johannessen, O.G.; Nielsen, N.C.; Levitt, M.H. *Chem. Phys. Letters* **1995**, 242, 304. (2.88)

Lehrer, S.S. *Biochemistry* **1971**, 10, 3254. (3.54, 7.11)

Leenheer, J.A.; Wershaw, R.L.; Reddy, M.M. *Environ. Sci. Technol.* **1995**, 29, 393. (6.15)

Leenheer, J.A.; Wershaw, R.L.; Reddy, M.M. *Environ. Sci. Technol.* **1995**, 29, 399. (6.16)

Lentz, H.; Ludemann, H.D.; Ziechmann, W. *Geoderma*, **1977**, 18, 325. 2.39)

Lévesque, M. *Soil Sci.* **1972**, 113, 346. (2.17)

Levitt, M.H.; Suter, D., Ernst, R.R. *J. Chem. Phys.* **1986**, 84, 4243. (2.84, 3.33)

Leyden, D.E.; Cox, R.H. Analytical Applications of NMR; John Wiley & Sons, New York, 1977. (3.4)

Lloyd, J.B.F. *Nature* **1971**, 231, 64. (3.49)

Lloyd, J.B.F.; Evett, I.W. *Anal. Chem.* **1977**, 49, 1710. (3.50)

Lowe, I.J. *Phys. Rev. Ltters* **1959**, 2, 285. (2.50, 3.26)

Ludemann, H.D. *Erdoel und Kohle, Ergas, Petrochemie vereinigt mit Brennstoff-Chemie*, **1973**, 26, 506. (2.38)

Lumb, M.D. in Luminescence Spectroscopy: Lumb M.D. (ed.); Academic Press, New York, 1978. (3.16)

Lund, W. *Fresenius J. Anal. Chem.* **1990**, 337, 557. (1.9)

Luster, J.; Llyod, T.; Sposito, G.; Fry, I.V. *Environ. Sci. Technol.* **1996**, 30, 1565. (7.9)

Maciel, G.E.; Bartuska, V.J.; Miknis, F.P. *Fuel* **1979**, 58, 391. (2.56)

Malcolm, R.L. *Anal. Chim. Acta.* **1990**, 232, 19. (4.27)

Marks, D.; Vega, S. *J. Magn. Reson. Ser. A* **1996**, 118, 157. (3.34, 4.16)

Martin, R.B. in Concepts On Metal Ion Toxicity: Vol. 20 of the series: H. Sigel (ed.), Vol. 20 of the series, Metal Ions in Biological Systems; Marcel Dekker, 1986. (1.5)

McBride, M.B. *Soil Sci.* **1978**, 126, 200. (7.12)

Metz, G.; Wu, X.; Smith, S.O. *J. Magn. Reson. Ser. A.* **1994**, 110, 219. (1.28, 2.94, 3.42, 4.15, 5.2)

Miano T.M.; Senesi N. *Sci. Total Environ.* **1992**, 117/118, 41. (6.2)

Miano, T.M.; Sposito, G.; Martin, J.P. *Soil Sci. Soc. Am. J.* **1988**, 52, 1016. (2.32)

Mikinis, F.P.; Maciel, G.E.; Bartuska, V.J. *Org. Geochem.* **1979**, 1, 169. (2.57)

Morrison, G.M.P. in Trace Element Speciation: Analytical Methods and Problems: G.E. Batley (ed.); CRC Press, Boca Raton, 1989. (1.8)

Nanny, M.A.; Minear, R.A.; Leenheer, J.A. Nuclear Magnetic Resonance Spectroscopy in Environmental Chemistry; Oxford University Press, New York, 1997. (3.20)

Newman, R.H.; Tate, K.R. *J. Soil Sci.* **1984**, 35, 47. (2.71)

Newman, R.H.; Tate, K.R.; Barron P.F.; Wilson, M.A. *J. Soil Sci.* **1980**, 32, 623. (2.46)

Ogner, G; Gronneberg, T. *Geoderma* **1977**, 19, 237. (2.45)

Oka, H.; Sasaki, M.; Itoh, M.; Suzuki, *A. Nenryo Koyokai-shi*, **1969**, 48, 295. (2.37)

Olson, D.L.; Shuman, M.S. *Anal. Chem.* **1983**, 55, 1103. (1.32)

Opella, S.J.; Frey, M.H. *J. Am. Chem. Soc.* **1974**, 101, 5854. (4.25)

Pan, V.H.; Maciel, G.E. *Fuel* **1993**, 72, 451. (1.17)

Parker, C.A. Photoluminescence of Solutions: With Applications to Photochemistry and Analytical Chemistry; Elsevier Publishing Company, New York, 1968. (3.14)

Peersen, O.B.; Wu, X.; Kustanovich, I.; Smith, S.O. *J. Magn. Reson. Ser. A* **1993**, 104, 334. (2.91)

Peersen, O.B.; Wu, X.; Smith, S.O. *J. Magn. Reson. Ser. A.* **1994**, 106, 127. (2.92, 3.44)

Petersen, R. *Environ. Sci. Technol.* **1982**, 16, 443. (1.7)

Pfeffer, P.E.; Gerasimowicz, W.V.; Piotrowski, E.G. *Anal. Chem.* **1984**, 56, 734. (2.109)

Pines, A.; Gibby, M.G.; Waugh, J.S. *J. Chem. Phys.* **1972**, 56, 1776. (2.48)

Power, J.F. PhD thesis, Concordia University, Montreal, 1986. (6.3)

Power, J.F.; Lesgae, R.; Sharma, D.K.; Langford, C.H. *Environ. Technol. Lett.* **1986**, 7, 425. (2.25, 6.8)

Preston, C.M. *Soil Sci.* **1996**, 161, 144. (1.10, 2.6)

Preston, C.M.; Blackwell, B.A. *Soil Sci.* **1985**, 139, 88. (2.47, 4.17)

Preston, C.M.; Dudley, R.L.; Fyfe, C.A.; Mathur, S.P. *Geoderma* **1984**, 33, 245. (2.108)

Preston, C.M.; Newman, R.H. *Geoderma*, **1995**, 68, 229. (1.20)

Preston, C.M.; Ripmeester, J.A. *Can. J. Spectrosc.* **1982**, 27, 99. (2.69)

Preston, C.M.; Schnitzer, M. *Soil Sci. Soc. Am. J.* **1984**, 48, 305. (1.19)

Pruski, M.; dela Rosa, L.; Gerstein, B.C. *Energy Fuels*, 1990, 4, 160. (1.27, 3.39)

Pullin, M.J.; Cabaniss, S.E. *Environ. Sci. Tech.* **1995**, 29, 1460. (4.8)

Purcell, E.M.; Torrey, H.C.; Pound, R.V. *Phys. Rev.* **1946**, 69, 37. (3.24)

Retkofsky, H.L.; VanderHart, D.L. *Fuel* **1978**, 57, 421. (2.55)

Rothwell, W.P.; Waugh, J.S. *J. Chem. Phys.* **1980**, 73, 2559. (3.30)

Ruggiero, P.; Interesse, F.S.; Sciacovelli, R. *Geochim. Cosmochim. Acta* **1979**, 44, 603. (2.44)

Ryan, D.K.; Ventry, L.S. *Anal. Chem.* **1990**, 62, 1523. (2.30)

Ryan, D.K.; Weber, J.H. *Anal. Chem.* **1982**, 54, 986. (2.22, 4.11, 7.4)

Ryan, D.K.; Weber, J.H. *Environ. Sci. Technol.* **1982**, 16, 866. (2.23, 4.12, 7.5)

Saar, R.A.; Weber, J.H. *Anal. Chem.* **1980**, 52, 2095. (2.21, 4.10, 7.3)

Sanders, J.K.M.; Hunter, B.K. Modern NMR Spectroscopy: A Guide for Chemists; Oxford University Press, New York, 1993. (3.7)

Sardashti, M.; Maciel, G.E. *J. Magn. Reson.* **1987**, 72, 467. (1.25, 2.79, 3.37)

Schaefer, J.; Stejskal, E.O. *J. Am. Chem. Soc.* **1976**, 98, 1031. (2.53)

Schaefer, J.; Stejskal, E.O.; Buchdahl, R. *Macromolecule* **1975**, 8, 291. (2.52)

Schnitzer, M. *Nature* **1985**, 316, 658. (2.107)

Schnitzer, M. Skinner, S.I.M. *Soil Soc.* **1968**, 105, 392. (4.2)

Schnitzer, M.; Barton, D.H.R. *Nature* **1963**, 198, 217. (2.35)

Schnitzer, M.; Ghosh, K. *Soil Sci. Soc. Am. J.* **1981**, 45, 25. (2.20)

Schnitzer, M.; Neyroud, J.A. *Can. J. Chem.* **1974**, 52, 4123. (2.42)

Schnitzer, M.; Preston, C.M. *Soil Sci. Soc. Am. J.* **1986**, 50, 326. (1.24, 2.72, 4.13)

Schnitzer, M.; Skinner, S.I.M. Isotopes and Radiation in Soil Organic Matter Studies, Proceedings of the Second International Atomic Energy Agency, Vienna, 1968. (2.36)

Schulman, S.G. Fluorescence and Phosphorescence Spectroscopy: Physiochemical Principles and Practice; Pergamon Press, New York, 1977. (3.17)

Seal, B.K.; Roy, K.B.; Mukherjee, S.K. *J. Indian Chem. Soc.* **1964**, 41, 212. (2.10)

Senesi, N. *Anal. Chim. Acta* **1990**, 232, 77. (2.1)

Senesi, N.; Miano T.M.; Provenzano, M.R.; Brunetti, G. *Soil Sci.* **1991**, 152, 259. (6.1)

Senesi, N.; Miano, T.M., Provenzano, M.R., Brunetti, G. *Sci. Total Environ.* **1989**, 81, 143. (2.33)

Senesi, N.; Schnitzer, M. in Environmental Biogeochemistry and Geomicrobiology: Krumbein, E. W., Ed.; Ann Arbor Science, Ann Arbor, MI, 1978. (6.17)

Shuman, M.S.; Collins, B.J.; Fitzgerald, P.J.; Olson, D.L. in Aquatic and Terrestrial Humic Materials: Christman, R.F.; Gjessing, E.T. (eds.); Ann Arbor Sci., Ann Arbor, Mich., 1983. (1.31)

Skjemstad, J.O.; Clarke, P.; Taylor, J.A.; Oades, J.M.; Newman, R.H. *Aust. J. Soil Res.* **1994**, 32, 1215. (1.21)

Snape, C.E.; Axelson, D.E.; Botto, R.E.; Delpeich, J.J.; Tekely, P.; Gerstien, B.C.; Pruski, M.; Maciel, G.E.; Wilson, M.A. *Fuel* **1989**, 68, 547. (1.18, 2.83)

Sohár, P. Nuclear Magentic Resonance Spectroscopy: Volume 1; CRC Press Inc. Boca Raton, Florida, 1983. (3.5)

Solomon, I. *Phys. Rev.* **1955**, 99, 559. (3.47)

Sposito, G.; William, S. *Soil Sci Soc. Am. J.* **1990**, 54, 933-935. (7.8)

Stejskal, E.O.; Memory, J.D. High Resolution NMR in the Solid State: Fundamentals of CP/MAS; Oxford University Press, New York, 1994. (3.10, 4.21)

Stejskal, E.O.; Scaefer, J.; Waugh, J.S. *J. Magn. Reson.* **1977**, 28, 105. (2.78, 3.36, 4.14)

Stevenson, F.J. Humus Chemistry, Genesis, Composition, Reactions (2nd ed.); John Wiley & Sons, Toronto, 1994. (1.3, 6.12, 3.23)

Sullivan, M.J.; Maciel, G.E. *Anal. Chem.* **1982**, 54, 1615. (2.68)s

Sunda, W.G.; Lewis, J.A.M. *Limnol. Oceanogr.* **1978**, 23, 870. (1.6)

Suwelack, D.; Rothwell, W.P.; Waugh, J.S. *J. Chem. Phys.* **1980**, 73, 2559. (3.29)

Tessier, A.; Campbell, P.G.C.; Bisson, M. *Can. J. Earth Sci.* **1980**, 17, 90. (1.30)

Underdown, A.W. PhD thesis, Carlton University, Ottawa, 1982. (4.28)

Underdown, A.W.; Langford, C.H.; Gamble, D.S. *Environ. Sci. Technol.* **1985**, 19, 132. (2.24, 6.9)

VanderHart, D.L.; Earl, W.L.; Garroway, A.N. *J. Magn. Reson.* **1981**, 44, 361. (3.31)

VanderHart, D.L.; Garroway, A.N. *J. Chem. Phys.* **1979**, 71, 2773. (3.28)

Vassallo, A.M.; Wilson, M.A.; Collin, P.J.; Oades, J.M.; Waters, A.G.; Malcolm, R.L. *Anal. Chem.* **1987**, 59, 558. (2.74)

Ventry, L.S.; Ryan, D.K.; Gilbert, T.R. *Microchem. J.* **1991**, 44, 201. (7.6)

Vila, F.J.; Lentz, H.; Ludemann, H.D. *Biochem. Biophys. Res. Comm.* **1976**, 72, 1063. (2.43)

Vo-Dinh, T. *Anal. Chem.* **1978**, 50, 396. (3.51)

Vo-Dinh, T. *Appl. Spectrosc.* **1982**, 36, 576. (3.52)

Voelkel, R. *Angew. Chem. Int. Ed. Engl.* **1988**, 27, 1468. (4.18)

Wang, Z.D. PhD. Thesis, Concordia University, Montreal, 1989. (4.7, 6.14, 7.1)

Wang, Z.D.; Gamble, D.S.; Langford, C.H. *Environ. Sci. Technol.* **1992**, 26, 560. (4.6)

Wang, Z.D.; Pant, B.C.; Langford, C.H. *Anal. Chim. Acta.* **1990**, 232, 43. (4.5)

Wershaw, R.L.; Mikita, M.A. (eds.) NMR of Humic Substances and Coal: Techniques, Problems and Solutions; 1987, Lewis Publishers, Chelsea, MI. (1.12, 2.3)

Wilson, M.A. J. *Soil Sci.* **1981**, 32, 167. (2.2)

Wilson, M.A. *J. Soil Sci.* **1984**, 35, 209. (2.61, 4.26)

Wilson, M.A. NMR Techniques and Applications in Geochemistry and Soil Chemistry; Pergamon Press, Oxford, 1987. (1.11, 2.4, 4.19, 6.11)

Wilson, M.A.; Jones, A.J., Williamson, B. *Nature*, **1978**, 276, 487-489.2.40

Wilson, M.A.; Vassallo, A.M.; Perdue, E.M.; Reuter, J.H. *Anal. Chem.* **1987**, 59, 551. (1.22, 2.75)

Wind, R.A.; Dec, S.F.; Lock, H.; Maciel, G.E. *J. Magn. Reson.* **1988**, 79, 136. (2.80, 3.38)

Worobey, B.L.; Webster, G.R.B. *Nature* **1981**, 292, 526. (2.70)

Wu, X; Zilm, K.W. *J. Magn. Reson. Ser. A* **1993**, 104, 154. (2.87)

Xia, K.; Bleam, W.; Helmke, P.A. *Geochim. Cosmochim. Acta* **1997**, 61, 2211. (7.14)

Xia, K.; Bleam, W.; Helmke, P.A. *Geochim. Cosmochim. Acta* **1997**, 61, 2223. (7.15)

Zhang, M.; Maciel, G.E. *Fuel* **1990**, 69, 557. (1.23, 2.82)

Zhang, S. *J. Magn. Reson. A* **1994**, 110, 73.2.93

Zhang, S. *J. Magn. Reson. Ser. A* **1994**, 111, 73. (2.93, 3.45)

Zhang, S; Czekaj, C.L.; Ford, W.T. *J. Magn. Reson. A* **1994**, 111, 87. (2.95)

Ziegler, R.C.; Wind, R.A.; Maciel, G.E. *J. Magn. Reson.* **1988**, 79, 299. (1.26, 2.81)

Note: The number or numbers inside the brackets at the end of the reference is or are the exact place the reference is used in dissertation.

TEST TARGET (QA-3)

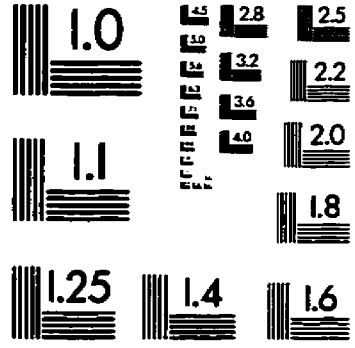

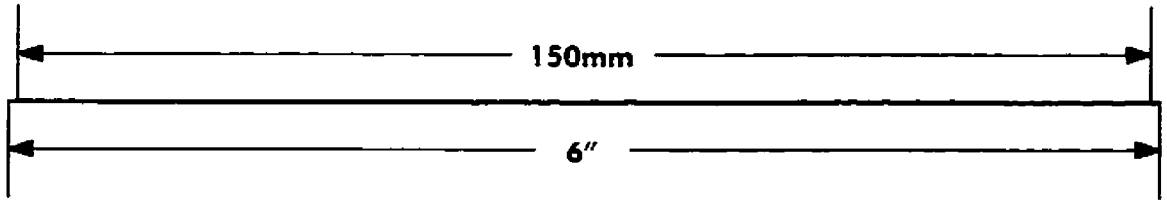

APPLIED IMAGE, Inc
1653 East Main Street
Rochester, NY 14609 USA
Phone: 716/482-0300
Fax: 716/288-5989